

UNCLASSIFIED

AD

402 076

*Reproduced
by the*

DEFENSE DOCUMENTATION CENTER

FOR

SCIENTIFIC AND TECHNICAL INFORMATION

CAMERON STATION, ALEXANDRIA, VIRGINIA



UNCLASSIFIED

NOTICE: When government or other drawings, specifications or other data are used for any purpose other than in connection with a definitely related government procurement operation, the U. S. Government thereby incurs no responsibility, nor any obligation whatsoever; and the fact that the Government may have formulated, furnished, or in any way supplied the said drawings, specifications, or other data is not to be regarded by implication or otherwise as in any manner licensing the holder or any other person or corporation, or conveying any rights or permission to manufacture, use or sell any patented invention that may in any way be related thereto.

63-32

ASD-TDR-63-175

CATALOGED BY ASTIA
AS AD NO. 402076

STUDY OF ELECTRICAL AND PHYSICAL
CHARACTERISTICS OF SECONDARY EMITTING SURFACES

TECHNICAL DOCUMENTARY REPORT NO. ASD-TDR-63-175
March 1963

Electronic Technology Laboratory
Aeronautical Systems Division
Air Force Systems Command
Wright-Patterson Air Force Base, Ohio

Project 4156, Task No. 415605

(Prepared under Contract No. AF 33(657)-8040
by: Department of Electrical Engineering
University of Minnesota, Minneapolis 14, Minnesota
Edited by: W. T. Peria)

402 076

ASTIA
APR 24 1963
TISIA

NOTICES

When Government drawings, specifications, or other data are used for any purpose other than in connection with a definitely related Government procurement operation, the United States Government thereby incurs no responsibility nor any obligation whatsoever; and the fact that the Government may have formulated, furnished, or in any way supplied the said drawings, specifications, or other data, is not to be regarded by implication or otherwise as in any manner licensing the holder or any other person or corporation, or conveying any rights or permission to manufacture, use, or sell any patented invention that may in any way be related thereto.

Qualified requesters may obtain copies of this report from the Armed Services Technical Information Agency, (ASTIA), Arlington Hall Station, Arlington 12, Virginia.

This report has been released to the Office of Technical Services, U. S. Department of Commerce, Washington 25, D. C., in stock quantities for sale to the general public.

Copies of this report should not be returned to the Aeronautical Systems Division unless return is required by security considerations, contractual obligations, or notice on a specific document.

ASD-TDR-63-175

FOREWORD

This report summarizes work carried out in the Physical Electronics Research Laboratory of the University of Minnesota during the period from January 16, 1962 to October 15, 1962, under Contract No. AF 33(657)-8040. The technical work was directed by Mr. B. E. Rambo (Electronics Technology Laboratory, ASD) as project engineer. This is the final report on the contract.

The individual sections were written by members of the research staff whose names appear in the Table of Contents under the pertinent section heading and who carried out the work described therein. The report was assembled and edited by W. T. Peria, Associate Professor of Electrical Engineering.

ABSTRACT

Results are presented which show that it is necessary to sputter-clean titanium crystals in the study of the variation of secondary emission with the angle of incidence of the primary beam. The nature and cause of the errors introduced when titanium is not sputter-cleaned are described. The asymmetrical structure observed in the angular dependence studies is attributed to misalignment of the crystals and some experimental results are given as evidence. The energy dependence of the magnitude of the structure in the angular dependence curves for tungsten is examined and found to be basically the same as for titanium and germanium. It is also demonstrated that sputter-cleaning is not necessary for angular dependence studies in the case of tungsten.

The techniques for production of unbacked gold films are outlined. Preliminary results of studies of the energy distribution of electrons transmitted through one of these films are reported.

Further results of studies of MgO films formed by the oxidation of a Mg film on a metal substrate are presented and analyzed. The concentrated study of two particular MgO films formed on Mo and W substrates has led to a quite detailed picture of the trapping centers that can occur in MgO films. Preliminary results for a second set of films are also reported.

A method involving use of the destructive interference of reflected light from anodized tantalum has been devised for the determination of the ion current density as a function of position, on the target face, during the sputter-cleaning operation. An optical arrangement for measuring the amount of sputtering as a function of position on a Ta₂O₅-Ta target has been built and preliminary measurements indicate the feasibility of the measuring technique.

The difficulties encountered in the study of the dissociation of NaCl thin films by low energy electron bombardment are described. The migration of Na⁺ ions to the film surface is believed to be the cause of the difficulties. Results of dissociating MgO thin films are presented and the problem of adsorbed gas on the target surface is discussed.

Slow electron diffraction from the (001) surface of a MgO crystal reveals two different types of surface structure. One is a fc structure with the MgO lattice constant. The other has a double spacing in those azimuths for which the sum of the indices is even. The effects of heating and sputtering on the pattern from the fc structure are described. The effect of these treatments on the secondary electron emission is also described. A qualitative explanation of the "extra" intensity maxima in slow electron diffraction patterns is presented.


A new model is proposed to explain the major peaks observed in the curves of the variation of secondary emission from single crystals as a function of the angle of incidence of the primary beam. Qualitative explanations of the manner in which the magnitude and width of these peaks vary with primary energy are given in terms of the model. The reason for the differences in the characteristics of the peaks for metals and insulators is also suggested by the model. The small peaks which occur between and superimposed upon major peaks can also be explained if the new model is combined with parts of a model previously proposed. The disagreements between this model and some of the standard assumptions in secondary emission theories are briefly discussed.

Using a previous calculation as a starting point, the influence of an internal electric field on the secondary emission from ionic crystals is computed. The results are in fair agreement with experiment for the case of MgO.

PUBLICATION REVIEW

The content of this report represents the scientific findings of an Air Force sponsored program. It does not direct any specific application thereof. The report is approved for publication to achieve an exchange and stimulation of ideas.

FOR THE COMMANDER:



A. H. Dicke
Chief, Thermionics Branch
Electronic Technology Laboratory

TABLE OF CONTENTS

	Page
1. Introduction and Summary	1
1.1 Interactions between Electrons and Solids	1
1.1.1 The Variation of the Secondary Yield from Single Crystals with the Angle of Incidence of the Primary Beam	1
1.1.2 Transmission of Electrons through Thin Gold Films	2
1.2 Experiments Intended to Improve the Understanding of Processes Occurring in Practical Dynodes	2
1.2.1 MgO Thin Film Studies	2
1.2.2 Secondary Emission Characteristics of Al ₂ O ₃ Thin Films	3
1.2.3 Dissociation of Compounds by Electron Bombardment	4
1.2.4 Diffraction of Slow Electrons by MgO	4
1.3 Theoretical Studies	5
1.3.1 Theoretical Model of the Mechanism Resulting in Structure in the Variation of Secondary Emission with Angle of Incidence of the Primary Beam	5
1.3.2 Effect of an Electric Field on the Escape of Secondary Electrons from Polar Crystals	6
2. Summary of Technical Progress	6
2.1 Interactions between Electrons and Solids	6
2.1.1 The Variation of the Secondary Yield from Single Crystals with the Angle of Incidence of the Primary Beam -- G. G. Goetz	6
2.1.2 Transmission of Electrons through Thin Gold Films -- K. F. Ramacher	17
2.2 Experiments Intended to Improve the Understanding of Processes Occurring in Practical Dynodes	18

TABLE OF CONTENTS (continued)

	Page
2.2.1 MgO Thin Film Studies -- H. J. Boll, F. Hornstra and M. P. Prins	18
2.2.2 Secondary Emission Characteristics of Al ₂ O ₃ Thin Films -- W. B. Shepherd	29
2.2.3 Dissociation of Compounds by Electron Bombardment -- J. W. Coburn	32
2.2.4 Diffraction of Slow Electrons by MgO -- D. C. Johnson	35
2.3 Theoretical Studies	41
2.3.1 Theoretical Model of the Mechanism Resulting in Structure in the Variation of Secondary Emission with the Angle of Incidence of the Primary Beam -- G. G. Goetz	41
2.3.2 Effect of an Electric Field on the Escape of Secondary Electrons from Polar Crystals -- W. S. Khokley and K. M. van Vliet	48
Appendix I	54
3. Conclusions	60
3.1 Interactions between Electrons and Solids	60
3.1.1 The Variation of the Secondary Yield from Single Crystals with the Angle of Incidence of the Primary Beam	60
3.1.2 Transmission of Electrons through Thin Gold Films	60
3.2 Experiments Intended to Improve the Understanding of Processes Occurring in Practical Dynodes	61
3.2.1 MgO Thin Film Studies	61
3.2.2 Secondary Emission Characteristics of Al ₂ O ₃ Thin Films	61
3.2.3 Dissociation of Compounds by Electron Bombardment	61
3.2.4 Diffraction of Slow Electrons by MgO	62

TABLE OF CONTENTS (continued)

	Page
3.3 Theoretical Studies	62
3.3.1 Theoretical Model of the Mechanism Resulting in Structure in the Variation of Secondary Emission with Angle of Incidence of the Primary Beam	62
3.3.2 Effect of an Electric Field on the Escape of Secondary Electrons from Polar Crystals	62
4. Recommendations	63
Bibliography	66

LIST OF ILLUSTRATIONS

Figure

- 1 δ of a Titanium Crystal vs. Angle of Incidence before and after Sputtering and Annealing
- 2 δ of a Sputtered Titanium Crystal vs. Angle of Incidence before and after Annealing
- 3 δ of a Sputtered Titanium Crystal vs. Angle of Incidence for Two Annealing Temperatures
- 4 δ of an Outgassed Tungsten Crystal vs. Angle of Incidence before and after Sputtering, and after Sputtering and Annealing
- 5 Possible Misalignments of the Plane of the Primary Beam with Respect to a Crystal Plane
- 6 δ of an Electropolished Tungsten Crystal vs. Angle of Incidence for Two Different Orientations
- 7 Correspondence between the Curves of δ vs. Angle of Incidence for Equal and Opposite Alignment Errors
- 8 Transmission and Reflection Yield of an Unbacked Gold Film
- 9 Retarding Potential Characteristics of Electrons Transmitted Through an Unbacked Gold Film
- 10 Energy Distribution of Electrons Transmitted Through an Unbacked Gold Film
- 11 High Energy Peak in Energy Distribution of Electrons Transmitted Through an Unbacked Gold Film
- 12 The Dependence of Secondary Yield on the Surface Potential of a MgO Film (Film #1)
- 13 The Dependence of Secondary Yield on the Surface Potential of Film No. 2

LIST OF ILLUSTRATIONS (continued)

Figure		Page
14	Surface State Model	82
15	Photoemissive Yield of Film No. 1	83
16	Photoemissive Yield of Film No. 2	84
17a	Continuous Distribution of Surface States	85
17b	Discontinuous Distribution of Surface States	85
18	Surface-to-Bulk Photoelectric Yield	86
19	Contact Potential Changes with Film Thickness	87
20	Possible Potential Configurations near the Surface of the MgO Film (a) High Temperature Case and (b) Room Temperature Case	88
21	Variation in δ as a Function of Primary Electron Beam Displacement for Several Collector Voltages	89
22	The Dependence of the Na_{23}^{+} Ion Current on the Bombarding Current for an Unbombarded NaCl Film	90
23	The Dependence of the Cl_{35}^{+} Ion Current on the Bombarding Current for an Unbombarded NaCl Film	91
24	The Dependence of the O_{16}^{+} Ion Current on the Bombarding Current for an MgO Film	92
25	The Dependence of the Mg_{24}^{+} Ion Current on the Bombarding Current for an MgO Film	93
26	The Dependence of the O_{16}^{+} Ion Current on the Bombarding Electron Energy for a MgO Film	94
27	The Transient Behavior of the Mg_{24}^{+} Ion Current	95

LIST OF ILLUSTRATIONS (continued)

Figure		Page
28	The Dependence of the Overshoot of the Mg_{24}^+ Ion Current on the Time without Bombardment	96
29	Electron Diffraction Chamber	97
30	Circuit for Sputtering MgO	97
31	Electron Diffraction Pattern from (001) MgO	98
32	Three Dimensional fcc Unit Cell	98
33	Two Dimensional fcc Unit Cell	98
34	Electron Diffraction Pattern from (001) MgO Showing Half Order Beams	99
35	Surface Structure Half Order Beams	99
36	Electron Diffraction from (001) MgO [110] Azimuth	100
37	Electron Diffraction from (001) MgO [100] Azimuth	101
38	Electron Diffraction from (001) MgO [310] Azimuth	102
39	Secondary Electron Yield from MgO	103
40	Half Width of the Normal Incidence Peak for Titanium vs. Primary Energy	104
41	Distribution Function Ψ_1 Against Distance $x - x_0$ from a Plane Source at x_0 for $a = 0.1$, $n = 2$, $\alpha = 1$	105
42	Variation of δ_0 with Electric Field for a Plane Source Situated at Range d	106
43	Effect of Electron Affinity on Secondary Emission without Field for Uniform Source for Various Primary Energies Assuming Range $d = 300$ (ϵ_p)1.35	107
44	Effect of an Electric Field on Secondary Emission Coefficient δ_1 for Uniform Source for Various Primary Energies	108

LIST OF ILLUSTRATIONS (continued)

Figure		Page
45	Experimental Results Obtained by H. J. Boll for Small Values of the Electric Field	109
46	Slope of δ_1/δ_0 vs. Electric Field Curves against Primary Energy for Various Values of Electron Affinity	110

LIST OF TABLES

<u>Table</u>		Page
I	Parameter Deduced from the Thermal Decay of the Surface Potential	20
II	Comparison of Measured and Calculated Changes in the Photoelectric Threshold	22
III	Change in Surface Potential as a Result of Irradiation at Various Quantum Energies	23
IV	Summary of Threshold Values for the 1300 Å Film	25
V	Contact Potential Difference between Tungsten and MgO Films	26

1. INTRODUCTION AND SUMMARY

1.1 Interactions between Electrons and Solids

1.1.1 The Variation of the Secondary Yield from Single Crystals with the Angle of Incidence of the Primary Beam

Because of its importance to the theory of the production of secondary electrons, the variation of the secondary emission coefficient with the angle of incidence of the primary beam (SEAI) has been studied in these laboratories for the past several years. The yield is found to pass through many maxima and minima as the angle is varied. This "structure" is superimposed on a "background" which increases monotonically with increasing angle of incidence. Early interpretations of the SEAI structure placed the main emphasis on the crystalline structure of the material under study, but later more detailed investigations showed that other factor(s) also were important. The experiments carried out during the present contract period were aimed at an evaluation of the role of surface cleanliness in the cases of Ti and W. The experimental tube was modified so that the surface under investigation could be bombarded with argon ions in order to remove any desired amount of material.

Ion bombardment of a clean, previously annealed titanium crystal resulted in SEAI curves with no minor peaks but those corresponding to alignment of the electron beam with the major zone axes of the crystal were still observable (Fig. 2). Annealing the crystal at about 500°C restored the minor peaks and increased the magnitude of the major peaks. The combined effects of sputtering and annealing introduced peaks not previously observed (Fig. 1). Annealing at a higher temperature (750°C), however, reduced the magnitude of all peaks (Fig. 3). These results are all consistent with the postulate that the crystal getters residual gases during the high temperature anneal and that the diffusion of these contaminants into a thin region near the surface causes a modification of the SEAI curves. In this view, the SEAI structure observed after sputtering and annealing at 500°C corresponds to the clean Ti crystal.

In the case of tungsten, neither sputtering nor annealing was found to have an appreciable influence on the SEAI curves (Fig. 4). Previous studies of tungsten (ref. 7, p. 22) showed that the SEAI curves were not symmetrical about normal incidence. Data have now been obtained which show that the asymmetry is obtained even when polishing damage is removed by extensive sputtering and also when the crystal surface is prepared by electropolishing (curve A,

Manuscript released by the author 23 January 1963 for publication as an ASD Technical Documentary Report.

Fig. 6). Studies of the tungsten crystal in a tube in which the angle of incidence could be varied in two mutually perpendicular directions showed that the asymmetry was in fact a consequence of misalignment of the surface with respect to the primary electron beam (curve B, Fig. 6). The alignment was found to be quite critical, errors of $\pm 1/2$ degree causing an observable asymmetry. The sensitivity to misalignment is however dependent on the lack of coincidence of a low-index crystallographic plane with the surface under examination. All results previously obtained can now be understood in terms of coincidence and misalignment errors.

1.1.2 Transmission of Electrons through Thin Gold Films

It is obvious that a better understanding of the secondary emission process could be obtained if, in addition to measuring the number and angular and energy distributions of the reflected secondaries, the same quantities were to be measured for primary electrons which have lost a fraction of their energy. This can be done if the amount of material available for interaction with primary electrons is limited, i.e., if an unbacked film is used as the target. Furthermore, the study of the transmitted electrons has practical implications because of the uses, and potential uses, of electron-transparent films in various types of devices. Consequently, a study of unbacked MgO films was instituted during a previous contract period and the results have been reported (ref. 7, p. 23).

During this period a study of gold films was instituted. Gold was chosen, not because of any belief in its practical importance but rather because highly-oriented (or single-crystal) films, free from pinholes and charging effects, are desired. It seems to be possible to make gold films satisfying these conditions; other materials may be used at a later date.

Two unbacked gold films were successfully mounted in the experimental tube and one of them was studied. The reflection and transmission yield were measured (Fig. 8) and the transmitted electrons were energy-analyzed (Figs. 9, 10, and 11). Interpretation of the data is presently in progress.

1.2 Experiments Intended to Improve the Understanding of Processes Occurring in Practical Dynodes

1.2.1 MgO Thin Film Studies

In a previous report (ref. 7, p. 5) a new tube and some new techniques were described; it was there pointed out that the improved characterization of MgO films now possible should lead to an improved understanding of their complex behavior when used as secondary emitters. During this period more data have been obtained and a more detailed analysis of all the data has been carried out.

Measurements of the secondary emission coefficient as a function of surface potential show that δ is not a single-valued function of V_s (Fig. 12). Particularly interesting are the two

branches obtained for positive surface potential. The uppermost branch shows little dependence of δ on V_s and suggests that the electric field in the region penetrated by the primaries is small (especially for low primary energy). This would be so if the positive charge were distributed throughout the bulk. When slow electrons are added to the positive surface a much steeper curve (e.g., B in Fig. 12) is obtained. This suggests that the negative charge resides on the surface, providing a retarding field just inside the surface in spite of the fact that the net charge on the film is positive. The postulate that electrons tend to be trapped on the surface (Fig. 14) was previously found to be consistent with the manner in which the surface potential decays with time (ref. 7, p. 43, Eq. (19)). The manner in which the photoelectric yield curves shift with negative charging (Fig. 15) is also consistent with this postulate.

The discharge of negatively charged films by optical irradiation has been studied as a function of quantum energy. The results (Fig. 18) are interpreted to give the energy difference between the uppermost filled state and the bottom of the conduction band. It is pointed out however that the energy difference measured in this way is not the same as that measured thermally and the difference is accounted for in terms of polarization of the MgO lattice by the electron.

A series of films varying in thickness from 10 Å to 120 Å was prepared and the contact potential difference between each film and clean tungsten was measured (Table V). Very little change was observed over the thickness range 15 to 120 Å; this result implies that the electric field in the film, in thermal equilibrium, is essentially zero at distances from the substrate in excess of 15 Å.

A second set of MgO films was prepared and their evaluation begun. The most obvious difference between the properties of this group and those of the previous group lies in the intense cathodoluminescence now observed. Furthermore the present films charge in a nonuniform fashion and exhibit "patch" fields.

A brief investigation of the uniformity of the yield of alloy-based MgO films was also carried out. Although the data are rather meager, it appears that suitably prepared alloy-based films may be more uniform than those prepared by oxidizing an evaporated Mg layer (Fig. 21).

1.2.2 Secondary Emission Characteristics of Al_2O_3 Thin Films

The previous report (ref. 7, p. 49) summarized the results of a study of the secondary emission of anodized aluminum. This study included an examination of the effect of ion-bombardment cleaning on the yield. In the course of the experiment it became obvious that the particular arrangement used led to a

nonuniform reduction in the film thickness. Since many of the experiments presently underway utilize a similar arrangement and depend on the assumption of uniform sputtering rate, a method for the determination of the sputtering current distribution was developed.

In this method, anodized tantalum targets are sputtered under known conditions and after removal from the vacuum system the reflectivity of the Ta₂O₅ film is measured as a function of wavelength at various positions on the film. From the wavelength of the reflectivity minimum the film thickness can be calculated with sufficient accuracy for the present purpose.

1.2.3 Dissociation of Compounds by Electron Bombardment

The lack of reproducibility of the results obtained in the study of the dissociation of NaCl (ref. 7, p. 63) is believed to be due to electrolysis of the film. For this reason the basic study of the dissociation process is better done using a material with negligible ionic conductivity. Attention was therefore shifted to MgO which had been studied previously in this laboratory (ref. 20) using a different experimental technique.

The evolution of Mg⁺ and O⁺ from the target appear to be linearly related to the bombarding current (Figs. 24 and 25) and the O⁺ evolution shows the expected type of variation with electron energy (Fig. 26). At the present time however, it is not clear whether the true dissociation process is being observed. One possibility is that the observed evolution is the result of the bombardment-induced desorption of adsorbed species, continuously replenished from the residual gases in the tube. Experiments in which the transient ion current is observed when the electron beam is turned on after a quiescent period, suggest that only a small fraction of the ion current can be due to such processes.

1.2.4 Diffraction of Slow Electrons by MgO

The study of the diffraction of slow electrons by MgO has three purposes. One is the investigation of adsorption processes on a MgO surface. The others are the development of techniques for producing a clean MgO surface and for monitoring the condition of the surface while other measurements are in progress. Preliminary data were reported previously (ref. 7, p. 70); the most recent results are summarized below.

It was found that the use of an auxiliary "flood" gun allowed observation of the diffraction pattern for primary energies as low as 6 eV. Thus, more useful data can now be obtained.

The observed diffraction pattern from the (001) MgO face is that of a face-centered square lattice (Fig. 33) having the lattice parameter of MgO. It is not yet clear whether this pattern is associated with the crystal itself or with an ordered adsorbed layer.

A certain region of this surface shows additional "half-order" beams which could be the result of an arrangement of surface atoms as shown in Fig. 35. If these surface atoms are in fact foreign adsorbed atoms it can be said that they are rather firmly bound, since heating the crystal to 900°C for 34 hours had no effect on the half-order beams.

The intensity maxima, shown for 3 azimuths in Figs. 36, 37 and 38, do not occur at the positions of the Laue beams and furthermore there are more maxima than would be predicted by the three von Laue equations. This is characteristic of the slow electron diffraction from many materials and can be made plausible by a qualitative discussion of Bethe's dynamical theory.

The pattern of Fig. 31 was observed immediately after the crystal was placed in the tube and its geometry was not changed by any of the subsequent treatment. However, the intensity of the pattern was increased by heating the crystal at 900°C and a new intensity maximum occurred in the (11) beam. Exposure to air at atmospheric pressure removed this extra maximum but it reappeared upon further heating in vacuum. Argon-ion bombardment of the MgO surface diminished the intensity of the whole pattern and the extra maximum disappeared. Annealing at 900°C restored the main pattern but not the extra maximum.

The secondary electron yield was also measured after the treatments outlined above (Fig. 39). The most interesting effect is the reduction of the yield by ion bombardment and its partial recovery by annealing.

1.3 Theoretical Studies

1.3.1 Theoretical Model of the Mechanism Resulting in Structure in the Variation of Secondary Emission with Angle of Incidence of the Primary Beam

Up to the present time, only one theory has been proposed to explain the presence of structure in the curves of the variation of secondary emission from single crystals with the angle of incidence of the primary beam (SEAI) (refs. 9, 10). This theory was based upon a model which employed diffraction of the primary electrons. Attempts to obtain quantitative agreement between this theory and the experimental results were unsuccessful (refs. 4, p. 24 and 5, p. 34), and it was concluded that it is impossible for diffraction of the primary electrons to produce peaks of as

large a magnitude as are experimentally observed for the major peaks (see Sec. 2.1.1).

A new model is now presented and its qualitative consequences described. The basic postulate in the new model is that the high-energy primary is localized at the site of an inelastic collision and can be represented thereafter as a spherical wave strongly peaked in the direction of its initial momentum. If this initial momentum direction coincides with a major zone axis of the crystal, along which the lineal density of nuclei is high, and further, if the electron distribution is concentrated in the vicinity of the nucleus, then a peak will be observed in the yield simply because the primary energy is expended most efficiently in this way and the resulting secondaries are closer to the surface than they would otherwise be. The model explains in a qualitative way the observed dependence of the magnitude of the SEAI structure on the primary energy and also predicts differences between metals and insulators.

1.3.2 Effect of an Electric Field on the Escape of Secondary Electrons from Polar Crystals

The transport of internally created secondary electrons to the surface and their escape over the surface barrier are of course processes of very great interest in the study of secondary electron emission. Two aspects are of particular interest in view of the experimental program presently underway in this laboratory. The first is the manner in which the total secondary electron yield depends on the electron affinity of the surface and the second the influence of an internal electric field on the transport and escape of secondaries. During a previous contract period (ref. 7, p. 73) a solution to the first of these was given for the case of polar crystals. Treating the field as a perturbation to this solution, the effect of an internal electric field has now been determined.

The numerical results (summarized in Figs. 44 and 46) can only be obtained by assuming values for several parameters which are not very well known in the case of MgO. Nevertheless, fair agreement with the experiments (Sec. 2.2.1) was obtained (Figs. 42 and 45).

2. SUMMARY OF TECHNICAL PROGRESS

2.1 Interactions between Electrons and Solids

2.1.1 The Variation of the Secondary Yield from Single Crystals with the Angle of Incidence of the Primary Electron Beam

It has been known for several years that the variation of the secondary yield with the angle of incidence of the primary electron beam (SEAI) is not the same for single crystals as for

polycrystalline targets (refs. 9, 10, 11). Whereas the secondary yield of polycrystalline targets increases smoothly with increasing angle, θ , between the primary beam and the normal to the surface, the yield for crystals exhibits relative maxima and minima for a number of angles of incidence. This structure appears to be the result of peaks (and possible dips) superimposed upon the usual smooth curve for polycrystalline targets. The major peaks in this structure correspond to the alignment of the primary beam with major zone axes of the crystal. In addition, there are smaller peaks located between and superimposed upon the major peaks. Since this structure in the SEAI curves for single crystals appears to be the result of some basic influence of the crystal structure upon the secondary emission, the SEAI has been studied fairly extensively for a number of materials.

The SEAI from single crystals of three materials have been studied in this laboratory. They are titanium, germanium and tungsten. Most of the results for these materials have been previously reported (ref. 7, pp. 16-23). However, it was apparent from those measurements that some factor(s) in addition to the lattice structure of the crystals was influencing the results, particularly in the case of titanium. It is known from slow electron diffraction studies (ref. 12) that it is not possible to completely clean the surface of a titanium crystal by outgassing. Consequently it was desirable to determine whether the contaminants, remaining on or near the surface of a titanium crystal after outgassing, alter the SEAI results. It was also desirable to determine whether the asymmetrical SEAI curves obtained for tungsten and germanium were caused by some sort of disruption (impurities, dislocations, cracks, etc.) of the lattice structure on, or near, the surface of the crystal.

In order to examine the above questions, the experimental tube (ref. 3, p. 33) was modified to permit argon sputter-cleaning and annealing (ref. 7, p. 16) of the crystals being studied; otherwise the experimental tube was unchanged. As before, the crystals were mounted on a tungsten rod which could be rotated through 360 degrees. The secondary yield was also measured by the same method previously described (ref. 3, p. 31) which permits measurements of changes in the yield with only 0.1 percent error.

The titanium crystal, referred to as crystal No. 1 in previous reports, and a tungsten crystal were mounted in the modified experimental tube. The titanium crystal was mounted, as in previous studies, such that the primary beam lay in the (1100) plane of the crystal and was incident upon the (0001) face. The tungsten crystal was mounted such that the primary beam was incident upon the polished (100) face and lay in the (010) plane. However, because of inaccuracies in the determination of the crystal planes in the tungsten crystal, there were larger errors in its orientation than there were for the titanium crystal.

The SEAI curves of these crystals were examined after outgassing and after they were sputter-cleaned and annealed, in order to observe any effect of contaminants that are not removed by outgassing. The SEAI curves were also examined after the crystals were sputtered (before annealing) in order to determine the effect of the disruptions introduced in the crystal lattice by the ion bombardment. Finally, the influence of the temperature of the anneals given the crystals after they were sputtered was examined because this factor was found to be important in the case of the titanium crystal. The results for the two crystals will be considered separately because there are several features which are quite different in the two cases.

Titanium

The titanium crystal was outgassed in the same manner as in the previous studies of titanium. This consisted of heating the crystal to 760° for many hours until the pressure was less than 10^{-9} Torr with the crystal hot. This resulted in SEAI curves which were similar to those which had been previously obtained from this crystal. The subsequent sputtering and annealing produced marked changes in the SEAI curves. This is illustrated in Fig. 1 where the SEAI curves obtained before and after sputtering and annealing are shown for primary energies of 500 eV and 1000 eV.* The cleaning procedure resulted in a general increase in the magnitude of all the peaks. In addition, there are several small peaks near normal incidence that were not in evidence until the crystal was sputter-cleaned. Thus, it is clear that the contaminants remaining on or near the surface of outgassed titanium crystals have affected the SEAI results that have been previously obtained. The importance of this will be discussed after additional results have been considered.

The results of ion bombardment of a titanium crystal without an anneal are also of interest. In Fig. 2 the SEAI curves for primary energies of 500 eV, 1000 eV, and 2300 eV are shown both before and after a 500°C anneal which was subsequent to an ion bombardment. The peaks corresponding to the major zone axes in the crystal are quite pronounced even when the lattice disruptions produced by the ion bombardment have not been removed by an anneal. There is an increase in the magnitude of these peaks when the crystal is annealed but there is no major change in them. However, the small structure between, and superimposed upon, the major peaks is obviously much more adversely affected by the lattice disruptions produced by ion bombardment. This is most clearly seen with the curves for a primary energy of 2300 eV.

*The measured angle (θ) is about 5 degrees different from the true angle of incidence; the latter can be determined from the symmetry of the curves.

After the ion bombardment, there is little evidence of any structure superimposed upon the major peaks. (The peak at an angle of incidence of 17.3 degrees corresponds to a "second order" zone axis.) Following the anneal there are so many small peaks superimposed upon the major structure that it is not possible to locate the 17.3° peak. These results suggest that there is an important difference between the mechanism which produces the major peaks and that producing the small structure. The former is apparently not as sensitive to imperfections near the surface of the crystal as is the latter. This is consistent with the new model which has been proposed to explain the major peaks and with the modified explanation of the small peaks (Sec. 2.3.1). It is postulated that the major peaks are the result of a direct interaction between the primary electrons and the lattice electrons which is important over the entire depth from which secondaries can escape. The small peaks involve diffraction of the primaries within a small region (small compared to the escape depth of the secondaries) at the surface of the crystal followed by the direct interaction. A cooperative phenomenon such as diffraction would be expected to be more adversely affected by lattice imperfections than a direct interaction process, particularly since both the diffraction and the imperfections due to the ion bombardment are believed to be restricted to regions near the surface.

As indicated above, it was also observed that the annealing temperature was an important factor in the SEAI structure obtained after the titanium crystal was sputtered. This can be seen in Fig. 3 where the SEAI curves are shown for a primary energy of 1000 eV after a 500°C anneal (just glowing) and after a 750°C anneal. The 500°C anneal results in a structure that is larger in magnitude than that for a 750°C anneal. The same results are obtained after a 750°C anneal independent of whether any lower temperature anneal preceded it. However, the process is not reversible, i.e., if the crystal is given a 500°C anneal after a 750°C anneal the structure corresponding to the 750°C will still be obtained. After a 750°C anneal, the 500°C structure can be restored only by resputtering and then annealing at 500°C. This cycle of sputtering and annealing can be repeated many times with the same results.

The investigators studying the sputter-cleaning of the surface of titanium crystals (with slow electron diffraction) have also observed differences between the results of a 500°C anneal and a 750°C anneal (ref. 12). The diffraction pattern obtained after a 500°C anneal was characteristic of the titanium lattice whereas the 750°C anneal yielded a unidentified diffraction pattern. It was concluded that a contaminant in the bulk of the crystal was diffusing to the surface during the 750°C anneal. These results indicate that the large amplitude of the SEAI peaks after the 500°C anneal is characteristic of the titanium crystal and the decrease in their magnitude after the 750°C anneal is the result of the introduction of a contaminant. This contaminant must be restricted to a thin region near the surface because the

removal of the equivalent of about 7 atom layers by sputtering* will restore the amplitude of the peaks after a 500°C anneal.

If the crystal is annealed at 750°C for times much longer than necessary for the removal of the argon, the magnitude of the peaks is decreased even more than for a normal 750°C anneal. This indicates that an additional amount of contaminant is introduced into the region near the surface. However, it appears that the effect of the contaminant is self-limiting because a great deal of additional heating is necessary to produce small additional changes. Because the contaminated layer could be obtained even after the cycle of sputtering and heating the crystal at 750°C was repeated many times, it appears more likely that it is a reaction with a residual gas than the result of diffusion of impurities from the bulk.

The effect of annealing the titanium crystal at temperatures below 500°C was also examined. If the temperature was too low it was apparent that the crystal was not annealed. However, for higher temperatures (determined by power input) but still below glowing, a structure was obtained in the SEAI curves that was different from any of the results for higher temperature anneals. This structure was not stable (except in one instance) and after a period of electron bombardment it would change to the 500°C structure. Furthermore, each time the crystal was resputtered and annealed below 500°C the period of electron bombardment, required to bring about the change to the 500°C structure, became shorter. After several cycles of sputtering and annealing the structure changed after such a slight amount of electron bombardment it was no longer possible to obtain quantitative measurements before the change occurred. It has been suggested that this unstable structure could be related to the presence of hydrogen in the titanium crystal. Since titanium releases absorbed hydrogen at temperatures above about 400°C this is possible, but it is not clear how electron bombardment could have the observed effect.

Since a thin contaminated region near the surface of the crystal apparently can alter the SEAI structure it might be expected that adsorbed gases on the surface of the crystal could have an important effect. However, there was no evidence of changes in the structure as a result of gases adsorbing on the surface after the crystal was sputter-cleaned. Furthermore, intentional exposure of the crystal to residual gases at a pressure of 10^{-4} Torr did not significantly alter the structure even though enough gas was adsorbed to change the secondary yield about 3.5 percent for all angles of incidence. Therefore, it is

*There is some evidence that the sputtering may not be uniform because the bombarding ions are focussed toward the center of the crystal.

fairly certain that the structure in the SEAI curves is not influenced by a monolayer or less of adsorbed gases.

In view of all the above results it seems that the difference between the SEAI structure before and after the titanium was initially sputter-cleaned is the result of a contaminated region near the surface. This contaminated region is probably similar to the one which forms during a 750°C anneal, but thicker and with a larger concentration of the contaminant. Because a considerable amount of data has been obtained from titanium crystals that had not been sputter-cleaned, it would be desirable to determine just what effect this contaminated region had on the results. Such a determination might be attempted by taking SEAI measurements on a titanium crystal before and after the initial sputter cleaning for a wide range of primary energies. However, it is questionable whether the results would justify the effort because they probably would not directly apply to the previously obtained data. Factors such as the pressure and composition of the gases present when the crystal is outgassed, would be expected to influence the characteristics of the contaminated region and they could not be duplicated. Therefore, it is probably best to estimate the effect of the contaminated region on the basis of the available data.

An examination of the curves in Fig.1 reveals an important feature of the contaminated region. The presence of this region causes decreases in the magnitude of the peaks and eliminates a few of them, but there is no evidence that any peaks are produced that are not characteristic of the titanium crystal. This indicates that while the structure obtained in measurements on unsputtered titanium crystals may not include all the peaks characteristic of the crystal, there are no false peaks.* This fact is important because the explanations of the structure are based upon the assumption that the observed peaks are characteristic of the titanium crystal structure.

The only peaks that are eliminated by the contaminated region are some small peaks that do not correspond to any zone axis of the crystal. In most cases, the measurements on unsputtered crystals showed evidence of these small peaks only for primary energies above 1000 eV. Thus, it appears that the contaminated region eliminates the small peaks for primary energies below a certain value (nominally 1000 eV). This is also consistent with the idea that these small peaks are the result of diffraction of some of the primaries. Because the distance from the surface in which this diffraction occurs increases with primary energy, it might be expected that the small peaks would be observed only for primary energies sufficiently high to cause the diffraction region to extend beyond the contaminated region.

*This may not be true when a titanium crystal was not outgassed at 750°C.

The manner in which the magnitudes of the major peaks are decreased by the contaminated region is somewhat complicated. There are marked differences among the various peaks with the peaks corresponding to "second" and "third" order zone axes (17.3° and 22.6°) much more adversely affected than the others. This could account for the fact that little evidence of these peaks was obtained with most unsputtered titanium crystals except for high primary energies. The primary energy also appears to be important in determining the extent to which the contaminated region decreases the peaks. It would be expected that the effect would be less for high primary energies, but measurements before and after sputter-cleaning were not taken for sufficiently high primary energies to determine this.

Tungsten

The results for the tungsten crystal were quite different from those for titanium in several aspects. The SEAI curves for tungsten exhibited a structure that was quite asymmetrical. Except for what appeared to be normal incidence peak, there was little evidence of peaks corresponding to major zone axes. The general properties of the structure were much like that previously obtained for a germanium crystal (ref. 7, p. 21 and Fig. 21). The cause of this asymmetry was examined further and will be considered later.

The other respect in which the results for tungsten are different from those for titanium is in the effect of sputter-cleaning upon the SEAI structure. After the tungsten crystal was well outgassed, sputtering followed by an anneal caused virtually no change in the structure. Furthermore, even sputtering without annealing produced only a minor change in the structure. This can be seen in Fig. 4 where SEAI curves for tungsten are plotted for a primary energy of 1000 eV. Curves are shown for the three cases, before sputtering, after sputtering, and after sputtering and annealing.

Because the crystal was mechanically polished, it was possible that the resulting damaged region near the surface was not completely removed by the subsequent etch. Such a damaged region could cause the observed structure and mask any effect the sputter cleaning might have. Therefore, a considerable amount of material was sputtered from the crystal in an attempt to remove any such layer. However, after close to 3000 atom layers were removed by sputtering there was no evidence of any significant change in the structure and it was concluded that at least a major portion of the structure in the SEAI curves was characteristic of the crystal structure. This has been verified by subsequent work in which the crystal was electropolished.

The difference between the importance of sputter-cleaning for titanium and for tungsten may be a direct result of the difference in their gettering properties. Titanium is a good bulk

getter at high temperatures and therefore readily takes up gases into the bulk which could cause a contaminated layer near the surface. However, gettering by tungsten is largely a surface effect such as the formation and evaporation of an oxide. Therefore, under reasonable outgassing conditions a contaminated region would not be expected to form in a tungsten crystal. Since surface gases do not appear to be important in the SEAI structure, sputtering and annealing would not alter the structure.

The failure of ion bombardment without annealing to produce any major changes in the structure is perhaps more surprising than the unimportance of sputter-cleaning. It could be considered as evidence against the idea that the production of the small peaks involves diffraction of the primaries. However, it has been found by several investigators that the disruptions in a tungsten crystal which are caused by ion or neutron bombardment are at least partially annealed at room temperature (ref. 13 and 14). Therefore, the observed results are quite reasonable and consistent with the diffraction idea.

Some additional measurements were taken with the tungsten crystal to determine the behavior of the SEAI structure for low and high primary energies. The low energy range was examined in order to observe, if possible, the characteristics of the structure for primary energies so low that the escape probability is essentially the same for all the secondaries. However, at the lowest energy obtainable with the electron gun (about 40 eV) it was evident from the SEAI curve that there were significant differences in the escape probabilities of the secondaries. Since tungsten has a fairly high secondary yield for a metal, these results indicate that the condition of equal escape probabilities cannot be obtained for metals with the available equipment.

The high energy range was examined to determine whether for sufficiently high energies, the relative magnitude* of the SEAI structure decreases with increasing primary energies as predicted by the model (Sec. 2.3.1). This was determined by examining the normal incidence peak but the results were complicated by what appeared to be small peaks superimposed upon the basic peak. These small peaks were present for some primary energies and not for others. This resulted in a number of relative maxima in the variation of the magnitude of the normal incidence peak with the primary energy. However, there did not appear to be any basic difference between the energy dependence of the major peaks of tungsten and the other materials studied; and although it was necessary to examine comparatively high energies, a decrease in the relative magnitude with increasing primary energy was observed.

*The relative magnitude of a peak is the ratio of the increase in the secondary yield as a result of the peak to the value the secondary yield would be without the peak.

Asymmetrical Structure

On the basis of the model proposed to explain the structure in the SEAI curves (Sec. 2.3.1) it is not obvious how an asymmetrical structure could be obtained. Since an asymmetrical structure has been observed for all the materials examined, it is quite important that the model be consistent with such results. Therefore, an attempt was made to determine the cause of the asymmetrical structure in the SEAI curves for tungsten.

There appear to be three possible causes of the asymmetrical structure observed in the case of the tungsten crystal. Certain errors in the alignment of the crystal with respect to the primary beam could result in an asymmetrical structure. Also, lattice dislocations introduced during the mechanical polishing might be influencing the SEAI results and producing the asymmetry. Finally, an error in the cutting of the face of the crystal which results in a face that is not parallel to the (100) plane would introduce an asymmetry.

There are two ways in which the crystal can be misaligned. They are shown in Fig. 5. The first case can be seen by considering the intersection of both the (010) plane and the plane of the primary beam with the (001) plane of the crystal. When the lines of intersection form an angle α the crystal is misaligned. The second case is seen by considering the intersection of the (010) plane and the plane of the beam with the (100) plane of the crystal. When these lines of intersection form an angle β the crystal is also misaligned and the primary beam in general will not lie in the (010) plane unless α and β are zero.*

An examination of the location of the crystal atoms in or very near the plane of the primary beam for the different possible conditions leads to the following conclusions:

- a) If $\beta = 0$ the array of atoms will be symmetric about the intersection of the plane of the beam and the (001) plane independent of α .
- b) If $\alpha = 0$ the array of atoms will be symmetric about the intersection of the plane of the beam and the (001) plane independent of β .
- c) If α and β are nonzero the array of atoms will be symmetric about the intersection of the plane of the beam and the (001) plane only for certain special values of α and β .

On the basis of the model, a nonsymmetric array of atoms (except in some special cases) would result in an asymmetrical structure in the SEAI curves. Therefore, it might be expected that when

*In general α and β will be angles between the plane of the primary beam and the crystal plane in which the beam is to lie.

the crystal is misaligned such that both α and β are nonzero the SEAI structure would be asymmetrical. However, it is very difficult to predict how large α and β must be in order that asymmetry may be observed, or, whether asymmetries as pronounced as have been observed for tungsten and germanium would be expected.

To examine the importance of the alignment of the tungsten crystal on the asymmetry of the SEAI results, it was mounted in an experimental tube in which the orientation of the crystal could be varied in two mutually perpendicular directions (ref. 5, Fig. 14). With this tube it was possible to examine the SEAI curves for various values of the angle α which could be varied over a range of four degrees in steps of one degree and another four degrees in steps of two degrees. Unfortunately, the possible measurements are limited because β cannot be varied. However, it is still possible to test whether the observed asymmetrical structure could be the result of crystal misalignment. As indicated above by (b), if the asymmetry is caused by misalignment it should be possible to obtain a symmetrical structure by adjusting α alone.

As previously suggested, there are two other possible causes of the asymmetrical structure which, if important, could complicate the results of the above experiment. To insure removal of any remaining lattice disruptions produced by the mechanical polishing, more than 70 microns* of material were removed from the surface of the crystal by electropolishing. Nothing could be done to eliminate the effects of a possible error in the cutting of the face of the crystal.

Upon examination of the SEAI curves the structure was found to be quite dependent upon the value of α . This observation is consistent with previous results for titanium (ref. 7, p. 20). For one value of α the structure of the SEAI curves was very similar to that previously obtained for the crystal (curve A, Fig. 6). This suggests that the value of β was not changed greatly when the crystal was remounted and that the electropolishing produced little change. A change of three degrees in α resulted in a major change in the structure (curve B, Fig. 6). The structure appears to be symmetrical except for a shift in the position of the peaks with respect to the gross curve** of the secondary yield. This structure can be interpreted in the following manner:

*It has been observed in the case of germanium crystals that mechanical polishing can disrupt the crystal to depths of 70 microns from the surface (ref. 15).

**The gross curve is the curve which would be obtained if all the peaks in the SEAI curve were removed.

- a) The value of α for curve B is zero (or very nearly zero) and consequently the resulting SEAI structure is basically symmetrical.
- b) There was a cutting error which resulted in a lack of coincidence between the face of the crystal (which determines the gross curve) and the (100) plane of the crystal (which determines the location of the peaks).

The combined effect of (a) and (b) would cause a SEAI structure just like that of curve B and consequently, these results can be considered evidence that the asymmetrical structure was basically caused by misalignment of the crystal. Furthermore, the alignment of the crystal appears to be quite critical. The SEAI structure for $\alpha = -1$ degree was definitely asymmetrical for a primary energy of 1000 eV and the asymmetry was more pronounced for higher energies.

The experimental tube was modified to permit the examination of the SEAI curves for $\alpha = +1/2$ degree and the structure was still definitely asymmetrical. This can be seen in Fig. 7 where the SEAI curve is shown for $\alpha = +1/2$ degree at a primary energy of 4000 eV. However, SEAI curves for $\alpha = +1/2$ degrees yielded further evidence as to the cause of the asymmetry because they were almost mirror images. This is also shown in Fig. 7 where the positive-angle half of the SEAI curve for $\alpha = +1/2$ degree is shown with the negative-angle half for $\alpha = -1/2$ degree and vice versa. It can be shown that the array of atoms in the plane of the primary beam for $+\alpha$ is the mirror image of the array for $-\alpha$ (independent of β). Consequently, the above results are further evidence that asymmetrical SEAI structure is a direct result of the nonsymmetrical array of atoms in the plane of the beam when the crystal is misaligned such that both α and β are nonzero.

If the above explanation is correct, it should apply to all the materials studied. While the results for tungsten and germanium appear consistent with this explanation there may be some question in the case of titanium. Because the crystals were always visually aligned it is likely that there were alignment errors greater than $1/2$ degree. Yet, only in one case (ref. 7, p. 18, Figs. 13 and 14) was any significant asymmetrical structure observed and it was not nearly as pronounced as for tungsten and germanium. Furthermore, little evidence of asymmetry was found when α was varied for a titanium crystal (ref. 7, p. 20, Figs. 19 and 20) in the same manner as for the tungsten crystal.

There are two possible reasons for these differences. The first has simply to do with the differences in the crystal structure of the materials. While both tungsten and germanium have cubic crystal structures, titanium has a hexagonal structure. Consequently, the array of atoms in the plane of the primary beam may in general be less asymmetric for titanium than for tungsten

and germanium when α and β are nonzero. It would be very difficult to determine quantitatively whether this is the case. However, the fact that the cubic crystals have only a four-fold symmetry about a normal to the face whereas the hexagonal structure has a six-fold symmetry may be an indication in this direction.

A second possible reason for the differences in the SEAI structure arises from the differences in the errors in the orientations of the crystals. The titanium crystals grow with major crystal planes for the boundaries of the crystal. Consequently, it is possible to determine the orientation of the crystals visually and visual alignment of the crystals can be quite accurate. It is possible to mount the titanium crystals with a β alignment error of about 1 degree. The situation for tungsten is quite different. The orientation of the crystal was determined by the supplier, using X-ray diffraction, and the crystal was marked. However, this marking was rather crude and the orientation of the crystal could be determined only within about 5 degrees by these marks. Furthermore, it is much more difficult to align the crystal by these marks during mounting. As a result the β alignment error for the tungsten crystal may be 7 to 8 degrees. In the case of germanium the orientation of the crystal perpendicular to the face was not known so it is quite likely that β was large. Consequently the large difference between titanium and the other two materials in the effect of α alignment errors could be mainly a result of a large difference in β .

2.1.2 Transmission of Electrons through Thin Gold Films

The unbacked gold films were produced by vacuum deposition of gold on (100) surfaces of heated sodium chloride crystal blanks (ref. 16). The gold was mounted on a molybdenum filament. The films were removed from the sodium chloride crystal blanks by slowly dipping into deionized water. As the substrate dissolved, the gold film floated to the surface of the water. The films were mounted on a nickel "target ring" by bringing the target ring up obliquely from below the film. Two of the films were placed in a vacuum tube so that their secondary electron emission properties could be studied.

The vacuum tube used to study the secondary electron emission of the unbacked gold films is that previously used in the study of unbacked MgO films (ref. 5, p. 1). This tube was designed to measure the transmission yield, the reflection yield, and the energy distributions of the reflected and transmitted electrons. Measurement of the above properties of unbacked gold films was less difficult than similar measurements on unbacked MgO films because it was not necessary to use pulse techniques in the case of gold. Standard secondary electron emission measurement techniques (ref. 7, p. 10) were used throughout the study.

The reflection and transmission yield of one unbacked gold film are plotted vs. primary electron energy in Fig. 8. The reflection yield shows a maximum of 1.616 at 800 eV primary electron energy. The transmission yield measurements show that the film was quite opaque to electrons with primary energy less than 4000 eV. The thickness of the film, estimated to be somewhat less than 1000 Å, will be measured after removal from the tube. The transmission yield increased, with primary electron energy above 4000 eV, to 0.712 at 13,500 eV, the maximum primary energy used. The transmission yield of the film is plotted vs. retarding potential in Fig. 9 for a primary electron energy of 5000 eV. The transmission yield decreased rapidly as the retarding potential was increased from 0 to 100 volts. At this point, the curve broke sharply and the transmission yield decreased much more slowly. Then, when the retarding potential was increased from 4500 to 4600 volts the transmission yield cut off to zero. That portion of the curve between the break at 100 volts and the cut-off at 4600 volts shows strong evidence of structure. The measurement method used is, however, not adequate to resolve this structure with any certainty. The transmission yield vs. retarding potential data was numerically differentiated to give the energy distribution of the electrons transmitted through the film. This energy distribution of transmitted electrons is shown in Fig. 10. Again, there are indications of considerable structure in the energy distribution of the transmitted electrons. Of considerable interest is the peak in the energy distribution curve corresponding to the cutoff in the transmission yield vs. retarding potential curve (Fig. 9). This shows that a large number of electrons is transmitted through the film with a loss in energy of 400 to 500 eV. Transmission yield vs. retarding potential curves were made for primary electron energies from 3500 to 5500 eV. This data was numerically differentiated in the region of cutoff so that the peak in the energy distributions of the transmitted electrons could be studied as a function of primary electron energy. The results are shown in Fig. 11. It is evident that the peaks change in width and height as the primary energy is changed. Also, it is noticed that all peaks are not displaced by the same amount.

These are preliminary results, and experiments are in progress which will determine the width and height of the peaks as well as their position, with greater accuracy.

2.2 Experiments Intended to Improve the Understanding of Processes Occurring in Practical Dynodes

2.2.1 MgO Thin Film Studies

In this series of experiments, a concentrated effort was directed toward the study of two particular MgO films. After the study of these films was essentially complete, the experimental tube was accidentally opened; subsequent work was therefore carried out on a new set of films. The first part of this section

summarizes the detailed results obtained for the first set of films, while the preliminary results for the second set are given towards the end of the section.

The results of previous studies of the dependence of the secondary yield on the surface potential of the films (ref. 7, p. 47) have strongly supported the hypothesis that when slow electrons were deposited onto the films, they became trapped within 100 Å or less from the surface, whereas, when the films were bombarded with high energy electrons, the holes that were generated became trapped throughout the bulk. The arguments which led to this conclusion have been given previously, but are repeated here for the sake of completeness.

The manner in which the secondary yield varied with the surface potential of the two films is shown in Figs. 12 and 13. These results were obtained in the following way. The secondary yield of the thermally discharged film was first measured. The film was then charged 2 V negative by depositing slow electrons onto its surface after which the secondary yield was again measured. This step-by-step procedure was followed until the spontaneous decrease in the surface potential became so rapid that it was no longer possible to take accurate measurements. The data obtained in this way correspond to curve A in Fig. 12.

Next, the film was again thermally discharged and allowed to cool, after which it was charged positively by bombarding it with electrons of 70 eV energy. After the film had become charged to its most positive value, the secondary yield was measured. The step-by-step procedure of adding slow electrons to the film and measuring the yield was then followed. These data correspond to curve B of Fig. 12.

The film was next charged positively again, but instead of adding slow electrons, the film was heated in a step-by-step procedure until thermal equilibrium was reached. Between heatings, the film was allowed to cool, after which the yield and the surface potential were measured. The data obtained in this way correspond to curve C in Fig. 12.

When the film was charged negatively and then discharged thermally in the step-by-step manner described above, the secondary yield followed curve A.

The results described above seem to be consistent with the postulate that the MgO film contains on its surface a high density of electron trapping sites and a much lower density of hole trapping sites. This is evident from the curves of Fig. 12 where, at a primary energy of 300 eV (in which case the primaries do not penetrate very deeply into the MgO), the secondary yield decreases rapidly as electrons are added to the surface. If the electrons were trapped only in the bulk, the strength of the

electric field would be zero at the surface. Hence, at low primary energy the change of yield with negative surface potential should be quite small. When the film is charged positively, on the other hand, the yield is increased only slightly, which by the same arguments used above, indicates that trapping is predominantly in the bulk. Since the electric field near the surface of the positively charged film is small, when electrons are deposited onto the surface of the film, this field is easily overcome by a small negative surface charge. Hence, when electrons are added to the surface of the film, the field near the surface reverses direction, retarding the escape of internal secondaries. As a result, the secondary yield represented by curve B decreases rapidly with decreasing surface potential, and remains below that of curves A and C.

Naturally, the slopes of curves A and C became more nearly alike at higher primary energies because the primaries penetrate deeper into the MgO, where the field is no longer small in the positively charged case. Furthermore, it is to be noted that in the case of the thinner of the two films (Fig. 13) the effects of surface and bulk trapping do not differ so greatly because the penetration depth of the primaries is a larger fraction of the film thickness.

Relaxation of the Surface Potential with Time

Studies of the spontaneous decrease in the surface potential with time were conducted to determine the energy distribution of the trapping centers. These studies, the results of which were reported previously, showed that the surface potential of the negatively charged films decreased logarithmically with time. These results are believed to be best interpreted in terms of the model shown schematically in Fig. 14. It is assumed that the current through the film is carried by electrons that are thermally excited out of surface states which are uniformly distributed with respect to energy with a density Z . These surface states, which are empty in thermal equilibrium, are assumed to extend from an energy E_0 up to the conduction band edge, E_c .

By comparing the mathematical expressions derived from this model with the experimental results (ref. 7, p. 42), the parameter values given in Table I were obtained.

Table I
PARAMETERS DEDUCED FROM THE
THERMAL DECAY OF THE SURFACE POTENTIAL

Estimated Film Thickness	$E_c - E_0$	Z
1300 Å	1.3 eV	$2 \times 10^{13}/\text{cm}^2\text{eV}$
700 Å	.52	3.7×10^{13}

In the surface state model, when electrons are deposited on the surface of the film they occupy the lowest energy levels, and as more electrons are added, higher energy states become filled. The energy E to which the states are filled is given by the equation, (ref. 7, p. 42)

$$E = E_0 + \frac{V_s \epsilon}{eZD} ,$$

where V_s is the surface potential of the film, ϵ is the dielectric constant, and D is the thickness of the film. The results of the photoemission experiments described below have been used to check this relationship.

Photoemission Experiments

The apparatus and techniques used in this phase of the work have been described previously (ref. 8, p. 28). The photoelectric yields of the two films discussed above are plotted in Figs. 15 and 16 as a function of the incident photon energy. The results, obtained for various values of surface potential show that the photoelectric threshold decreased whenever the films were charged, whether positively or negatively. The discrepancy between the two yield curves (Fig. 15) that were obtained with the tungsten lamp and the hydrogen arc, is believed to be the result of an error in the calibration of the monochromator output.

In the mathematical treatment of the surface state model (ref. 7, p. 42) it was shown that the energy E to which the surface states are filled is related to the surface potential V_s by the equation

$$E = E_0 + \frac{V_s \epsilon}{eZD} ,$$

where ϵ is the dielectric constant, and D is the film thickness. With reference to Fig. 17, if the energy state E_0 is filled in thermal equilibrium, and if the electrons in the surface states can be excited photoelectrically, then the photoemissive threshold is expected to decrease by an amount $V_s \epsilon / eZD$ compared with the threshold in the uncharged state, when the film is charged V_s volts negative. If the surface states do not extend down to the Fermi energy E_F , then E_0 will be empty in thermal equilibrium. When electrons are deposited onto the surface of the film, the level E_0 becomes filled, and in this case (Fig. 17b), the photoelectric threshold should decrease discontinuously by the energy difference between E_0 and the energy of the highest filled state in thermal equilibrium, E_m . Thereafter, the addition of more electrons should lead to a further decrease in threshold of $V_s \epsilon / eZD$.

Unfortunately, because the shape of the photoemissive yield curves are not all the same, those curves (the 16V negative case in Fig. 15 and the 6V case in Fig. 16) whose shapes deviate considerably from the others cannot be used in this analysis. The origin of the change in the shape of the curves is not known. However, the difference in the photoemissive threshold between the similarly shaped curves (A and B in Fig. 15 and Fig. 16) have been compared with the expected change (V_{SE}/eZD), that is obtained from the results. This comparison is given in Table II.

Table II

COMPARISON OF MEASURED AND CALCULATED
CHANGES IN THE PHOTOELECTRIC THRESHOLD

	Measured Threshold Change	Calculated Threshold Change
1300 Å film	0.22 eV	0.18 eV
700 Å film	0.15 eV	0.10 eV

It is noted that although the correlation is not exact, the results are in sufficiently close agreement that they strongly support the surface state model of electron trapping.

The large change in threshold (Fig. 16) observed when the 700 Å film was charged from 0 to 1 V negative is believed to reflect the previously discussed discontinuous reduction in threshold which results from a gap $E_0 - E_m$ (Fig. 17b) in the surface state distribution. An estimate of $E_0 - E_m$ in this case may be obtained as follows: Since the surface states are filled to an energy V_{SE}/eZD above E_0 , the total change in threshold is given by

$$\Delta E_T = E_0 - E_m - \frac{e}{eZD}$$

when the film is charged 1 V negative. Hence, since ΔE_T from Fig. 16 is approximately 0.2 eV, and e/eZD calculated from the results of Table I is -0.02 eV, $E_0 - E_m$ is approximately 0.18 eV.

Photoconduction Experiments

Measurements of the photoconduction current have also supported the surface state model of electron trapping. However, these measurements were very difficult to make because it was not possible to make electrical contact to the surface of the MgO film except by means of the electron stream from the gun. The

method used consisted of the measurement of the surface potential of a charged film, before and after a 2 hour irradiation with light of the desired quantum energy. The ratio of the rate of decrease of the surface potential to the intensity of the incident light was then considered to be a measure of the photoconductive current in the film. However, a simple analysis is valid only when it is assumed that the internal electric field E is assumed to be constant throughout the film. Fortunately, in the case of the negatively charged films, the assumption that the electric field strength is uniform throughout the film is supported by the results of the previously described studies of the dependence of secondary yield on the surface potential.

The change in the surface potential of the 1300 Å film as a result of a 2 hr. irradiation with light is given in the following table for two different values of surface potential.

Table III

CHANGE IN SURFACE POTENTIAL
AS A RESULT OF IRRADIATION AT VARIOUS QUANTUM ENERGIES

Quantum Energy (eV)	$V_s = -7$ V	$V_s = -14$ V
2.4		.04 .03 .00
2.5		.12 .10 .04
2.6		.08
2.7		.04
2.8	.01	.07
2.9	.04	
3.0	.09	.08
3.1		
3.2	.09	.13
3.3		
3.4		.14
3.5	.065	
3.6		.12
3.7	.036	
3.8		.12
3.9		
4.0	.02	.04

The values in Table III have not been corrected for changes in the monochromator output as a function of quantum energy. In the -14V case, a number of measurements were made at 2.4 eV and 2.5 eV to obtain a more accurate value for the threshold energy. Unfortunately, the spontaneous decrease in surface potential was so rapid that the threshold changed significantly between measurements. It is emphasized that because the surface potential decreased so little during the irradiation, and because it was necessary to make allowance for the decrease in surface potential resulting from the thermal decay of trapped charge, these measurements are considered to be very crude. Hence, the only result of significance here is the position of the photoconductive threshold, and this could be in error by 0.1 eV.

Since the photoconductive threshold decreased as the film was charged negatively just as the photoemissive threshold did, it is natural to assume that the photoconduction also involves the excitation of electrons residing in surface states. If it is assumed that the electrons excited out of these states go to the substrate without becoming retrapped, then a photoconductive yield may be defined as the number of photoelectrons reaching the substrate per incident photon. This photoconductive yield has been plotted in Fig. 18 as a function of the photon energy. The change in threshold is approximately 0.3 eV, while the value obtained from the relation $\Delta E_T = \Delta V_{sc}/eZD$ yields only 0.14 eV. Although the agreement here is not very good, the difference may be ascribed to inaccuracies in the measurements.

It is recalled at this point that the optical and thermal energies required to excite an electron in an ionic crystal may differ considerably. Hence, the above comparison between optical and thermionic data is open to question. However, the following discussion of this problem shows that a comparison between changes in photoelectric and thermionic activation energies are probably valid but that a comparison between their magnitudes is not.

The Correlation of Thermionic and Photoelectric Data

The difference between optical and thermionic activation energies arises from the Frank-Condon principle which states that when an electron is excited optically the nuclei of the surrounding ions remain at rest during the process. After the excitation, the ions move to new equilibrium positions, and in the process an energy P is lost to the lattice in the form of vibrational motion. Estimates of the magnitude of P involve the calculation of the energy of polarization before and after the removal of the electron. On the other hand, when the electron is excited thermally, the process occurs slowly enough that the ions are essentially in their equilibrium positions throughout the process, and no energy is lost to the lattice. Since the end state is the same, namely, the electron has been moved a large distance from its trapping center, the photoelectric activation

energy, E_p , is greater than the thermionic activation energy, E_t , by an amount P .

The above generally accepted analysis does not take into account the energy of polarization of the lattice by the released electron. If it is assumed that the polarization energy associated with the free electron is equal to that of the trapped electron, then the photoelectric and thermionic activation energies differ by $2P$, because an additional energy P is lost as the result of the buildup of polarization around the free electron.

If the trapping site resides on the surface, the polarization energy will be approximately $1/2 P$. Therefore if the electron is excited into the bulk, an energy $3P/2$ is lost to the lattice, whereas if it is emitted from the surface into the vacuum, only $1/2 P$ is lost. Hence, if the electrons involved are trapped on the surface, E_{pC} , the photon energy required to excite an electron into the conduction band, should be $3P/2$ greater than E_{tC} , the thermionic energy required. Furthermore, if the photoemission from a thermally discharged film is assumed to involve electrons near the Fermi energy, as was indicated by the photoemission experiments, then the photoemissive threshold should be $P/2$ greater than the thermionic threshold or work function.

This analysis is now applied to the thermionic and photoelectric results obtained with the 1300 Å film which are summarized in the table below.

Table IV

SUMMARY OF THRESHOLD VALUES FOR THE 1300 Å FILM

Thermionic Conductivity Threshold, E_{tC}	Photoconductive Threshold, E_{pC}	Work Function E_{tE}	Photoemissive Threshold, E_{pE}
1.3 eV	2.6 eV	2.6 eV	3.1 eV

Substituting the results of Table IV into the relation $E_{pC} = E_{tC} + 3P/2$ yields $P = 2/3(2.6 - 1.3) = 0.87$ eV. This value of P when substituted into the relation $E_{pE} = E_{tE} + 1/2 P$ yields the result that the photoelectric threshold should exceed the work function by 0.44 eV, while from Table IV, the measured value is approximately 0.5 eV. If the generally accepted analysis had been used, the energies lost to the lattice during photoconductive and photoemissive excitations would be equal, in which case, $E_{pC} - E_{tC} = E_{pE} - E_{tE}$, a relation that is definitely in disagreement with the experimental results.

Since the polarization energy associated with an electron on the surface of the film is expected to be the same, independent of the energy of the surface state in which it resides, the difference between optical and thermionic activation energies is the same, independent of the energy of the surface state. Hence, the magnitudes of the changes observed in the thermionic and photoelectric thresholds, as higher energy surface states become filled, should be the same. Thus, a comparison between changes in thermionic and photoelectric activation energies seems to be valid.

Contact Potential Measurements

Because the MgO films with a work function of approximately 2.6 eV are in contact with high work function substrates, the energy bands of the film are expected to be bent as shown in Fig. 19a. Here the usual model of a metal-semiconductor contact is assumed to be valid, where the barrier height is equal to the work function of the metal, less the electron affinity of the semiconductor. Hence, the work function of the film is expected to increase with decreasing film thickness as shown in Fig. 19b and c. If the film is very thin, its contact potential is expected to be approximately equal to that of its substrate.

An experiment designed to test this supposition was conducted as follows: MgO films of various thicknesses were prepared on Mo and W substrates, and the contact potential differences between the films and a clean tungsten substrate were measured. The results, given in Table V below show that there is very little change in contact potential with thickness down to about 15 Å.

Table V

CONTACT POTENTIAL DIFFERENCES BETWEEN TUNGSTEN AND MgO FILMS

Film Thickness	Contact Potential Difference	Substrate Material
10 Å	1.2 V	Mo
15 Å	1.9 V	W
20 Å	1.3 V	Mo
25 Å	1.75V	W
30 Å	1.8 V	Mo
50 Å	1.8 V	W
60 Å	1.8 V	Mo
100 Å	1.85V	W
120 Å	1.9 V	W

The result with the 20 Å film was considered anomalous because the substrate in this case contained a region of abnormal appearance, possibly as the result of a contaminant. Since the measured contact potential differences between the clean tungsten and the 700 Å and the 1300 Å films were measured to be approximately 2 eV, it is seen that in thermal equilibrium, the energy bands of the MgO in these films are bent very little over the range from 15 to 1300 Å from the substrate.

This result is not surprising because the Debye length in an insulating material is expected to be long compared with the film thickness. However, the observation that there is 1.9 V contact potential difference between a 15 Å tungsten-based film and clean tungsten is quite surprising, because the density of charge necessary to effect this magnitude of potential change is extremely high. The other alternative is that the simple model of a metal-semiconductor contact does not apply here. It is to be noted that this simple model has been criticized by Bardeen on the basis of its assumption that the work functions of the two materials are not modified by the contact. He showed that if surface states exist on the surface of the semiconductor, with a density of approximately 10^{13} states/cm² eV, then the barrier height is essentially independent of the work function of the metal, and is approximately the same as that occurring at the free surface of the semiconductor.

Since the Debye length is expected to decrease with increasing temperature, the energy bands may be more curved at a high temperature. Hence, the contact potential of two MgO films was measured at ambient temperature and at 550°C to determine whether any changes, which may result from changes in the curvature of the bands, could be observed. The results showed that any change in contact potential, if it occurred at all, could not have exceeded approximately 0.1 V the limit of accuracy of the measurement method. Since the migration of internal secondaries is influenced by the curvature of the energy bands, it may be possible to utilize the secondary emission mechanism to detect changes in curvature. For example, if at a high temperature the Debye length is shortened so that the bands are bent as shown in Fig. 20a compared with the low temperature case shown in Fig. 20b, then a plot of secondary yield as a function of primary energy is expected to reflect this change. For example, at a low primary energy, where the penetration depth of the primaries is small, the yield is expected to be greater at the high temperature, while at a high primary energy little change in yield is expected. Unfortunately, the analysis is complicated by the fact that the secondary yield is also affected by the lattice vibrations. Nevertheless, measurements of secondary yield as a function of primary energy were made (ref. 8, Fig. 19) to determine whether significant changes could be detected. The change in yield with temperature was found to be small at low primary energies but quite appreciable at high primary energies. This is the opposite behavior to that expected on the basis of the diagrams of Fig. 20.

Hence it is concluded that the change in yield observed is the result of scattering of internal secondaries by lattice vibrations and that little change in band curvature occurs with increasing temperature.

The Second Set of MgO Films

After the tube was accidentally opened, new films were processed with much difficulty in that the glass admission valves would frequently open during bakeout. The resulting films are somewhat unique in that they exhibit an intense cathodoluminescence. In addition, the films are also apparently quite nonuniform as they exhibit both a variation in the yield and in the maximum surface potential over the surface of the film. Patch-field effects are also observed such that increased collector potential is necessary to saturate the yield.

The luminescence is visible at a primary energy as low as 100 eV and a current density as low as $0.005 \mu\text{A}/\text{cm}^2$. The intensity decreases with time of bombardment in an apparent exponential fashion, decreasing quite rapidly at first, but even after several hours of bombardment with 1200 volt electrons a faint blue luminescence is still observable. The original intensity may be restored by heating the target to approximately 600°C for a few minutes; this heating also discharges the film. It has not been possible to restore the intensity by electrically discharging the film, indicating that there is some difference between the two methods of discharge.

The luminescence does offer an advantage in that the characteristics of the film may be observed as a function of beam position. The yield was measured as the beam was moved over the film with the aid of an external magnet. For a primary energy of 300 eV, a collector voltage of 90 volts, and a beam diameter of approximately 2 mm, a variation in yield of 16 percent was observed for one film and 10 percent for another film.

The maximum yield obtained by the dc method for each film was originally quite small (below 10); however, it was observed that heating the film increased the yield. It was thought that the original yield may have been limited by patch fields which are decreased by heating. To reduce the effect of the patch fields, the collector voltage was increased above the original 90 volts. A substantial increase in yield was observed. In fact, about 250 volts were necessary to make the yield saturate with collector voltage. The films have not been studied at this high collector potential.

The maximum positive surface potential on film 3-1 varied from 10 to 50 volts, depending on beam position, when a beam diameter of approximately 2 mm was used. The portion of the film which exhibited the lowest value was characterized by a rapid rate of decrease in surface potential; therefore the value of 10 is

probably low since a finite time is required before the potential of the film may be measured after it is charged.

Negative surface potential measurements were not made as a function of the beam position since the film does not luminesce at the low energies used in charging the film. In addition, when the film is being charged negatively the beam is swept over the entire surface of the film by rf induction coils. It was possible to charge film 3-1 to an indicated negative 70 volts and film 2-1 to an indicated negative 40 volts. If the film charges nonuniformly, as it undoubtedly does, these potentials correspond to the most positive portion of the film since the potential is determined by the potential of the filament with respect to the target at which electrons are just able to reach the film.

It is possible in the present tube to prepare the film, explore its characteristics and then destroy the film by heating the substrate to a high temperature. The necessity of opening the tube between each new set of films would be eliminated if a method existed whereby the thickness of the film could be determined without removing it from the tube. Some work has been done on such a method. Briefly, the process involves measuring the amount of charge necessary to produce a known increment of voltage across the film; however, a more detailed evaluation of this method must be made.

Yield Inhomogeneities in Alloy-Based MgO Films

Experiments, in which the variations in yield occurring over the surface of a MgO film were measured, were reported previously (ref. 5, p. 54). The films used were formed by oxidizing Mg which had been evaporated onto a metal substrate. The behavior of the yield was very erratic. The purpose of the present experiment was to make the same measurements on films made by oxidation of a Mg-Ag alloy and compare the results with those obtained for the metal-backed films. The preparation of the targets was described in detail in a previous report (ref. 8, p. 41). Typical traces of the yield as a function of beam position are shown in Fig. 21. The measurements demonstrate that the non-uniform yields, previously found in the case of films prepared by the oxidation of evaporated Mg, (ref. 5, Fig. 21) are also present in the alloy-based films. No explanation of this lack of uniformity is offered but it is evident that it is intimately related to the details of the preparation process.

2.2.2 Secondary Emission Characteristics of Al_2O_3 Thin Films

In a previous report (ref. 7, p. 49), the work done on films prepared by oxidizing evaporated aluminum was summarized. At the same time, an extension of this work, using anodized aluminum, was described. The data obtained in the latter experiment is still being analyzed. It was apparent early in the experiment

however that the ion-bombardment (used in an attempt to clean the surface) resulted in a nonuniform reduction in the film thickness. In order to ascertain the extent of this nonuniformity the work described below was carried out. The technique developed may also be used to evaluate modifications of the sputtering arrangement aimed at providing uniform sputtering over the surface of the target. Such modifications are considered necessary since several experiments now in progress depend on the assumption that the sputtering rate is uniform over the face of the target.

The method used to determine the sputtering rate is based on the dependence of the reflectivity of oxide films on their thickness. Haas (ref. 17) and Vermilyea (refs. 18 and 19) report having made thickness measurements of Al_2O_3 and Ta_2O_5 films on Al and Ta substrates by making use of the colors produced by the films through destructive interference of reflected light. Assuming no absorption in the films and zero conductivity in the oxide the reflected and transmitted light energies can be calculated for both Al and Ta. It is found that for Al the ratio of energy reflected from the air-oxide boundary to that from the oxide-metal boundary is roughly 1 to 14 while for Ta- Ta_2O_5 the corresponding ratio is roughly 1 to 1. Thus the optical method for determining thicknesses is more suitable in the case of Ta_2O_5 . This fact suggests the use of anodized Ta targets for the determination of the sputtering rate. Such an approach is attractive because it offers a detailed observation of the sputtering beam, within the limit of the optical system used to examine the thickness profiles of the bombarded films; it closely duplicates the Al- Al_2O_3 system in that it presents an insulating oxide layer on a conducting substrate to the sputtering beam and it allows for an estimation of the sputtering rate of argon on Ta_2O_5 and possibly on Al_2O_3 if the sputtering beam can be made uniform.

Preliminary optical measurements indicated that thickness determinations would be possible, and that quite good resolution could be obtained with the Ta_2O_5 films. All measurements have depended on data given by Vermilyea who reports that the thickness of Ta_2O_5 formed by anodization at constant current goes as

$$t = 19 + 16.32 V$$

for an initial current of 2 mA/cm^2 which decays to 0.1 mA/cm^2 at constant final voltage V . t = thickness in angstrom units and V = the final voltage across the film. Vermilyea also gives the index of refraction of the oxide as $n = 2.21$ at 7000 \AA and $n = 2.53$ at 4000 \AA .

The thickness of the films from optical null methods is determined according to:

$$t = \frac{\lambda}{2n} \left(\frac{1}{2} - \frac{\delta}{2\pi} \right) \cos \phi$$

where

t = thickness in angstrom units

λ = the wavelength of light at the null in angstroms

n = the refractive index of the film

ϕ = the angle of incidence of the light beam

$\delta/2\pi$ = a constant which accounts for phase changes at the reflecting boundaries.

On the strength of the preliminary results a more refined optical system has been constructed. It consists of a tungsten ribbon filament light source which illuminates the diffraction grating of a Bausch and Lomb 250 mm monochromator. When both the input and output slits have the same setting the monochromator produces light having a bandwidth of 66 angstroms per mm of slit width. The monochromatic light falls on a front surface aluminum concave mirror and is brought to focus at an angle of incidence of $45^\circ + 11^\circ$, on an area of the target 2 mm in diameter. The target is rigidly mounted on an adjustable microscope stage and all but the 2 mm spot is masked from the incident light. The light reflected from the spot is collected by an RCA 926 vacuum phototube situated at 45° from the normal to the target. The target mounting and masking arrangement allows for study of 25 distinct areas on the target.

A number of targets have been prepared, one set having thicknesses in the range 524 Å to 544 Å in 10 Å steps, and the other set with thicknesses 385 Å to 395 Å. The targets in the first set were found to yield detectable minima in the reflectivity vs. wavelength curves for slit widths of 1 mm and to give very clear minima when the slits were opened to 1.5 mm. However, no differences among the films could be detected, indicating a resolution of thickness no better than 30 Å. This is in part attributable to the spread in the incident angle of the light beam, and in the finite bandwidth of the light used. Vermilyea also reports a resolution of only 30 Å for films in the 500 Å to 900 Å range. Measurements were made on the second set of films, and discernible minima were obtained for slit widths of 1.5 mm. In the case of these films the difference in thickness was evident in a very marked difference in colors, and in well separated minima. Here the resolution is at least 10 Å and according to Vermilyea can be made as good as 2 Å. The resolutions agree with data obtained earlier while observing areas of the films approximately 3 times as large.

Present data are encouraging and it is expected that measurements of good resolution can be made on the sputtering beams using targets in the 400 Å film thickness range. This corresponds well to the thicknesses used in the Al_2O_3 studies. It must be

noted that this approach does not depend on a detailed knowledge of Ta₂O₅ film properties since only relative changes are of interest. Further, there is considerable room for refinement of the optical system allowing for improvement of resolution and incident light intensity and purity.

2.2.3 Dissociation of Compounds by Electron Bombardment

The results obtained by bombarding a thin film of NaCl on a palladium substrate with low energy (less than 300 eV) electrons have been given in a previous report (ref. 7, p. 63). In summary it was found that strong currents of Na⁺ and Cl⁻ ions were produced but that these currents decreased drastically with continued electron bombardment. These ion currents were never seen to return to their original values or even to increase significantly. Also considerable visible damage, in the form of a purple coloration, was produced in the films by the electron bombardment. The intensity of the color increased with continued electron bombardment. This behavior made it difficult to obtain consistently reproducible results particularly in efforts to obtain the dependence of ion current on bombarding current. This purple coloration of the film, indicative of excess sodium in the NaCl lattice, suggests that the conduction of the bombarding current through the film is accomplished to some extent by migration of the Na⁺ ions to the film surface. It is quite possible that the resulting excess sodium near the film surface is the reason for the visible deterioration of the film and the decrease in the dissociation rate. An experiment was performed to investigate this postulate using KCl thin films, since these films had been previously prepared for possible dissociation work and were readily available. One KCl film was bombarded in the same manner as the NaCl films, that is, with the substrate potential more positive than any of the surroundings, thus ensuring the return of secondary electrons to the film surface. This causes the film surface to become negative with respect to the substrate and the migration of Na⁺ ions to the surface is encouraged. It is necessary to perform the dissociation work in this way in order to measure the bombarding current and to draw the dissociated positive ions from the film surface to the spectrometer. The KCl film subjected to electron bombardment under these conditions turned a brown color and deteriorated in a manner very similar to the NaCl films discussed earlier. Another KCl film was bombarded but this time no electrical connection was made to the film substrate. The potential of the target remained at the potential of the surroundings since the secondary emission coefficient is greater than unity at the bombarding energy of 100 eV which was used. In this situation there is no electric field across the film and no tendency for ion migration. This film showed no discoloration nor any evidence of flaking away from the substrate after electron bombardment. However, it did show evidence of dissociation in that the film was completely removed over small areas of high bombarding current density. This experiment was repeated twice with similar results. The conclusion is that the observed deterioration of the NaCl films under electron bombardment

is due in part to migration of Na^+ ions to the film surface. In view of this it does not appear feasible to continue study of the dissociation of alkali halides since all alkali halides are known to conduct current by migration of one or both ions through the lattice. In the case of the last NaCl film studied, care was taken to minimize the electron bombardment in an effort to obtain some data before the film was disrupted. Figures 22 and 23 show the dependence on bombarding current of the Na_{23}^+ and Cl_{35}^+ ion currents respectively for the case of a fresh film of NaCl . These curves were taken before any decay of the ion currents was observed with the exception of that evidenced by the curvature at the high current end of Fig. 23. The reproducibility, before these last few points on Fig. 23 were taken, was excellent. It is possible that absorbed sodium and chlorine on the film surface may have influenced these results. In fact the change in slope of Fig. 22 could be due to the removal of adsorbed material. However at this time it was decided to study the dissociation of a new material in which electrical conduction is predominately an electronic and not an ionic process.

Magnesium oxide was selected as the new material to be used for dissociation studies partly because of earlier dissociation work done on this material by Wargo (ref. 20) and partly because the secondary emission properties of MgO have been studied in detail in this laboratory. The electrical conduction mechanism in MgO is believed to be essentially an electronic process. The MgO films which are being used for the dissociation work were formed by heating electropolished Ag-Mg alloy (ref. 2, p. 5) to about 700°C in 100 microns of oxygen for about 15 minutes. The thickness of one MgO film formed in this manner has been measured by an electrolytic conduction technique (ref. 1, p. 20) and was found to be 650 \AA . During low energy electron bombardment of these MgO films in the dissociation tube, ion currents of O_{16}^+ and Mg_{24}^+ have been seen. The intensity of these ion currents is considerably less than the intensity of the Na_{23}^+ and Cl_{35}^+ ion currents observed during the dissociation of NaCl . The dependence of the O_{16}^+ and Mg_{24}^+ ion currents on the bombarding current has been observed and appears to be linear as is shown on Figs. 24 and 25. The dependence of the O_{16}^+ ion current on the energy of the bombarding electrons has been measured and is shown on Fig. 26. It should be noted that the energy dependence may be slightly in error because of the necessity of changing the magnetic field used to focus the bombarding electrons onto the target. This changing magnetic field could change the fraction of the ions from the target that reach the mass spectrometer. However in view of the large electric field drawing the ions from the target, the effect of the changing magnetic field is not expected to be large. It is hoped that this effect can be determined using a thermal ion source in the target position.

During the bombardment of MgO the most intense ion current that is seen is that due to chlorine. This large amount of chlorine was first thought to be due to the re-evolution from the titanium

sputter pump of some of the chlorine which had been pumped during the dissociation of NaCl. However the installation of a new sputter pump did not change the amount of chlorine noticeably. It is now believed that during the dissociation of NaCl the metal parts inside the dissociation assembly became coated with NaCl resulting from the adsorption and recombination of the Na and Cl dissociation products. Subsequent unintentional electron bombardment of these metal parts might dissociate this NaCl film and a substantial background pressure of chlorine and sodium would be established. Although it is possible that the chlorine might combine chemically with the MgO film, it is believed that the chlorine ion current results from the ionization by the bombarding electrons of chlorine atoms which are adsorbed on the target surface. Another possible explanation for the large amount of chlorine observed is that the titanium ion pump may form one or more of the titanium chlorides, $TiCl_2$, $TiCl_3$, or $TiCl_4$ when pumping chlorine. In addition several components of the tube structure are made of titanium and the chlorine liberated during the dissociation of NaCl could form titanium chloride on the surfaces of these components. All of the chlorides of titanium have a sufficiently high vapor pressure to contaminate the tube and the target surface. Electron bombardment of the target could then dissociate the titanium chlorides giving a chlorine ion current. Although the mass scale of the spectrometer has not been calibrated for high masses, peaks have been seen which correspond roughly with the masses of the three chlorides of titanium.

A more serious problem than the effect of chlorine on the dissociation process is the possibility that previously dissociated oxygen and magnesium may be adsorbing on the film surface and contributing significantly to the observed ion currents of oxygen and magnesium. The potentials of the target, spectrometer, and intervening grids have been arranged so that only ions which are formed on the target surface are able to reach the spectrometer. This arrangement severely reduces the intensity of the ion current reaching the spectrometer but eliminates any ions which are formed by ionization of ambient gas atoms by the bombarding beam enroute to the target. However the problem of ambient gas atoms which are adsorbed on the target surface and then ionized by the bombarding electron beam, is more difficult. One approach to the problem has been to vary the pumping speed of the ion pumps and observe the changes in the O^+ ion current resulting from the changes in the ambient pressure of oxygen. From this data the fraction of the ion current which is dependent upon background pressure can be determined and has been found to be about 4 percent. Unfortunately the same experiment when applied to the mass 28 ion current (CO^+ and/or N_2^+) suggests that only 10 percent of this ion current is dependent on ambient pressure whereas intuitively one would expect 100 percent pressure dependence. This simple approach neglects the possibility that the surface is largely covered by adsorbed atoms during electron bombardment. It is known that the number of atoms adsorbing on a surface per unit time decreases

strongly with the number of atoms already adsorbed. If the surface were largely covered with adsorbed atoms, even at the highest pumping speed available, changes in pressure would not cause any appreciable increase in the number of adsorbed atoms on the surface. However this implies that the factor limiting the number of adsorbed atoms on the surface is the inefficiency of the adsorption process at high coverage of the surface and not the electron bombardment; this implication is however contradicted by the following work.

A second approach to the problem has been to observe the transient behavior of the ion current. If the target is left un-bombarded for a time T (usually a few minutes) and the ion current of oxygen (or magnesium) is observed as the bombardment is started, an overshoot of the ion current is seen. This is shown in Fig. 27. The dependence of this overshoot on T is shown in Fig. 28. This overshoot of the ion current is believed to be due to desorption and ionization by electron bombardment, of atoms which were adsorbed on the target surface during the quiescent period T . This interpretation implies that the electron bombardment is an important factor in limiting the number of adsorbed atoms on the film surface. From Figs. 27 and 28 it is possible to obtain an estimate of the percentage of the total ion current that is due to adsorbed gas. At this time, this calculation has been carried out for only one set of measurements of the Mg_{24}^+ ion current, and the results indicate that less than 20 percent of the total ion current is due to adsorbed gas. In summary, the problem of adsorbed atoms on the film surface has not been resolved conclusively but indications are that the observed ion current is due mainly to dissociation of MgO by electron bombardment.

2.2.4 Diffraction of Slow Electrons by MgO

The apparatus for slow electron diffraction studies which was constructed during the last contract period (ref. 7, p. 64) has been used for studies of the (001) MgO surface. It is well known that the secondary electron emission from (001) MgO is extremely sensitive to surface contaminants. The purpose of the present experiments is to study this effect in some detail and to develop techniques for obtaining a clean surface. Most of the experimental techniques were described previously (ref. 7, p. 64) and will not be discussed again.

Surface Potential

During the early measurements on MgO it was found that a diffraction pattern could not be observed for primary energies less than approximately 100 eV. For lower energies the screen was covered with a diffuse glow rather than with the sharp diffraction beams which were present at higher energies. (The exact energy at which the pattern "washes out" depends on the prior treatment of the surface.) Moreover, operation of the flood gun with $\epsilon_f \leq 100$ eV (see Fig. 29) did not change the pattern at either low or

high values of ϵ_p . It was concluded that the first crossover ($\delta = 1$) occurred at $\epsilon_p \approx 100$ eV and that for lower energies the crystal became charged to the potential of the filament of the main gun. In that case the primary electrons would not be able to reach the crystal.

Subsequent measurement of δ however indicated that it was considerably greater than unity at $\epsilon_p = 100$ eV (see Fig. 39). It was also discovered that if the flood gun were operated with $\epsilon_f \geq 200$ eV the diffraction pattern would remain visible for ϵ_p as low as 6 eV. This is not understood. It seems possible that with the flood gun off, "patch fields" around the bombarded portion of the target could prevent the primary beam from reaching the target even when the bombarded portion of the target is not charged negatively. The reason for the necessity of such high energy electrons in order to dissipate the charge of the "patch fields" is not clear however.

For the data which will be presented here the flood gun was operated with $\epsilon_f = 1000$ eV. The potential of the surface of the crystal depends upon the relative magnitudes of the currents from the main gun and flood gun. These were adjusted so that the first strong maximum in the (00) beam (marked with an arrow in Fig. 36) occurred at 8.5 eV (for normal incidence). This is a rather arbitrary procedure and the precise value of the surface potential is not known.

Plane Grating Beams

It is quite natural from a theoretical point of view to discuss the plane grating beams and their relative intensities separately. The positions of the plane grating beams and their dependence upon energy can be calculated using the two von Laue equations which are appropriate for the particular crystal face upon which the electrons are incident (ref. 7, p. 67). However the correct dependence of the intensities of these beams upon energy cannot be predicted using the third von Laue equation. Hence, firm conclusions cannot be drawn from the variations of the intensities of the plane grating beams. This point will be discussed further below.

The diffraction pattern from the (001) face of MgO is shown in the sketch in Fig. 31. The sketch is drawn for a normally incident primary beam and is as seen looking along the direction of the primary beam. All of the beams are not visible at a particular energy and the (00) beam is only visible when the angle of incidence is not zero. The complete pattern exhibits the symmetry of a cube face and so can be constructed from that portion of the pattern shown.

This pattern is due to a two dimensional fcc structure with the MgO lattice constant. The notation in Fig. 31 is for the unit cell shown in Fig. 33. The colatitude angle is plotted vs.

energy for the beams in the $[\bar{1}10]$, $[\bar{1}00]$ and $[\bar{3}10]$ azimuths in Figs. 36, 37 and 38. The solid lines were calculated for an angle of incidence of 2° . The positions of the intensity maxima in the plane grating beams are indicated by the quadrangles. The areas of these figures indicate the precision of the measurements.

The pattern in Fig. 31 is typical of most of the area of the surface. When the primary beam is directed at a particular small portion of the surface however, additional "half-order" beams appear. These are sketched in Fig. 34. Half-order beams are present in those azimuths for which the sum of the indices is even ($[110]$, $[310]$, etc.); they are not present in those azimuths for which the sum of the indices is odd ($[100]$, $[210]$, etc.).* This pattern is the same as that reported by Farnsworth, et al., (ref. 21) for a clean (001) Ge surface and is interpreted in a similar way.

The surface is supposedly covered by patches of the type shown in Fig. 35. The open circles represent the structure which produces the half-order beams and the solid circles represent the underlying face centered structure. Other patches similar to that in Fig. 35 but rotated through 90° would produce the four fold symmetry of the pattern which is observed. It is obvious that such a structure would produce half-order beams in the $[\bar{1}\bar{1}0]$ azimuth and no half-order beams in the $[\bar{1}00]$ azimuth. A more detailed analysis shows that in fact half-order beams would be produced only in those azimuths for which the sum of the indices is even.

Except for the $(3/2, 1/2)$ beam the half-order beams are much weaker than the integral order beams. The colatitude angles for the $(1/2, 1/2)$, $(3/2, 3/2)$ and $(3/2, 1/2)$ beams are plotted vs. energy in Figs. 36 and 38. The $(5/2, 3/2)$, $(5/2, 1/2)$ and $(7/2, 1/2)$ beams are visible only at primary energies of 123 eV, 135 eV and 176 eV respectively.

In addition to these half-order beams, which are as sharp as the beams in the pattern of Fig. 31, there are much weaker beams which are diffuse in one direction. These are indicated by the lines in Fig. 34. They would be produced by patches like that in Fig. 35 which had only a few atomic rows in the direction $[\bar{1}\bar{1}0]$ and many atomic rows in the direction $[\bar{1}10]$ and which were not mutually coherent.

Intensity Maxima

The open quadrangles in Figs. 36, 37 and 38 actually correspond to the intensity maxima of the various beams. The dashed lines indicate the range over which the beams are continuously

*This nomenclature is slightly confusing. The (10) beam, for instance, would be considered a half-order beam; i.e., it would correspond to a double spacing in the $[\bar{1}00]$ azimuth. This is because of the choice of unit cell which was made in Fig. 33. It is used because it conforms to the usage in the literature.

visible. The closed circles are the positions of the Laue beams (the energies and angles which satisfy all three von Laue equations) for a three dimensional fcc lattice with the MgO lattice constant. The notation is for the unit cell shown in Fig. 32. The fact that these intensity maxima do not occur at the positions of the Laue beams and that there are more maxima than one would predict with the von Laue equations is characteristic of the slow electron diffraction from many materials (refs. 22 and 23). One would expect intensity maxima only at the positions of the Laue beams if the diffraction involved only single scattering processes. This is so since the three von Laue equations are derived from the first Born approximation (ref. 25). (In the theory of electron diffraction this is usually called the kinematical theory.) The physical content of the first Born approximation is that contributions to the scattering amplitude from multiple scattering processes are neglected, i.e., the distortion of the incident wave due to the crystal potential is neglected. It seems reasonable therefore to look for the cause of the "extra" maxima in multiple scattering processes. Laschkarew (ref. 24) has explained the "extra" maxima in the (00) beam from copper in this way. His argument is not strictly self-consistent however since he uses the kinematical theory and then introduces the multiple scattering in an artificial way.

Multiple scattering can be taken into account in several ways (refs. 27,28). Laschkarew suggested that his idea could be put on a more solid basis by using Bethe's dynamical theory of electron diffraction* (ref. 26) and this will be done here.

Bethe's theory is a zeroth order theory, i.e., the wave function inside the crystal is developed in powers of the crystal potential and then only those terms which are of zeroth order in the potential are retained. The result is that when the incident wave vector is not near a Brillouin zone boundary there is no interaction with the lattice, the electron remains free and hence there are no diffracted beams. (This is of course in direct contradiction to the experimental result that the plane grating beams are continuously visible for low energies. This point will not be considered further here however.) When the external incident wave vector is near a zone boundary there will be a number of internal incident wave vectors. Associated with each of these there will be a number of diffracted waves with amplitudes of zeroth order in the potential. These amplitudes and the values of the corresponding wave vectors will be given by the "dispersion equation" (Heidenreich's Eq. 8b) which involved the Fourier coefficients of the potential for all the zone boundaries which the

*Bethe's theory has appeared in the literature a number of times in equivalent but slightly different forms (refs. 29, 30, 31, 32, and 33). The best of these is that by Heidenreich (ref. 32).

incident wave vector is simultaneously near. The important point for our present purpose is that when the incident wave vector is near several zone boundaries, the amplitudes of the corresponding scattered waves cannot be calculated separately as they are in the kinematical theory. These amplitudes are "dynamically coupled" by the dispersion equation. Thus as the energy of the incident electron is varied so that its wave vector passes through a region containing several zone boundaries, the diffracted amplitudes will vary in a complicated way (given by the dispersion equation) and may have multiple maxima.

Even in the simplest case for MgO (the second intensity maximum in the (00) beam) one has to consider the interactions among nine diffracted beams. The dispersion equation actually consists of a set of nine linear homogeneous equations. The Hartree potentials are known to give good results for fast electron diffraction and could be used for the solution of these equations. Use of these potentials in the equations for the first intensity maximum in the (00) beam gave unreasonable results however. The Hartree potentials are apparently not a good approximation for slow electrons and the calculation has not therefore been carried through.

Effects of Heating and Sputtering

The pattern in Fig. 34 was discovered only recently. It is now known whether or not it was present from the beginning. Heating the crystal at approximately 900°C for 34 hours at a pressure of 10^{-9} mm Hg had no effect on the half-order beams. The effect which sputtering has on this pattern and on the secondary electron yield from those portions of the target covered with the structure of Fig. 35 remain to be determined.

It is not known whether the pattern in Fig. 31 is in fact due to the MgO lattice or whether it is due to an adsorbed fcc structure which has the MgO lattice constant. This pattern was visible immediately after the crystal was placed in the tube and it did not change (insofar as its geometry is concerned) when the crystal was heated or sputtered. The surface which produces this pattern is certainly not clean since it was cleaved in air and even after the heat treatment and sputtering the secondary electron yield was quite low (see Fig. 39).

The initial secondary electron yield of the crystal is shown in curve A of Fig. 39. After the tube had been baked at 300°C the yield was that shown in curve B of Fig. 39. The diffraction pattern was considerably brighter after the bake than before. (In measurements on another MgO crystal however the opposite effect had been observed, i.e., the pattern was brighter before the bake than it was afterward.)

Heating the crystal at 900°C for 8 hours at a pressure of 10^{-9} mm Hg resulted in the yield shown in curve C of Fig. 39. The pattern was again brightened and a new intensity maximum appeared

in the (11) beam (and in the three equivalent beams) at $\epsilon_p = 180$ eV. This behavior was reproducible. When the crystal was exposed to air at atmospheric pressure the maximum of 180 eV disappeared. After subsequent heating it reappeared. There were no other changes in the pattern when the heating period was increased to 34 hours. If the interpretation of the extra maximum given above is correct, then the heat treatment must have significantly changed the band structure of the crystal.

An attempt was then made to clean the surface by bombarding it with argon ions. Since the target is an insulator this must be accomplished with an rf accelerating field for the ions. The circuit used is shown schematically in Fig. 30. Since the mobility of the electrons in the plasma is much higher than that of the positive ions the crystal surface is positive over only a very short portion of the rf cycle in the steady states. The maximum accelerating voltage for the positive ions during each cycle is therefore very nearly the peak-to-peak voltage of the rf signal.

The diffraction pattern did not change during two 2 hour bombardment periods using peak-to-peak voltages of 500 and 1000 volts respectively. After 2 hours of bombardment with a peak-to-peak voltage of 2000 volts the diffraction pattern was considerably dimmer and the additional maximum at 180 eV had disappeared. The secondary electron yield is shown in curve D of Fig. 39.* Further bombardment at 2000 volts for 8 hours did not produce further changes in the diffraction pattern.

Annealing the crystal at approximately 500°C for two hours produced no change in the diffraction pattern. After the crystal had been annealed at 900°C for four hours the pattern was about as bright as before the sputtering but the 180 eV maximum did not reappear. The secondary emission yield after this treatment is shown in curve E of Fig. 39.

These measurements were made before the proper operating conditions for the flood gun were discovered. The pattern for $\epsilon_p \lesssim 100$ eV was not therefore observed. Similar measurements will be made using the improved discharging technique.

*The control electrode of the main electron gun became shorted to the filament before these measurements were made. The measurements for curves D and E were therefore made with the flood gun at an angle of incidence of 50°. The corresponding yield for normal incidence should be slightly higher for energies below the maximum and approximately 10% lower for energies near and beyond the maximum (ref. 11). Notice that this would tend to make curves D and E even more sharply peaked for normal incidence.

It seems probable that due to the high value of accelerating potential which was used argon ions were buried rather deeply in the crystal. The decrease in the yield after the sputtering might be due to this effect. The fact that the yield did not completely recover after the anneal probably indicates that all of the argon ions were not removed. It would therefore be desirable to effect the sputtering at a lower energy. In fact, however, even for these high energies the sputtering was apparently not as efficient as possible. E. D. Savoye (ref. 34) has observed that sputtering at 2000 V removed a macroscopic layer of a MgO crystal in a few hours. This is indicated by a noticeable thinning of the crystal and by the absence after sputtering of most of the striations which are visible on the cleavage surface of the crystal. These striations were visible in the present case even after the 8 hour sputtering treatment. The principal difference between Savoye's work and that described here appears to be that in the former the crystal was situated inside the discharge tube and thus closer to the plasma. The discharge tube is therefore being reconstructed to permit the crystal to be held closer to the plasma. Measurements similar to those described above will then be repeated.

2.3 Theoretical Studies

2.3.1 Theoretical Model of the Mechanism Resulting in Structure in the Variation of Secondary Emission with the Angle of Incidence of the Primary Beam

The structure in the SEAI curves for single crystals may be of considerable theoretical importance because it appears to be related to the crystal structure. Almost all of the existing theories of secondary emission assume that the production and escape of secondaries can be treated as if they were occurring within an isotropic medium. Furthermore, in the case of secondary emission theories for metals, it is generally assumed that the primary electrons essentially interact with only the conduction electrons of the crystal. Since these electrons are almost free, the crystal geometry is of little consequence in such interactions. Therefore, if the structure in the SEAI curves is a result of the direct influence of the crystal geometry on the production or escape of the secondary electrons, changes may be required in the formulation of secondary emission theories.

It may be the case that for polycrystalline secondary emitters the approximation of an isotropic medium could still be justified since the total emission is the sum of the emission from many randomly oriented crystallites. However, most of the basic research in the field of secondary emission involves single crystals and, consequently, a theory must be applicable to single crystals to be of much value. In the case of metals there is little question that interactions with the more tightly bound electrons must be important if the crystal geometry is directly involved in secondary emission.

A theory has been proposed to explain the structure in the SEAI curves (refs. 9, 10 and 3, p. 43) which avoids the above problems. This theory is based on a model in which the crystal geometry is important only in diffracting the primaries and is not directly involved in the secondary emission process. A number of the features of the SEAI structure for titanium can be qualitatively explained by this theory but it does not explain some of the SEAI results obtained from MgO single crystals (ref. 11). Furthermore, on the basis of the results of quantitative calculations for this theory (ref. 4, p. 24 and ref. 5, p. 39) it was concluded that it is impossible for diffraction of the primary electrons to produce peaks of as large a magnitude as are experimentally observed.

A new model has now been proposed to explain the presence of the structure in the SEAI curves for single crystals. This model is based upon localization of the primary electrons and the localization of the electron density within crystals and requires both nonisotropic production of secondaries and interactions between the primaries and the tightly bound lattice electrons for both metals and insulators. However, it appears capable of accounting, in a qualitative way, for the presence of the major peaks at angles of incidence corresponding to the direction of major zone axes in the crystal. Some aspects of the manner in which these peaks vary with the primary energy can also be qualitatively explained for both metals and insulators. If this model is combined with parts of the model previously proposed by Soshea (ref. 9), it is possible to account for the small structure between and superimposed upon the major peaks.

The model involves several postulates that appear to be reasonable. The basic postulate is that when a high energy electron enters a crystal and suffers an inelastic collision it becomes localized at the site of the collision. Then the wave function of the electron becomes a modified spherical wave centered about the site of the collision with an amplitude that is strongly peaked in the original direction of the electron. While it may not appear reasonable that the wave function would abruptly change, similar changes frequently are implicit assumptions in theoretical work. It is actually an artifice to avoid the treatment of the statistical ensemble of wave functions which a more rigorous treatment would require (ref. 35). The forward peaking of the wave function amplitude follows directly from the atomic scattering factor for high energy electrons. For lower energy electrons there would be some modifications introduced by the lattice potentials.

From the results of X-ray diffraction studies it is known that in a crystal the electron density has strong maxima in the vicinity of the nuclei. For example, in aluminum which has a nearest neighbor distance of 2.86 Å the following electron densities have been found (ref. 36):

- a. 100 electrons/ \AA^3 at 0.12 \AA from the nuclei
- b. 10 electrons/ \AA^3 at 0.35 \AA from the nuclei
- c. 1 electron/ \AA^3 at 0.57 \AA from the nuclei
- d. 0.208 electrons/ \AA^3 between ions.

Aluminum has an atomic number of only 13 and the peaking of the electron density would be even more pronounced for materials which have larger atomic numbers. Therefore, it is probable that the initial collision of a high energy electron entering a crystal would be in the vicinity of a nucleus. If one considers the probability per unit path length that the electron will have a second interaction it will be evident that there is a definite dependence upon the initial direction of the electron. If the incident electron is in the direction of a major zone axis of the crystal, the large amplitude portion of the altered wave function will pass through many more nuclei and regions of high electron density (per unit path length) than for some arbitrary incident direction. An immediate consequence of this would be that incident electrons directed along a major zone axis would produce secondaries* closer to the surface than an electron in a direction differing by several degrees. Since the secondaries nearer the surface would have a greater probability of escaping, this model predicts peaks in the secondary yield when the primary beam is in the direction of a major zone axes.

The model has the disadvantage that any quantitative calculations based upon it would be very laborious. Furthermore, the results of such calculations would be greatly dependent upon several factors that are not accurately known (i.e., interaction probabilities of the incident electron and the lattice electrons, escape probabilities of the secondaries, etc.). However, as previously indicated it is possible to estimate how the structure should vary with primary energy, and predict differences between metals and insulators. On the basis of the model, the existence of the structure is a direct result of differences in the depth at which the secondaries are formed. Since the depth of formation of the secondaries varies with primary energy (increasing with increasing energy), variations in the relative magnitude of the structure* with primary energy would be expected to have a similar origin.

*In this work the term secondaries includes all the emitted electrons. Most of these will be low energy electrons but the higher energy secondaries often referred to as backscattered electrons are also included.

**The relative magnitude of a peak is the ratio of the increase in secondary yield as a result of the peak to the value the secondary yield would be without the peak.

Primary energies below the energy corresponding to the maximum in the yield curve will be considered first. In this energy range most of the secondaries are produced sufficiently close to the surface to have a significant probability of escaping. As the primary energy is decreased the differences among the escape probabilities of the secondaries become smaller. For sufficiently low primary energies, for all angles of incidence, all the secondaries are produced so close to the surface that they all have virtually the same escape probability. Therefore, for this energy range it would be expected that the relative magnitude of the structure would decrease with decreasing primary energy. Furthermore, there might even be an inversion of the structure (i.e., dips where there were peaks) for the low end of this energy range. This could occur because when the primary beam is in line with a major zone axis the primary electrons are more likely to interact with the more tightly bound lattice electrons than for other angles of incidence. Thus, the average energy loss per secondary produced would be greater, resulting in fewer secondaries when the beam is aligned with a zone axes.

From the measurements on titanium, germanium, and tungsten it is clear that relative magnitude of the structure does decrease with energy for primary energies below the maximum in the yield curve. Unfortunately, limitations of the electron gun have prevented a determination of whether an inversion of the structure occurs at low energies in the case of the materials examined. However, it is questionable whether inversion would be present because the primary energy for which it could occur would apparently be so low (below 40 eV) that the atomic scattering factor would not be strongly peaked in the forward direction. However, an inversion of the structure for MgO single crystals has been observed by Whetten and Laponsky (ref. 37) along with a decrease in the magnitude for energies below the yield curve maximum (ref. 11).

Next, the variation of the relative magnitude of the structure will be considered for very high primary energies. Initially, only the low energy secondaries will be considered. Since the mean free path increases with energy, for sufficiently high primary energies, only the secondaries produced by the first several collisions of the primaries will be sufficiently close to the surface to have a significant probability of escaping. In this energy range a large percentage of the escaping secondaries will result from the initial collisions of the primaries and the percentage will increase with increasing primary energy. Because the wave functions of the primaries are not localized before the initial collision, the depth at which these secondaries are formed is not altered when the primary beam is aligned with a zone axis. Therefore, the relative enhancement of the yield due to alignment with a zone axes will decrease with increasing primary energy. If the primary energy is sufficiently high, virtually all of the escaping secondaries will result from the initial collisions and the relative peak magnitude will go to zero. The various peaks would disappear

at somewhat different energies because the depth of the initial collisions depends upon the angle of incidence, with those for normal incidence being the deepest. Consequently, the normal incidence peak should be the first to disappear with increasing primary energy.

It has been experimentally observed in the case of tungsten, titanium, and germanium crystals that for high primary energies the relative magnitude of the structure does decrease with increasing primary energies as the model predicts for low energy secondaries. Furthermore, in the case of titanium sufficiently high energies were examined to observe extinction of peaks (ref. 9, Fig. 9) and the normal incidence peak disappeared at a lower energy than most of the other peaks.* However, the same general variation in the peak magnitudes was observed for the total secondary yield as for the low energy secondaries. Since the depth from which the high energy secondaries escape is considerably greater, this similarity would not be expected for high primary energies on the basis of a straightforward application of the model. It is not certain that this is entirely the fault of the model because there are many details concerning the production of the high energy secondaries that are not well understood.

The results obtained by Whetten and Laponsky for MgO single crystals have been considered in contradistinction with the above results because they do not observe any evidence of a decrease in the relative magnitude of the SEAI peaks at high primary energies (ref. 11). However, in terms of the model these two sets of results can be seen to be quite consistent. At the highest primary energies examined by Whetten and Laponsky the total secondary yield was still much larger than the maximum for a metal. Under these conditions the secondaries produced by the initial collisions of the primaries make a negligible contribution to the total yield and the peaks would not be expected to decrease. A decrease in the relative magnitude of the peaks would not be expected until the primary energy was so high that a significant portion of the secondary yield (low energy) was a result of the initial collisions of the primaries. This indicates that the difference between the structure of the SEAI curves of metals and insulators is largely a result of the difference in primary energies required to establish similar conditions because the escape depth of secondaries is so much greater for insulators.

The results from titanium, germanium and tungsten are consistent with this idea. For these materials, both the maximum secondary yield and the corresponding primary energy is largest for tungsten and smallest for titanium. This indicates that, for

*The 51.2 degree peak disappeared at the same energy as the normal incidence peak, but this may be a result of the much smaller magnitude of 51.2 degree peak over the entire energy range.

a given high primary energy, tungsten would yield more escaping secondaries than germanium which in turn would yield more than titanium. Therefore, it would be expected from the above reasoning that a given percentage (high energy) decrease in the relative magnitude of the SEAI peaks would require the highest energy for tungsten and the lowest energy for titanium; this is in agreement with the observations.

The width (in angle) of the SEAI peaks has also been observed to vary with primary energy. In terms of the model, the widths of the peaks are dependent upon how sharply the wave functions of the scattered primaries are peaked in the forward direction. As previously stated, the forward peaking for low energies is probably affected by lattice potentials, but for high primary energies it should be determined by the atomic scattering factor. Since the half-width of the atomic scattering factor varies as the inverse of the square root of the energy, the half-width of the SEAI peaks should vary in a similar manner. A log-log plot of the estimated half-width of the normal incidence peak of titanium is shown in Fig. 40 for primary energies from 120 eV to 10,000 eV. For comparison a solid line is drawn with a slope of $-1/2$. Above 1,000 eV the agreement between the slope of the data and the slope of the line is quite good considering the errors in the estimated half-width caused by the small structure superimposed upon the main peak. The disagreement below 1,000 eV is understandable because the influence of the lattice potentials upon the scattering and also because the measurements were obtained on a crystal that was not sputter cleaned (Sec. 2.1.1).

A final feature of the SEAI peaks that can be qualitatively explained by the model concerns differences between the enhancement of low energy and high energy secondaries as a result of alignment of the primary beam. The very high energy secondaries (having energies which are a large fraction of the primary energy) are usually produced by large angle interactions of the primaries with either the very tightly bound lattice electrons or the nuclei (ref. 38). Therefore, the distance from the surface at which these secondaries are produced should be more strongly influenced by alignment of the primary beam with a zone axis than for the low energy secondaries, which can be produced between the nuclei. Consequently, the relative increase in the yield as a result of alignment of the beam would be expected to be larger for the very high energy secondaries than for the low energy secondaries. The situation is different for the secondaries with a small fraction of the primary energy even though these energies may be quite large on an absolute scale. It is believed that a fairly large number of interactions with the more loosely bound electrons occur before these secondaries escape (ref. 38). Thus, compared to the very high energy secondaries, their yield would not be expected to be as strongly influenced by alignment of the beam with a zone axis, particularly for high primary energies. The data obtained for the higher energy secondaries are consistent with this explanation (ref. 3, Figs. 22-24) but it is felt that both more extensive measurements and a more detailed explanation are needed.

As previously indicated, it is possible to account for the small structure between and superimposed upon the major peaks of the SEAI curves by combining the new model with parts of the model previously proposed by Soshea* (ref. 9, p. 1368). Two assumptions are involved in this new explanation and the first is the same as that used in the old model. It is assumed that some of the primary electrons are diffracted within a thin layer of material at the surface of the crystal. The thickness of this layer is determined by the mean free path for inelastic scattering of the primaries. It is further assumed that primaries diffracted in the direction of a major zone axis will produce more escaping secondaries by the same mechanism as for a primary initially directed along a zone axis. Thus, when conditions are satisfied for the diffraction of a significant number of primaries in the direction of a major zone axis, a small peak in the yield should be observed. The old model predicts the same conditions for the existence of a small peak except that it is required that the primaries be diffracted into a zone axis which is at a larger angle with the normal to the surface than the primary beam.** Consequently, the new model predicts all the small peaks predicted by the old model plus some additional peaks. An examination of the small peaks previously cited as examples of peaks predictable by the old model (ref. 9, Table I) reveals that one of them (the first one) actually is predicted only by the new model because it requires diffraction of the primaries into an angle closer to the normal than is the primary beam. Thus it is clear that even for the small structure in some cases the new model yields a satisfactory explanation of the observed results while the old model fails.

In summary, it can be stated that the model proposed here is limited by the lack of quantitative results and does not appear to account for some of the results observed for high energy secondaries at high primary energies. However, the model does give a qualitative explanation of sufficiently many of the observed characteristics to be seriously considered as a likely explanation of the mechanism involved in the production of the structure of the SEAI curves. If this model is correct, some significant objections can be made to assumptions made in existing secondary emission theories.

*Because of the excessive space required to thoroughly explain the old model, familiarity with it will be assumed.

**This was not stated but is implicit in the model.

2.3.2 Effect of an Electric Field on the Escape of Secondary Electrons from Polar Crystals

In the theory of secondary electron emission from insulators an electric field plays a role in several ways; it can cause drift of electrons; it can modify the production mechanism and it can increase or decrease the effective electron affinity at the surface (Schottky Effect). For large fields the secondary current consists of a constant part and of a field dependent part. The latter part is still proportional to the primary current (ref. 39) for fields up to 10^7 or 10^8 V/cm (in MgO) while for still larger fields the yield becomes more and more independent of the primary current (refs. 40, 41). The former effect has been explained by a Townsend type avalanche effect, while the latter is interpreted as field emission. The agreement between theory and experiments by Jacobs, et al., seems to be quite good. In the first case, the produced secondaries gain sufficient energy from the field to liberate new electrons by ionization. For larger fields in the second case, the emission becomes self-sustained presumably by field emission. In avalanche type field-dependent secondary emission the average energies range between 10 and 24 eV and δ is of the order of 27 in MgO, while for newly self-sustained emission δ up to several thousand has been observed. In both these effects the field is strong enough to create more electrons and so the production mechanism depends on the field. In this article, we shall deal with electric fields considerably smaller than stated above so that only the transport processes are effected by the field. Thus the effect of the electric field will be treated as a perturbation. The average energy of the emerging secondaries from MgO is of the order of 1 eV and this will not be appreciably affected in this situation. The contemplated effect on δ is also relatively small; a change of 20% for fields of the order of 10^4 to 10^5 V/cm has been reported by Boll (Sec. 2.2.1).

The Transport Equation

The differential equation without field was derived previously (ref. 7, p. 76) and reads as follows:

$$\mu v \frac{\partial F}{\partial x}(x, \epsilon, \mu) - a \frac{\partial}{\partial \epsilon} \left(\frac{v(\epsilon)}{\lambda(\epsilon)} F(x, \epsilon, \mu) \right) = S(x, \epsilon, \mu)$$

where

$$F(x, \epsilon, \mu) = 2\pi \sqrt{2\epsilon} \left(\frac{m}{\hbar^2} \right)^{3/2} f(x, \mathbf{k})$$

F refers to the distribution per unit range of x , ϵ , and μ ; $f(x, P/\hbar)$ is the original distribution in phase space.

Now we have an additional term arising from the electric field \underline{E} ;

$$\left(\frac{\partial f}{\partial t}\right)_{\text{field}} = \frac{e\underline{E}}{\hbar} \cdot \text{grad}_{\underline{k}} f(x, \underline{k}) \quad (1)$$

This equation will be written also in terms of the distribution $F(x, \epsilon, \mu)$ by noticing:

$$\epsilon = \frac{\hbar^2 k^2}{2m} \quad \text{and} \quad \mu = \frac{k_x}{k} \quad (2)$$

If the field is restricted in direction along the polar axis, the k_x component of the gradient is the only remaining component. Changing to (ϵ, μ) , the field term reads:

$$\begin{aligned} \left(\frac{\partial f}{\partial t}\right)_{\text{field}} &= \frac{eE_x}{\hbar} \frac{\partial f}{\partial k_x}(x, \underline{k}) \\ &= eE_x \mu \left(\frac{2\epsilon}{m}\right)^{1/2} \frac{\partial f}{\partial \epsilon}(x, \underline{k}) \\ &\quad + \frac{(1 - \mu^2)}{(2m\epsilon)^{1/2}} eE_x \frac{\partial f}{\partial \mu}(x, \underline{k}) \end{aligned} \quad (3)$$

or in terms of $F(x, \epsilon, \mu)$

$$\left(\frac{\partial F}{\partial t}\right)_{\text{field}} = eE_x \mu v \left(\frac{\partial F}{\partial \epsilon} - \frac{F}{2\epsilon}\right) + \frac{1 - \mu^2}{mv} eE_x \frac{\partial F}{\partial \mu}$$

The total transport equation now becomes:

$$\begin{aligned} \mu v(\epsilon) \frac{\partial F}{\partial x}(x, \epsilon, \mu) + \mu v(\epsilon) eE_x \left[\frac{\partial F}{\partial \epsilon}(x, \epsilon, \mu) \right. \\ \left. - \frac{1}{2\epsilon} F(x, \epsilon, \mu) \right] + \frac{eE_x}{mv(\epsilon)} (1 - \mu^2) \frac{\partial F}{\partial \mu}(x, \epsilon, \mu) \\ - a \frac{\partial}{\partial \epsilon} \left[\frac{v(\epsilon)}{\lambda(\epsilon)} F(x, \epsilon, \mu) \right] = S(x, \epsilon, \mu) \end{aligned} \quad (4)$$

Solution of the Transport Equation

Equation (4) will be solved only for small values of the electric field E_x . To do this, we assume a solution of the form:

$$F(x, \epsilon, \mu) = F_0(x, \epsilon, \mu) + eE_x F_1(x, \epsilon, \mu) \quad (5)$$

This is linear in E_x and all higher terms are neglected. The field E_x will be taken to be constant. F_0 is known and satisfies the following equation (ref. 7, p. 76)

$$\mu v(\epsilon) \frac{\partial F_1}{\partial x}(x, \epsilon, \mu) - a \frac{\partial}{\partial \epsilon} \left(\frac{v(\epsilon)}{\lambda(\epsilon)} F_1(x, \epsilon, \mu) \right) = S(x, \epsilon, \mu)$$

Substituting Eq. (5) in Eq. (4) and neglecting E_x^2 terms we obtain:

$$\begin{aligned} & \mu v(\epsilon) \frac{\partial F_1}{\partial x}(x, \epsilon, \mu) - a \frac{\partial}{\partial \epsilon} \left(\frac{v(\epsilon)}{\lambda(\epsilon)} F_1(x, \epsilon, \mu) \right) \\ & - v(\epsilon) \mu \frac{\partial F_0}{\partial \epsilon}(x, \epsilon, \mu) + \mu \frac{v(\epsilon)}{2\epsilon} F_0(x, \epsilon, \mu) - \\ & - \frac{(1 - \mu^2)}{mv(\epsilon)} \frac{\partial F_0}{\partial \mu}(x, \epsilon, \mu) \end{aligned} \quad (6)$$

To simplify the solution of Eq. (6) we change to:

$$\Psi_1(x, \epsilon, \mu) = \frac{v(\epsilon)}{\lambda(\epsilon)} F_1(x, \epsilon, \mu) \quad (7)$$

and $\Psi_0(x, \epsilon, \mu) = \frac{v(\epsilon)}{\lambda(\epsilon)} F_0(x, \epsilon, \mu)$. Equation (6) then reads:

$$\begin{aligned} & \mu \lambda(\epsilon) \frac{\partial \Psi_1}{\partial x}(x, \epsilon, \mu) - a \frac{\partial \Psi_1}{\partial \epsilon}(x, \epsilon, \mu) \\ & - \mu v(\epsilon) \frac{\partial}{\partial \epsilon} \left[\frac{\lambda(\epsilon)}{v(\epsilon)} \Psi_0(x, \epsilon, \mu) \right] + \frac{\mu}{2\epsilon} \lambda(\epsilon) \Psi_0(x, \epsilon, \mu) \\ & - \frac{(1 - \mu^2)}{mv(\epsilon)^2} \lambda(\epsilon) \frac{\partial \Psi_0}{\partial \mu}(x, \epsilon, \mu) \end{aligned} \quad (8)$$

The variable ϵ is now changed to η by the relation:

$$\eta = \int_0^{\epsilon} \lambda(\epsilon') d\epsilon'$$

to obtain finally:

$$\begin{aligned} \mu \frac{\partial \psi_1}{\partial x}(x, \eta, \mu) - a \frac{\partial \psi_1}{\partial \eta}(x, \eta, \mu) &= \psi_0(x, \eta, \mu) \\ \left[-\mu v(\eta) \frac{\partial}{\partial \eta} \left(\frac{\lambda(\eta)}{v(\eta)} \right) + \frac{\mu}{2\epsilon(\eta)} \right] - \mu \lambda(\eta) \frac{\partial \psi_0}{\partial \eta} \\ (x, \eta, \mu) - \frac{(1 - \mu^2)}{2\epsilon(\eta)} \frac{\partial \psi_0}{\partial \mu}(x, \eta, \mu) & \end{aligned} \quad (9)$$

Equation (9) is solved in Appendix I first for a general source function $S(x, \epsilon, \mu)$. This method is then applied to the case where the source function is $A\delta(x - x_0)e^{-\eta}$. After the usual transformation to η the above source function leads to the following solution:

$$\begin{aligned} \psi_1(x, \eta, \mu) &= \frac{B}{a} \left(\frac{c}{a+1} \right)^{1/(a+1)} \frac{(a+1)}{2\mu |\mu|} \left\{ \frac{\eta}{u^{a+1}} \cdot \right. \\ & \left[\frac{1}{a} (\mu^2(\gamma + 1 - 2a) - \gamma + 1) + \frac{\gamma}{2a+1} (\mu^2(2a+1) + 1) \right] \\ & - \eta^{\frac{a}{a+1}} u^{-\gamma} \frac{1}{a} \left[\mu^2(\gamma + 1 - 2a) - \gamma + 1 \right] - \eta^{\frac{2a+1}{a+1}} \\ & \left. u^{-(\gamma+1)} \frac{\gamma}{2a+1} \left[\mu^2(2a+1) + 1 \right] \right\} \end{aligned} \quad (10)$$

where

$$u = \eta + \frac{a(x - x_0)}{\mu}$$

$$\gamma = \frac{n+a}{a+1}$$

and

$$B = \frac{A}{c} \left(\frac{c}{a+1} \right)^{\frac{n+a}{a+1}}$$

This solution satisfies the boundary condition $\psi_1(x_0, \eta, \mu) = 0$, indicating that the field has no affect at the source.

An important feature of the solution (10) is that it changes sign when one goes from $x > x_0, \mu > 0$ to $x < x_0, \mu < 0$. This is to be expected because the unperturbed transport is a diffusion process, symmetrical with respect to the source at x_0 , whereas the drift due to the field either aids or opposes the transport of the secondaries away from the source (Fig. 41).

The complete solution (5) is valid only when $eE_x F_1 \ll F_0$ for the region (x, η, μ) of interest. This will be the case if the energy gained by an electron from the field in traversing a mean free path is small compared to the energy loss per collision. An equivalent condition can be derived from the inequality

$$eE_x \psi_1(x, \eta, \mu) \ll \psi_0(x, \eta, \mu) \quad (11)$$

Effect of the Electric Field on the Escape Mechanism

The additional current density due to the field will be given by:

$$j_1(\epsilon, \mu) = \mu \lambda(\epsilon) eE_x \psi_1(x, \epsilon, \mu) \quad (12)$$

The secondary emission coefficient δ_1 , caused by the field, can be found by integrating Eq. (12) with respect to ϵ and μ over the region D, described by

$$\mu^2 \epsilon \geq \omega$$

and

$$\left(\frac{\omega}{\epsilon_{00}} \right)^{1/2} \leq \mu \leq 1$$

where ϵ_{00} is the maximum energy of electrons at the surface and ω is the electron affinity. Hence

$$\delta_1 = \iint_D j_1(\epsilon, \mu) d\epsilon d\mu$$

Accordingly, the no-field yield calculated before will be denoted by δ_0 :

$$\delta_0 = \iint_D \mu \lambda \psi_0(x=0, \epsilon, \mu) d\epsilon d\mu$$

It is clear from Eq. (12) that the variation of δ with respect to the electric field is linear.

Example - (a) Plane Source at x_0 .

The above theory now will be applied to the case of an ionic crystal like MgO. The exponent in the excitation function will be chosen as $n = 2$. $\lambda(\epsilon) = 1.6\epsilon$ in Å where ϵ is in eV. The distance $d = x_0$ is of the order of the range of the primaries. We take an isotropic distribution for momentum of the electrons produced at the source. For this case the perturbing solution for $x < x_0$, $\mu < 0$ is much simplified:

$$\psi_1(x, \eta, \mu) = \frac{Ac}{4a} \left[\frac{1 + 3\mu^2}{2\mu^2} \eta^{3/2} u^{-5/2} - \frac{1 - \mu^2}{2\mu^2} \eta^{1/2} u^{-3/2} - \frac{2}{u} \right] \quad (13)$$

The perturbation treatment holds for fields up to 10^5 volts/cm. The secondary emission coefficient calculated by integrating (12) over the region D is plotted in Fig. 42. The calculations were done on an ERA 1103 computer, taking $\epsilon_{00} = 10$ eV and various values of ω and d , and for electric fields in the above mentioned range. Also some experimental data obtained by Boll from the variation of δ with change in surface potential (for $\epsilon_p = 900$ eV) are plotted for comparison. Evidently the magnitude of the calculated effect is close to the observed effect. The calculated values depend on a , $\lambda(\epsilon)$ and ω and d , none of these values are known with great accuracy and accordingly, the calculated result is only indicative as to the order of magnitude. The dependence on d reflects the dependence on primary energy to some extent; the slope of the curves increases as d increases, and therefore as ϵ_p increases. However, the range-energy relationship for a planar source model is not known; for that reason, we investigate in the next section a uniform source model, as employed in the "constant loss theory".

Example - (b) Uniform Volume Source for $x_0 \leq d$

From experimental evidence, it appears that the spatial distribution of sources in an insulator lies between a planar source at $x = x_0$ and a uniform volume source for $x_0 \leq d$. To test this hypothesis calculations were made for a uniform source where the source extends from 0 to d where d is given by the range energy relationship, $d = 300 \epsilon_p^{1.35}$ in Å when ϵ_p is in keV. The results can be obtained by integrating the planar source results, letting x_0 range from 0 - $d(\epsilon_p)$.

First of all, a new solution for ψ_0 and for δ_0 (no field) was obtained. The variation of δ_0 with electron affinity is given in Fig. 43. This result should be compared with the previous results (ref. 7, Fig. 76) which pertained to the δ -function source. The general behavior is the same. The effect of the electric field was obtained by integrating the ψ_1 solution, and by determining δ_1 as a function of ω and ϵ_p with the computer. The result is given in Fig. 44, where δ_1/δ_0 , i.e., the relative enhancement or deenhancement of the secondary emission yield, was plotted versus E . Of course, the relationship is linear in this perturbation approach; the slopes are indicative for the order of magnitude of the effect and for the variation with ϵ_p . The dependence on the electron affinity ω is apparently very small. For comparison, data by Boll are given in Fig. 45. It is noted that the general trend of the curves, in particular the dependence on ϵ_p , is comparable with the calculated effect. However, the observed magnitude differs by a factor 3 (notice that scales for δ_1/δ_0 in Figs. 44 and 45 differ). As said before, however, many not well known parameters enter into the calculated values so that this discrepancy should not be surprising. The measured effect seems to deviate from the linear approximation for high primary energy for relatively low fields. To obtain a result for higher fields, higher order perturbation terms are necessary, or another approach should be followed. A general curve giving the calculated slope $(\delta_1/\delta_0)/E$ versus ϵ_p for various values of ω is plotted in Fig. 46. The effect of ϵ_p on the slope is clearly manifest in this figure.

APPENDIX I

Presently we have to solve Eq. (9) (Sec. 2.3.2) which reads:

$$\begin{aligned} \mu \frac{\partial \psi_1}{\partial x}(x, \eta, \mu) - a \frac{\partial \psi_1}{\partial \eta} = \mu \psi_0(x, \eta, \mu) \left[-v(\eta) \frac{\partial}{\partial \eta} \left(\frac{1}{v(\eta)} \right) \right. \\ \left. + \frac{1}{2e(\eta)} \right] - \mu \lambda(\eta) \frac{\partial \psi_0}{\partial \eta}(x, \eta, \mu) - \frac{(1 - \mu^2)}{2e(\eta)} \frac{\partial \psi_0}{\partial \mu}(x, \eta, \mu) \end{aligned} \quad (9)$$

where $\Psi_0(x, \eta, \mu)$ is given by

$$\Psi_0(x, \eta, \mu) = \frac{1}{a} \int_{\eta}^{\eta_1} \sigma \left[x + \frac{\mu}{a} (\eta - \eta'), \eta', \mu \right] d\eta' \quad (I-1)$$

We note that the left hand side of (9) and of the inhomogeneous equation solved before for the field free case are similar (compare ref. 7, Eq. 49). Further if $\sigma(x, \eta, \mu)$ is a sum of many terms, i.e.,

$$\sum_i \sigma_i(x, \eta, \mu),$$

it is easily shown that the solution is additive. Equation (9) has a right hand side which can be considered as

$$\sum_i \sigma_i(x, \eta, \mu)$$

and then the solution for each one can be obtained from the previous result as given by (I-1) using proper sources

$\sigma_i(x, \eta, \mu)$. However, the solution obtained will be a Fourier transform solution satisfying the relevant boundary conditions employed previously; other boundary conditions can be satisfied by adding the homogeneous solution to the result.

From (I-1), we find that a particular solution resulting from the r.h.s. term of Eq. (9)

$$\mu \Psi_0 \left[\frac{1}{2\epsilon(\eta)} - v(\eta) \frac{\partial}{\partial \eta} \left(\frac{\lambda(\eta)}{v(\eta)} \right) \right]$$

is given by

$$\begin{aligned} \Psi_1^{(1)}(x, \eta, \mu) &= \frac{\mu}{a} \int_{\eta}^{\eta_2} \Psi_0 \left[x + \frac{\mu}{a} (\eta - \eta'), \eta', \mu \right] \\ &\cdot \left[\frac{1}{2\epsilon(\eta')} - v(\eta') \frac{\partial}{\partial \eta'} \left(\frac{\lambda(\eta')}{v(\eta')} \right) \right] d\eta' \quad (I-2) \end{aligned}$$

Substituting for Ψ_0 (I-1) we get:

$$\Psi_1^{(1)}(x, \eta, \mu) = \frac{\mu}{a^2} \int_{\eta}^{\eta^2} d\eta' \left[\frac{1}{2\epsilon(\eta')} - v(\eta') \frac{\partial}{\partial \eta'} \cdot \left(\frac{\lambda(\eta')}{r(\eta')} \right) \right] \int_{\eta}^{\eta^1} \sigma \left[x + \frac{\mu}{a} (\eta - \eta'), \eta'', \mu \right] d\eta'' \quad (I-3)$$

The term $-\frac{\partial \Psi_0}{\partial \eta}(x, \eta, \mu)$ in Eq. (9) contributes the following to the solution:

$$\Psi_1^{(2)}(x, \eta, \mu) = -\frac{\mu}{a} \int_{\eta}^{\eta^2} \lambda(\eta') \left[\frac{\partial \Psi_0}{\partial \eta}(x, \eta, \mu) \right] \begin{matrix} d\eta' \\ \eta' \rightarrow \eta' \\ x \rightarrow x + \frac{\mu}{a} (\eta - \eta') \end{matrix} \quad (I-4)$$

where again the zero order solution for Ψ_0 as given by (I-1) has to be substituted, yielding:

$$\frac{\partial \Psi_0}{\partial \eta}(x, \eta, \mu) = -\frac{\sigma(x, \eta, \mu)}{a} + \frac{1}{a} \int_{\eta}^{\eta^1} \frac{\partial}{\partial \eta} \left[\sigma \left\{ x + \frac{\mu}{a} (\eta - \eta''), \eta'', \mu \right\} \right] d\eta'' \quad (I-5)$$

Calling

$$\frac{\partial \sigma}{\partial x}(x, \eta, \mu) = \sigma_1(x, \eta, \mu) \quad (I-6)$$

$$\frac{\partial}{\partial \eta} \left\{ \sigma \left[x + \frac{\mu}{a} (\eta - \eta''), \eta'', \mu \right] \right\} = \frac{\mu}{a} \sigma_1 \left[x + \frac{\mu}{a} (\eta - \eta''), \eta'', \mu \right] \quad (I-7)$$

(I-4) reads:

$$\psi_1^{(2)}(x, \eta, \mu) = \frac{\mu}{a^2} \int_{\eta}^{\eta^2} \lambda(\eta') d\eta' \cdot \sigma \left[x + \frac{\mu}{a} (\eta - \eta'), \eta', \mu \right] - \frac{\mu}{a} \int_{\eta}^{\eta^1} d\eta'' \sigma_1 \left[x + \frac{\mu}{a} (\eta - \eta''), \eta'', \mu \right] \quad (I-8)$$

Similarly, the last term $-\frac{(1-\mu^2)}{2\epsilon(\)} \frac{\partial \psi_0}{\partial \mu}(x, \eta, \mu)$ gives the solution:

$$\psi_1^{(3)}(x, \eta, \mu) = -\frac{1-\mu^2}{2a} \int_{\eta}^{\eta^2} \frac{1}{\epsilon(\eta')} \cdot \left[\frac{\partial \psi_0}{\partial \mu}(x, \eta, \mu) \right]_{\substack{d\eta' \\ \eta \rightarrow \eta' \\ x \rightarrow x + \frac{\mu}{a} (\eta - \eta')}} \quad (I-9)$$

Calling

$$\frac{\partial \sigma}{\partial \mu}(x, \eta, \mu) = \sigma_2(x, \eta, \mu) \quad (I-10)$$

and using (I-6) we obtain:

$$\psi_1^{(3)}(x, \eta, \mu) = -\frac{1-\mu^2}{2a^2} \int_{\eta}^{\eta^2} \frac{d\eta'}{\epsilon(\eta')} \int_{\eta}^{\eta^1} d\eta'' \left\{ \frac{\eta' - \eta''}{a} \cdot \sigma_1 \left[x + \frac{\mu}{a} (\eta - \eta''), \eta'', \mu \right] + \sigma_2 \left[x + \frac{\mu}{a} (\eta - \eta''), \eta'', \mu \right] \right\} \quad (I-11)$$

Thus a particular solution for Eq. (9) reads

$$\psi_1(x, \eta, \mu) = \sum_{i=1}^3 \psi_1^{(i)}(x, \eta, \mu) \quad (I-12)$$

where $\psi_1^{(i)}(x, \eta, \mu)$, $i=1,2,3$ are defined by Eqs. (I-3), (I-8) and (I-11).

The solution of the homogeneous equation which is of the form $H(u)$ where $u = \eta + ax/\mu$ will be added to (I-12). The function $H(u)$ is arbitrary and has to be determined.

In what follows we shall confine ourselves to the special excitation function:

$$S(x, \epsilon, \mu) = A\delta(x - x_0)e^{-n}$$

the unperturbed solution was given by:

$$u_0(x, \epsilon, \mu) = \frac{B}{|\mu|} u_0^{-\gamma} \quad (I-13)$$

where

$$B = \frac{A}{c} \left(\frac{c}{\alpha + 1}\right)^\gamma, \quad \gamma = \frac{n + \alpha}{\alpha + 1} \quad (I-14)$$

and

$$u_0 = \eta + \frac{a(x - x_0)}{\mu} \quad (I-15)$$

and $\lambda(\epsilon)$ has been assumed to have the form $c\epsilon^\alpha$. Thus

$$\eta = \frac{c}{\alpha + 1} \epsilon^{\alpha + 1}.$$

Substituting (I-13) into (I-3) we obtain:

$$\begin{aligned} \psi_1^{(1)}(x, \eta, \mu) = & \frac{B}{a} \frac{\mu}{|\mu|} u_0^{-\gamma} \int_{\eta}^{\eta_2} \left[\frac{1}{\epsilon(\eta')} \right. \\ & \left. - \nu(\eta') \frac{\partial}{\partial \eta'} \left(\frac{\lambda(\eta')}{\nu(\eta')} \right) \right] d\eta'. \end{aligned} \quad (I-16)$$

In (I-3) it should be noted that the range of η'' is

$$\eta_1 \geq \eta'' \geq \eta' \geq \eta.$$

Further for the second term, we obtain (taking care in handling the derivative of the 8-function)

$$\Psi_1^{(2)}(x, \eta, \mu) = \frac{B}{a} \frac{\mu}{|\mu|} u_0^{-\gamma+1} \int_{\eta}^{\eta_2} \lambda(\eta^{\circ}) d\eta^{\circ} \quad (I-17)$$

Similarly for $\Psi_1^{(3)}$:

$$\Psi_1^{(3)}(x, \eta, \mu) = \frac{B(1-\mu^2)}{2a \mu |\mu|} u_0(x, \eta, \mu)^{-(\gamma+1)} \int_{\eta}^{\eta_2} \left[(1-\gamma)\gamma\eta^{\circ} \right] \frac{d\eta^{\circ}}{e(\eta^{\circ})} \quad (I-18)$$

Combining the solutions $\Psi_1^{(1)}$, $\Psi_1^{(2)}$, and $\Psi_1^{(3)}$, $\Psi_1(x, \eta, \mu)$ reads:

$$\begin{aligned} \Psi_1(x, \eta, \mu) = & \frac{B}{a} \left(\frac{c}{a+1} \right)^{\frac{1}{a+1}} \frac{1}{2a\mu |\mu|} \left[\mu^2(\gamma+1-2a) - \gamma + 1 \right] \\ & \cdot \left[\eta_2^{\frac{a}{a+1}} - \eta^{\frac{a}{a+1}} u_0^{-\gamma} + \frac{B}{a} \left(\frac{c}{a+1} \right)^{\frac{1}{a+1}} \right. \\ & \cdot \gamma \frac{a+1}{(2a+1) \mu |\mu|} \left[\mu^2(2a+1) + 1 \right] \\ & \left. \cdot \left[\eta_2^{\frac{2a+1}{a+1}} - \eta^{\frac{2a+1}{a+1}} \right] u_0^{-(\gamma+1)} + H\left(\eta + \frac{ax}{\mu}\right) \right] \quad (I-19) \end{aligned}$$

Now we apply the boundary condition: $\Psi_1(x, \eta, \mu) = 0$ for any η at $x = x_0$, indicating that the field has no effect on the solution at the source. This gives the function H , and finally substituting back in the result, we obtain:

$$\begin{aligned}
\psi_1(x, \eta, \mu) = & \frac{B}{a} \left(\frac{c}{a+1} \right)^{\frac{1}{a+1}} \frac{1+\alpha}{2\mu/|\mu|} \left\{ u_0^{-\frac{n}{a+1}} \right. \\
& \cdot \left[\frac{1}{a} \left(\mu^2(\gamma+1-2\alpha) \right) + \frac{\gamma}{2\alpha+1} \left(\mu^2(2\alpha+1)+1 \right) \right] \\
& - \eta^{\frac{\alpha}{a+1}} u_0^{-\gamma} \frac{1}{a} \left[\mu^2(\gamma+1-2\alpha) - \gamma+1 \right] - \\
& \left. - \eta^{\frac{2\alpha+1}{a+1}} u_0^{-(\gamma+1)} \frac{\gamma}{2\alpha+1} \left[\mu^2(2\alpha+1)+1 \right] \right\} \quad (I-20)
\end{aligned}$$

The above solution does not contain u_2 anymore, the specification of u_2 is not necessary since we used in the special model a δ -type source function.

3. CONCLUSIONS

3.1 Interactions between Electrons and Solids

3.1.1 The Variation of the Secondary Yield from Single Crystals with the Angle of Incidence of the Primary Beam

In the study of the variation of secondary emission with the angle of incidence of the primary beam, it is necessary that titanium single crystals be sputter-cleaned in order that reproducible results may be obtained. The errors introduced when titanium is not sputter-cleaned are largely related to the magnitude of the peaks. Tungsten, however, need not be so cleaned. The asymmetrical structure observed in the angular dependence studies is the result of misalignment of the crystals. The energy dependence of the magnitude of the structure in the angular dependence curves for tungsten is basically the same as for titanium and germanium.

3.1.2 Transmission of Electrons through Thin Gold Films

Gold films suitable for electron transmission experiments may be prepared by epitaxial growth on NaCl single-crystal substrates. The reflection and transmission yield of these films may be measured reproducibly. The energy distribution of the transmitted electrons seems to show considerable structure which cannot be resolved with confidence except at the high-energy end.

At energies several hundred eV below the primary energy however a large peak in the energy distribution occurs and measurements on this peak seem possible using the present measuring technique. No electrons having energies between those of the primary beam and of this peak are observed. This implies a characteristic energy loss of several hundred eV and furthermore gives assurance that the films used in these experiments are free from pinholes. The analysis of the experimental results is still in progress and more detailed conclusions must await its completion.

3.2 Experiments Intended to Improve the Understanding of Processes Occurring in Practical Dynodes

3.2.1 MgO Thin Film Studies

The results of contact potential measurements on MgO films of different thicknesses show that in thermal equilibrium the space charge region at the contact between the MgO film and its metal substrate is less than 15 Å in thickness. The technique which was developed to measure the surface potential is still proving useful in that it allows a much more detailed evaluation of a given MgO film than was previously possible. It has been possible, for example, to conclude for a particular group of films that electrons are trapped in surface states while holes are probably trapped in bulk states. The importance of a detailed evaluation of a given film is emphasized by the fact that films of a second group seem to behave quite differently in that they display an intense cathodoluminescence. Only by an intense study of the secondary emission, thermal decay of surface potential, photoemission and photoconductivity will it be possible to determine the real nature of such striking differences among various groups of films.

3.2.2 Secondary Emission Characteristics of Al₂O₃ Thin Films

The use of Ta₂O₅ films in the sputtering arrangement used in the Al₂O₃ study will allow a determination of the uniformity of the sputtering rate. The thickness of the sputtered film may be measured at various positions by locating the wavelength of the minimum reflectivity. The geometry of the sputtering tube can then be changed in order to achieve the uniform rate which is desirable for this experiment as well as for several others presently in progress.

3.2.3 Dissociation of Compounds by Electron Bombardment

As a result of the fact that electrical conduction in alkali halides is to a large extent an ionic process, a large fraction of the observed dissociation may be the result of electrolysis of the film. Thus it does not appear feasible to continue the study of these materials at this time.

The dissociation of MgO proceeds more slowly but reproducible results can be obtained. Transient effects occur however when the bombardment is initiated and these imply that some fraction of the observed ion current is in fact due to the desorption of surface atoms obtained from the residual gas when the target is not bombarded. A detailed analysis of the data implies that, in the steady state, the residual-gas effect is small but further confirmation is required.

3.2.4 Diffraction of Slow Electrons by MgO

The (001) surface of a MgO crystal which has been cleaved in air is covered with two different types of structure. One is a square structure which has the MgO lattice constant. The other is similar but has double spacing in those azimuths for which the sum of the indices is even. The surface of the crystal was not cleaned by the argon-sputtering experiments so far attempted but this may be a consequence of a tube design which prevented efficient sputtering.

3.3 Theoretical Studies

3.3.1 Theoretical Model of the Mechanism Resulting in Structure in the Variation of Secondary Emission with Angle of Incidence of the Primary Beam

It is possible to explain, in a qualitative way, many of the characteristics of the variation of the secondary emission from single crystals with the angle of incidence of the primary beam. The model used is based upon the assumption of localization of both the primary electron and the lattice electron density. The primary electron is assumed to be localized at the point of an inelastic collision and to be represented by a spherical wave thereafter. The spherical wave is however strongly peaked in the direction of the initial momentum and hence is expected to undergo other inelastic collisions along this line. Now, if the lattice electron density is localized in the vicinity of the nucleus most of the inelastic collisions will occur in this vicinity. Thus the energy loss per unit path length will be particularly large when the initial momentum coincides in direction with a crystallographic direction of high lineal atomic density, i.e., with a zone axis. Such angles of incidence should show peaks in the secondary yield as observed (for primary energies which are not too low). Several other features of the experimental results, notably the dependence of the peak width on primary energy, also follow from the model.

3.3.2 Effect of an Electric Field on the Escape of Secondary Electrons from Polar Crystals

The effect of relatively small electric fields (up to 10^6 V/cm) on the escape of secondary electrons from insulators has been calculated. The result is in fair agreement with

experiment. The change in the yield is proportional to the field in the approximation used and the way in which the proportionality factor was found to vary with primary energy is in agreement with experiment although its magnitude is somewhat less. Since the computation involves the use of some parameters whose numerical values are not well known, the agreement between the theory and the experiment is considered to be quite satisfactory.

4. RECOMMENDATIONS

The work described in the foregoing sections is a combination of pure research having to do with the interactions between electrons and solids, of other basic experimental research having a more obvious connection with the applications of secondary electron emission, and of theoretical studies carried out in support of, and as stimulation for, the experimental work. It is believed that this type of program leads most effectively towards the desired goal, viz., the improvement of the understanding of practical secondary emitters and of the secondary emission process.

The nature of the dependence of the secondary yield on the angle of incidence has an important bearing on the theory of secondary emission as is evidenced by the models proposed to account for the effect (Sec. 2.3.1). During this contract period definitive experimental results were obtained for the first time for the cases of Ti and W. It is hoped that these results may be repeated using a specimen of much lower atomic number (say Be) in order to test the predictions of the current model. Once this has been accomplished, attention should be focussed on the obtaining of a more detailed, semi-quantitative theory. Such a theory would no doubt suggest ramifications of the experiments already carried out. Furthermore, it seems that the details of the SEAI curves are sensitive to conditions near and/or at the surface and once a suitable understanding of the effect is obtained the measurement of SEAI curves might serve as a useful complement to the slow electron diffraction technique in the detailed study of surfaces.

The preliminary energy analyses of the electrons transmitted through gold films indicate that a characteristic energy loss of several hundred eV occurs. This loss may be due to plasma excitations and, if this is indeed the case, this study should be carried forward with some emphasis on this aspect of the experiment. The experiment which is presently in progress should be extended to higher primary energies and should be repeated with films of various thickness. In addition more attention should be given to the cleanliness of the film since some plasma modes will no doubt depend on the condition of the surface, i.e., on the boundary conditions on the plasma.

The energy loss discussed above is the lowest one observed. There are of course many of the transmitted electrons which have lost more than this amount of energy but attempts to obtain an

energy distribution curve for these electrons have so far been unsuccessful. Because of the likelihood that more characteristic loss peaks would appear in this energy region, the experimental technique should be changed to one capable of detecting such peaks. The most promising technique appears to be one in which a small audio-frequency voltage is superimposed on the dc collector potential and the ac component of the collector current is measured. This amounts to the measurement of the dc retarding potential characteristic followed by its electrical differentiation; the requirement of high-precision retarding-potential data is thus removed and more reproducible results should be obtainable.

The techniques applied to the study of MgO films during this contract period have proven valuable in providing information which is usually very difficult to obtain for a system as difficult to work with as an insulating thin film. The information so far obtained raises the hope that in the future one will be able to determine the electronic energy levels (surface and bulk) associated with a given method of preparation or with given deliberately added impurities. At this stage one could presumably introduce levels so as to achieve a desired effect. For example, the long-term yield changes which are observed are believed to be associated with long-term changes in the internal electric field which, in turn, are probably the result of slow changes in the occupancy of some type(s) of traps. If these traps could be dominated by a small time constant trap, deliberately introduced, stability of the yield might be achieved.

In view of the above remarks, it seems that several more groups of films ought to be thoroughly evaluated in order to correlate the properties with the preparation conditions and with the thickness. Subsequently the effects of known impurity concentrations should be investigated. In this latter connection it is believed that MgO films of known impurity content may be formed by sputtering from crystals containing the desired impurity.

At the present time the question as to the difference between the yields obtainable from MgO films and from MgO single crystals remains unresolved. Furthermore, the origin of the surface levels, whose existence was shown (Sec. 2.2.1), is unknown. Since it is likely that both of these questions are related to surface cleanliness, it is believed that the slow electron diffraction study of MgO should continue. This study offers the best possibility of allowing definite statements to be made as to the conditions required to obtain and maintain a clean MgO surface. Once the sputtering and annealing treatments required to provide a high-yield, ordered surface are established, this information should be used in a study of the influence of the sputtering treatment on the properties of MgO films.

The study of Al₂O₃ films was initiated in the hope that, when the surfaces were adequately cleaned, such films would show secondary yields high enough to be of practical interest. It

had already been shown that Al_2O_3 displays no field-enhancement effect and hence long-term stability was to be expected. Since the investigations have shown that sputter-cleaning does not accomplish the desired objective, it is recommended that this aspect of the program be discontinued, at least temporarily.

The studies of the dissociation of compounds under electron bombardment should be continued. In particular the study of MgO , where controversy still exists as to the dependence of the dissociation rate on current density, should be carried on. In this case, however, the dissociation rate is quite low and the measurements can be obscured by other processes such as the continual desorption by the electron beam of adsorbed atoms of the residual gases. Thus, great emphasis must be laid on the obtaining of low background pressures in the vicinity of the target. In the case of the alkali halides, where the dissociation rates are more rapid, this adsorption-desorption effect is less important but the electric field developed across the film appears to be a factor. Future work on such compounds should therefore be carried out under conditions such that this field is negligible.

The theoretical studies have proven valuable in their stimulation of the experimental program and in the interpretation of the experimental results. As indicated above a more quantitative theory is required for the understanding of the dependence of the secondary emission on the angle of incidence of the primary beam. Because of its importance for the interpretation of slow electron diffraction patterns the quantum mechanics of electron diffraction should also be examined. In fact, it is believed that the same theory may have a bearing on both of these problems. Along the same lines an elaboration of the quantum-mechanical production theory for metals is required in order to take into account the details of the band structure.

BIBLIOGRAPHY

1. W. G. Shepherd, Study of Electrical and Physical Characteristics of Secondary Emitting Surfaces, WADC Technical Report 57-760, Wright Air Development Center, Wright Patterson Air Force Base, Ohio, August 1958.
2. W. G. Shepherd, Study of Electrical and Physical Characteristics of Secondary Emitting Surfaces, WADC Technical Report 59-473, Wright Air Development Center, Wright Patterson Air Force Base, Ohio, December 1959.
3. W. G. Shepherd and B. V. Haxby, Study of Electrical and Physical Characteristics of Secondary Emitting Surfaces, Scientific Report No. 3, Contract No. AF 33(616)-6239, November 15, 1959.
4. W. G. Shepherd and B. V. Haxby, Study of Electrical and Physical Characteristics of Secondary Emitting Surfaces, Scientific Report No. 4, Contract No. AF 33(616)-6239, May 15, 1960.
5. W. T. Peria, Study of Electrical and Physical Characteristics of Secondary Emitting Surfaces, Scientific Report No. 5, Contract No. AF 33(616)-6239, December 31, 1960.
6. W. T. Peria, Study of Electrical and Physical Characteristics of Secondary Emitting Surfaces, Interim Report, Contract No. AF 33(616)-6239, June 30, 1961.
7. W. T. Peria, Study of Electrical and Physical Characteristics of Secondary Emitting Surfaces, Final Report, Contract No. AF 33(616)-6239, ASD-TDR-62-707.
8. W. T. Peria, Determination of Dynamics of Electron Emission from Solids as the Result of Impact, Interim Engineering Report No. 1, Contract No. AF 33(657)-8040, January 16, 1962 to July 15, 1962.
9. R. W. Soshea and A. J. Dekker, "Fine Structure of Secondary Emission vs. Angle of Incidence of the Primary Beam on Titanium Single Crystals," Phys. Rev. 121, 1362 (1961).
10. A. J. Dekker, "Variation of Secondary Electron Emission of Single Crystals with Angle of Incidence," Phys. Rev. Letters 4, 55 (1960).
11. A. B. Laponsky and N. R. Whetten, "Dependence of Secondary Electron Emission from MgO Single Crystals on Angle of Incidence," Phys. Rev. 120, 801 (1960).

BIBLIOGRAPHY (continued)

12. H. E. Farnsworth, et al., "Ion Bombardment-Cleaning of Germanium and Titanium as Determined by Low-Energy Electron Diffraction," *J. Appl. Phys.* 26, 252 (1955).
13. G. Ehrlich and T. G. Hudda, "Interaction of Rare Gases with Metal Surfaces," *J. Chem. Phys.* 30, 493 (1959).
14. G. H. Kinchin and M. W. Thompson, "Irradiation Damage and Recovery in Molybdenum and Tungsten," *J. Nuclear Energy* 6, 275 (1958).
15. E. N. Pugh and L. E. Samuels, "Etching of Absorbed Germanium Surfaces with CP-4 Reagent," *J. Electrochem. Soc.* 109, 409 (1962).
16. Avery Catlin and Walter P. Walker, "Mechanical Properties of Thin Single-Crystal Gold Films," *J. Appl. Phys.* 31, 2135 (1960).
17. G. Haas, "On the Preparation of Hard Oxide Films with Precisely Controlled Thickness on Evaporated Aluminum Mirrors," *J. Opt. Soc. Am.* 39, No. 7, 532-540 (1949).
18. D. A. Vermilyea, "The Kinetics of Formation and Structure of Anodic Films on Tantalum," *Acta. Met.* 1, 282-294 (1953).
19. D. A. Vermilyea, "The Formation of Anodic Oxide Films on Tantalum in Non-Aqueous Solution," *Acta. Met.* 2, 482 (1954).
20. P. Wargo and W. G. Shepherd, "Electron Bombardment Induced Dissociation of Alkaline Earth Oxides," *Phys. Rev.* 106, 694 (1957).
21. H. E. Farnsworth, R. E. Schlier, T. H. George and R. M. Burger, "Application of the Ion Bombardment Cleaning Method to Titanium, Germanium, Silicon and Nickel as Determined by Low-Energy Electron Diffraction," *J. Appl. Phys.* 29, 1150 (1958).
22. H. E. Farnsworth, "Diffraction of Low-Speed Electrons by Single Crystals of Cu and Ag," *Phys. Rev.* 40, 684 (1932).
23. H. E. Farnsworth, "Fine Structure of Electron Diffraction Beams from a Gold Crystal and from a Silver Film on a Gold Crystal," *Phys. Rev.* 43, 900 (1933).
24. W. E. Laschkarew, "Inner Potentials of Crystals and the Electron Diffraction," *Trans. Farad. Soc.* 31, 1081 (1935).
25. H. Raether, "Elektroneninterferenzen," *Hand. Phys.* 32, 466 (Springer-Verlag; Berlin, Goettingen and Heidelberg, 1957).

BIBLIOGRAPHY (continued)

26. H. Bethe, "Theorie der Beugung von Elektronen an Kristallen," Ann. d. Phys. 87, 55 (1928).
27. K. Fujiwara, "Application of Higher Order Born Approximation to Multiple Elastic Scattering of Electrons by Crystals," J. Phys. Soc. Japan 14, 1513 (1959).
28. J. Hoerni, "Multiple Elastic Scattering in Electron Diffraction by Crystals," Phys. Rev. 102, 1534 (1956).
29. E. Fues, "Zur Dynamischen Theorie der Raumgitterbeugung," Z. Phys. I, 109, 14 (1938); Z. Phys. II, 109, 236 (1938).
30. M. Blackman, "On the Intensities of Electron Diffraction Rings," Proc. Roy. Soc. A173, 68 (1939).
31. C. H. MacGillavry, "Zur Prufung der dynamischen Theorie der Elektronenbeugung am Kristallgitter," Physica 7, 329 (1940).
32. R. D. Heindenreich, "Theory of the 'Forbidden' (222) Electron Reflection in the Diamond Structure," Phys. Rev. 77, 271 (1950).
33. A. Howie and M. J. Whelan, "Diffraction Contrast of Electron Microscope Images of Crystal Lattice Defects," Proc. Roy. Soc. A263, 217 (1961).
34. Private communication, E. D. Savoye, Physical Electronics Laboratory, University of Minnesota.
35. David Bohm, QUANTUM THEORY, Prentice-Hall Inc., Englewood Cliffs, New Jersey, 1951, Chap. 22, Sec. 10.
36. H. Witte and E. Wolfel, "Electron Distributions NaCl, LiF, CaF₂ and Al," Rev. Mod. Phys. 30, 51 (1958).
37. A. B. Laponsky, General Electric Co., Research Laboratories, Schenectady, New York, private communication.
38. E. J. Sternglass, "Backscattering of Kilovolt Electrons from Solids," Phys. Rev. 95, 345 (1954).
39. H. Jacobs, J. Freely and F. A. Brand, "The Mechanism of Field Dependent Secondary Emission," Phys. Rev. 88, 492 (1952).
40. D. Dobischek, H. Jacobs and J. Freely, "The Mechanism of Self-Sustained Electron Emission from Magnesium Oxide," Phys. Rev. 91, 804 (1953).
41. F. A. Brand and H. Jacobs, "Energy Distribution of Field Dependent Secondary Electrons," Phys. Rev. 97, 81 (1955).

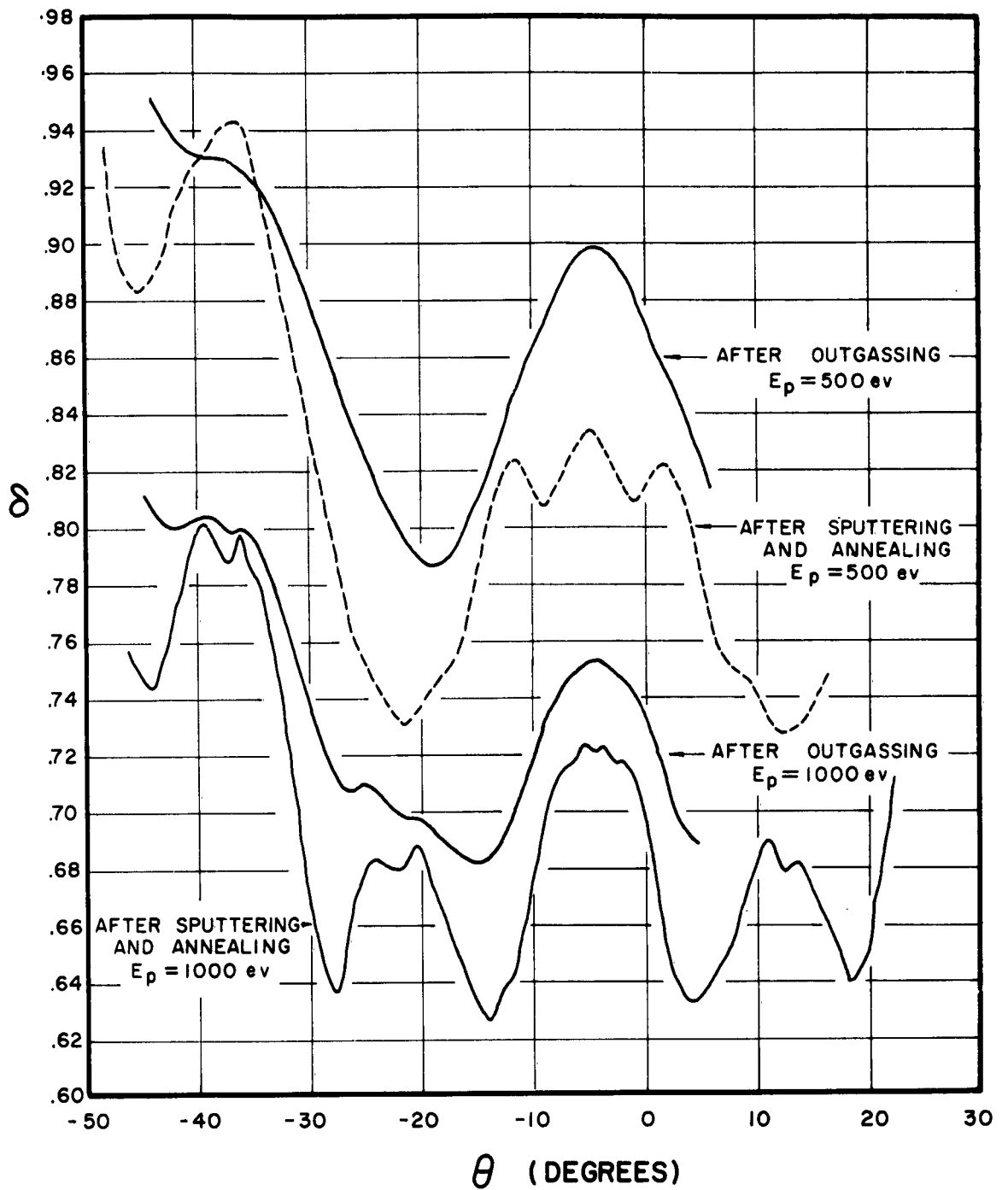


Fig. 1 δ of a Titanium Crystal vs. Angle of Incidence before and after Sputtering and Annealing

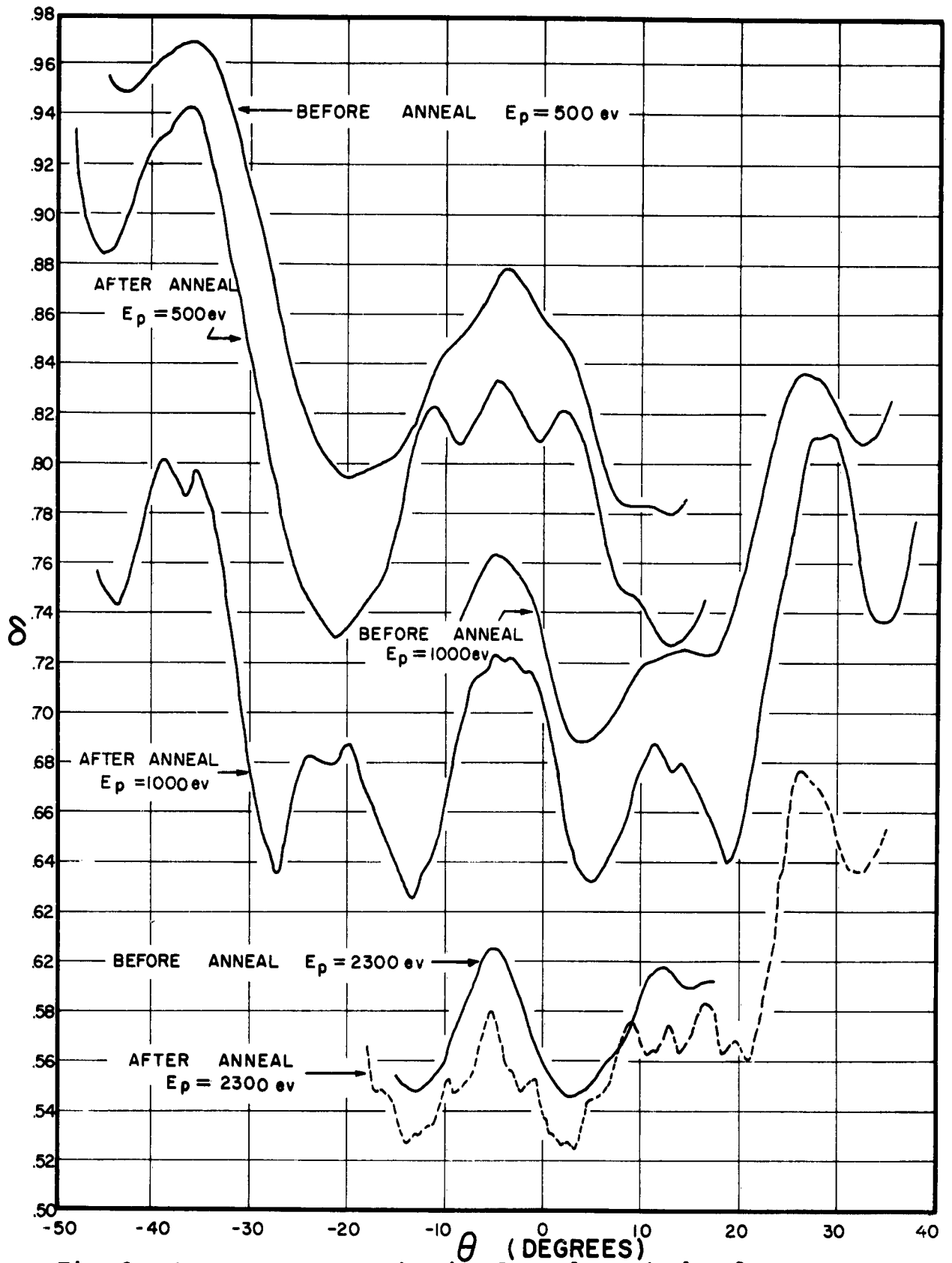


Fig. 2 δ of a Sputtered Titanium Crystal vs. Angle of Incidence before and after Annealing

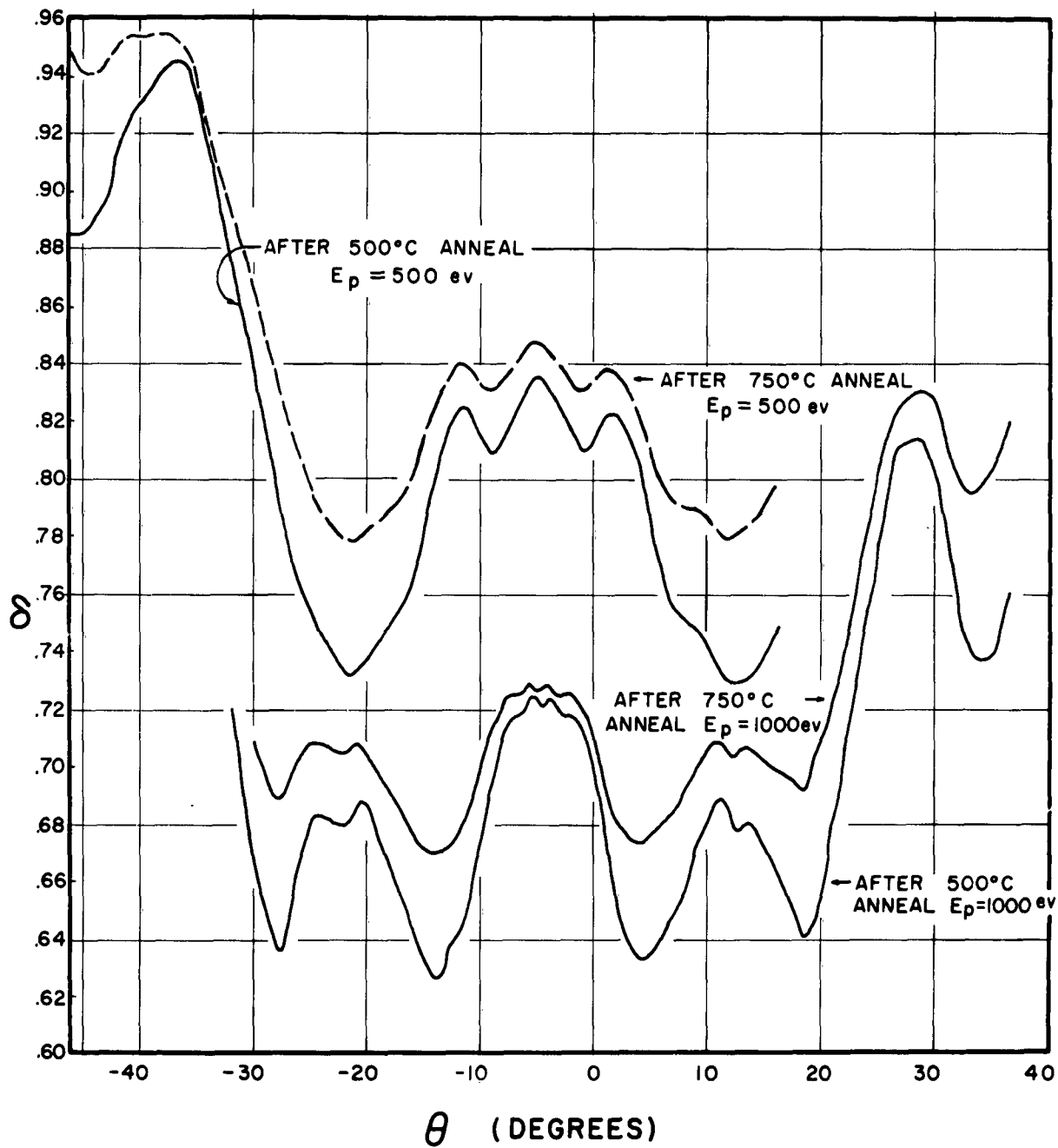


Fig. 3 δ of a Sputtered Titanium Crystal vs. Angle of Incidence for Two Annealing Temperatures

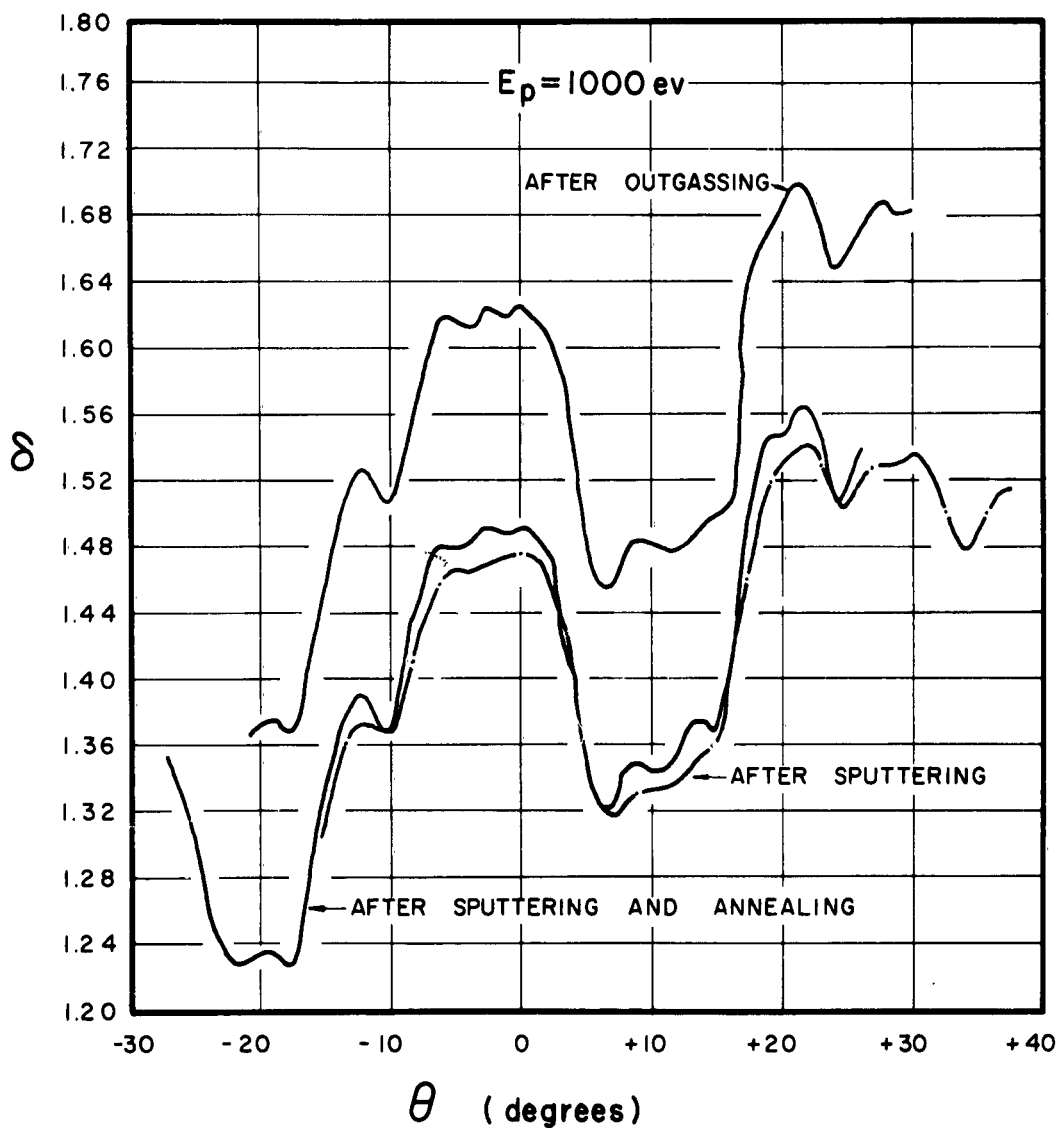


Fig. 4 δ of an Outgassed Tungsten Crystal vs. Angle of Incidence before and after Sputtering, and after Sputtering and Annealing

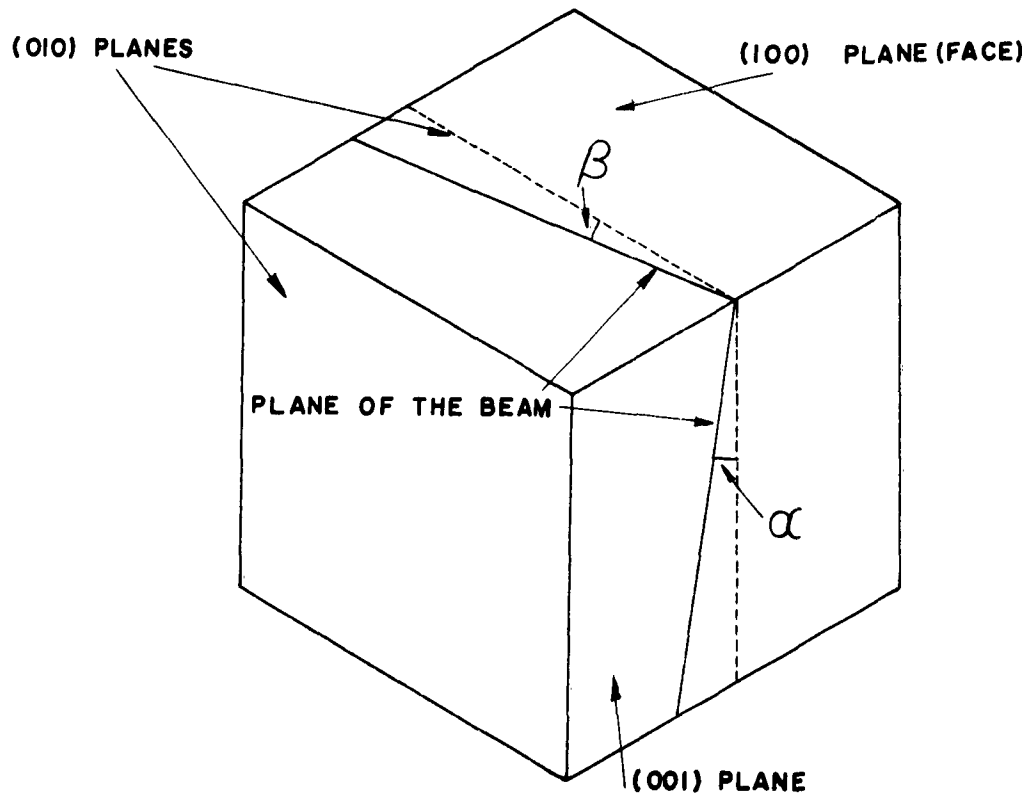


Fig. 5 Possible Misalignments of the Plane of the Primary Beam with Respect to a Crystal Plane

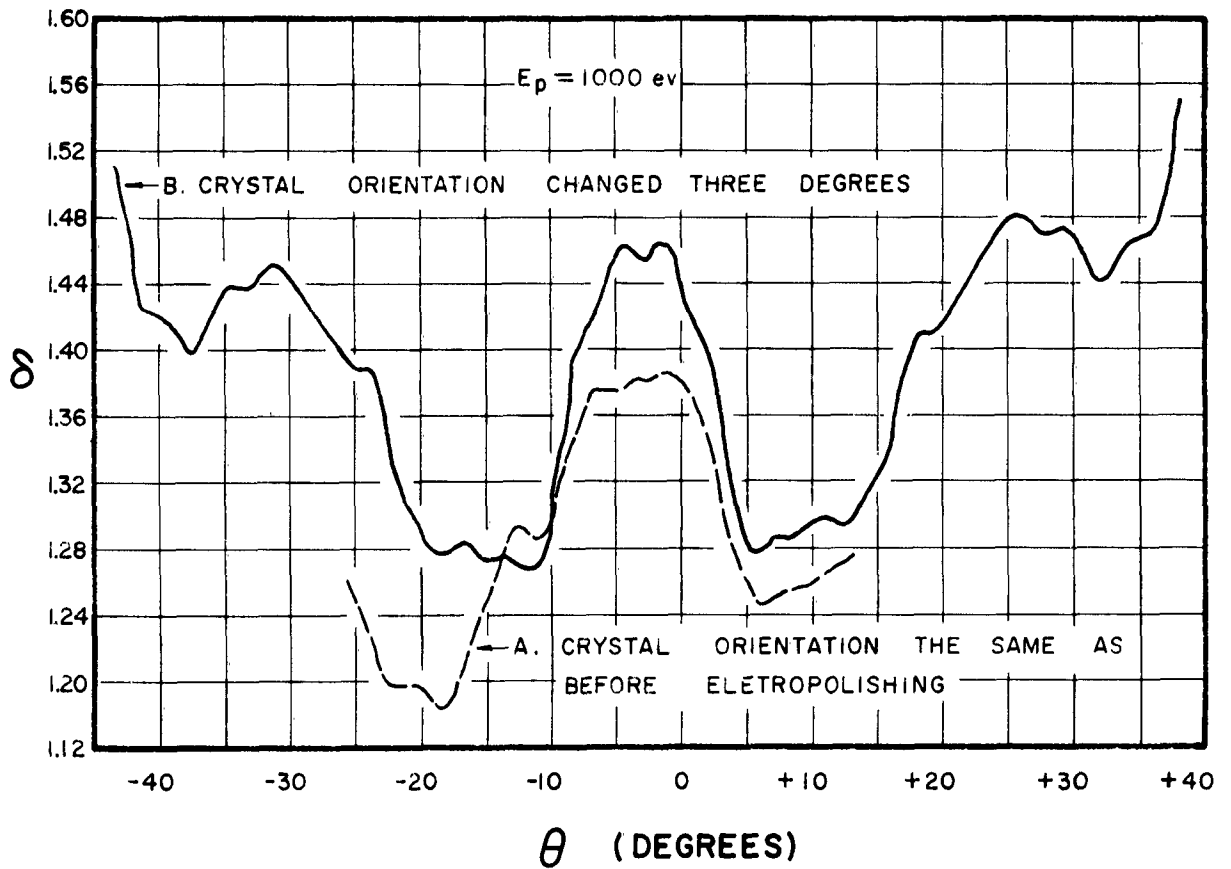


Fig. 6 δ of an Electropolished Tungsten Crystal vs. Angle of Incidence for Two Different Orientations

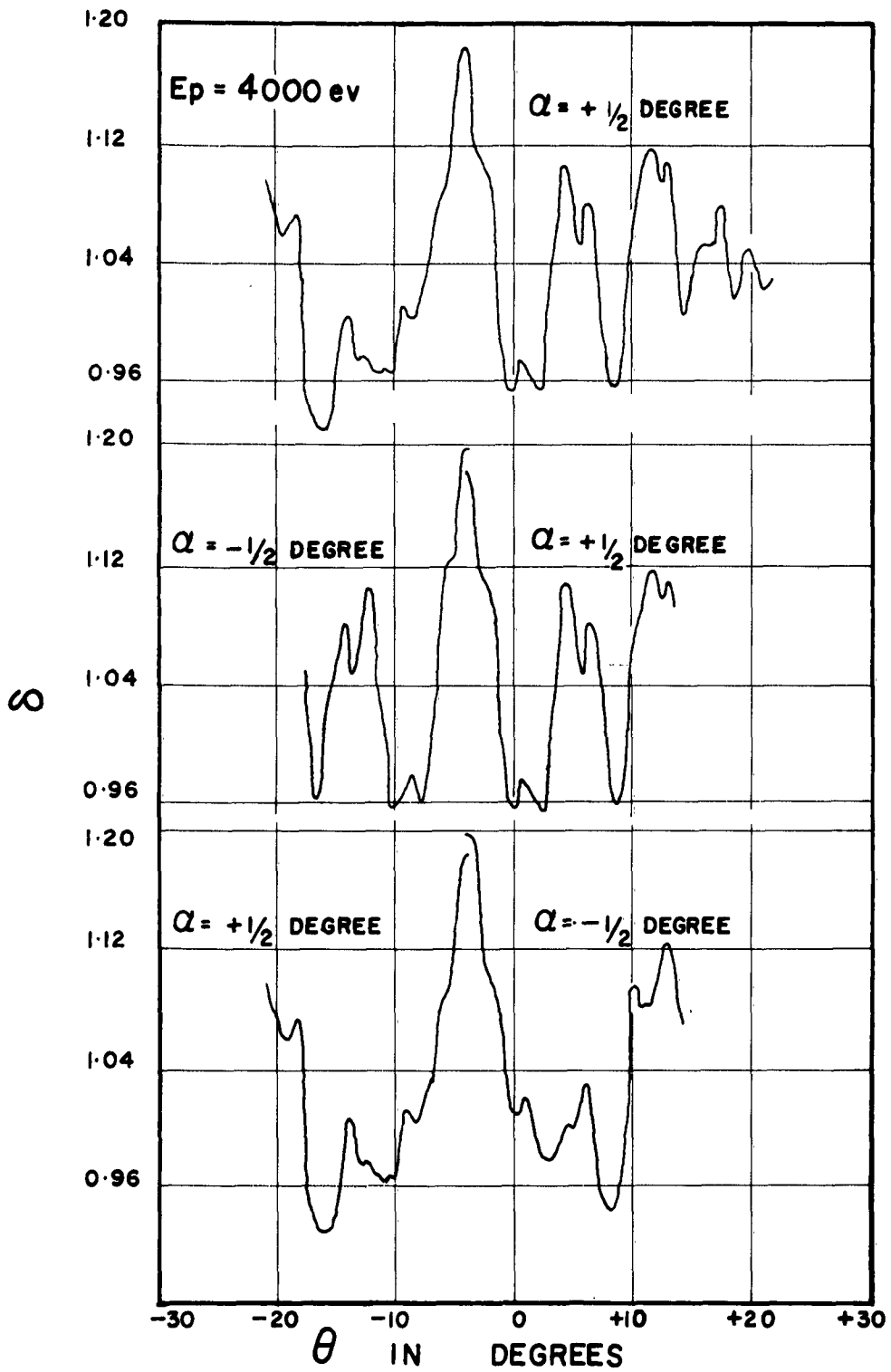


Fig. 7 Correspondence between the Curves of δ vs. Angle of Incidence for Equal and Opposite Alignment Errors

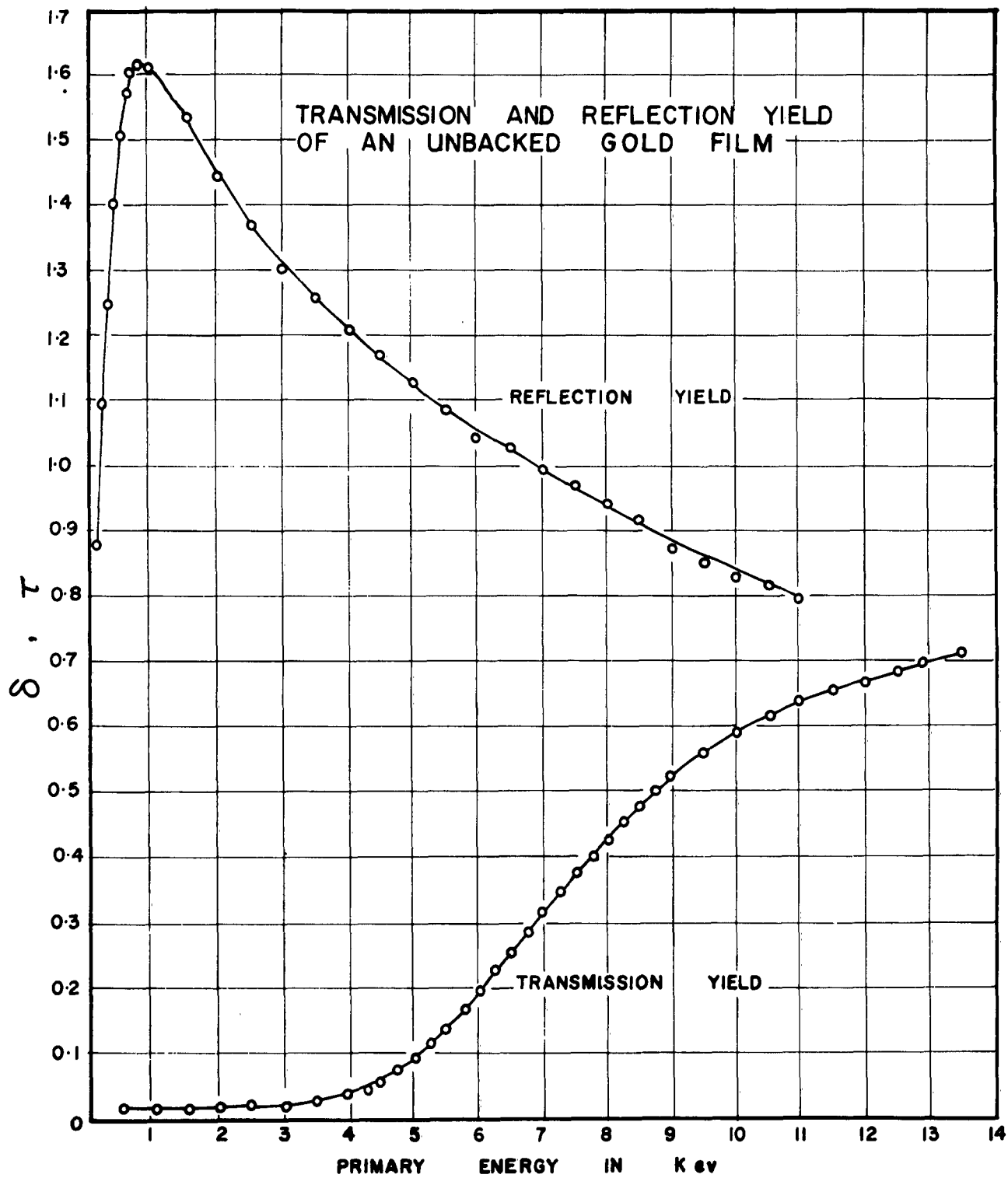


Fig. 8

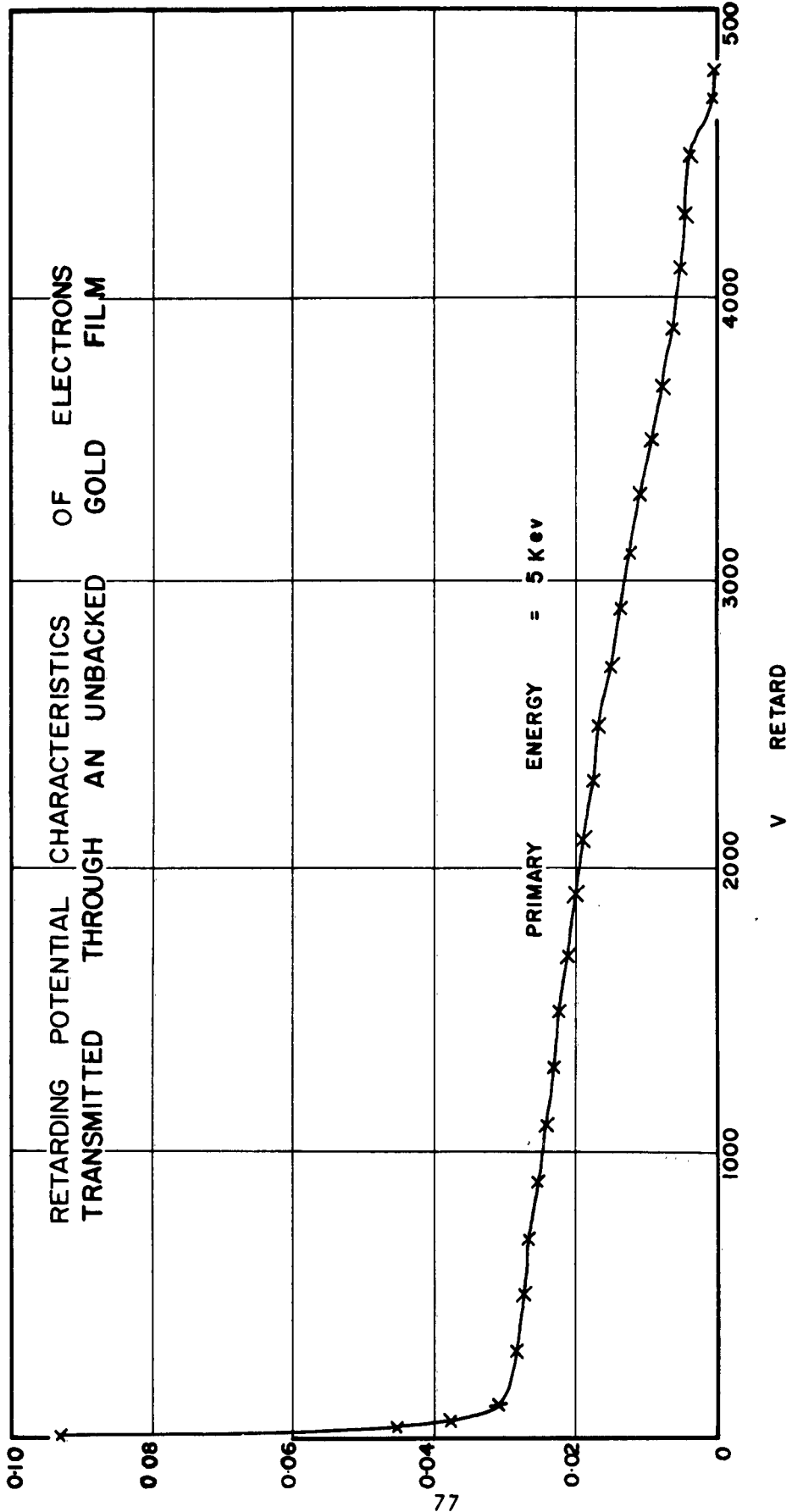


Fig. 9

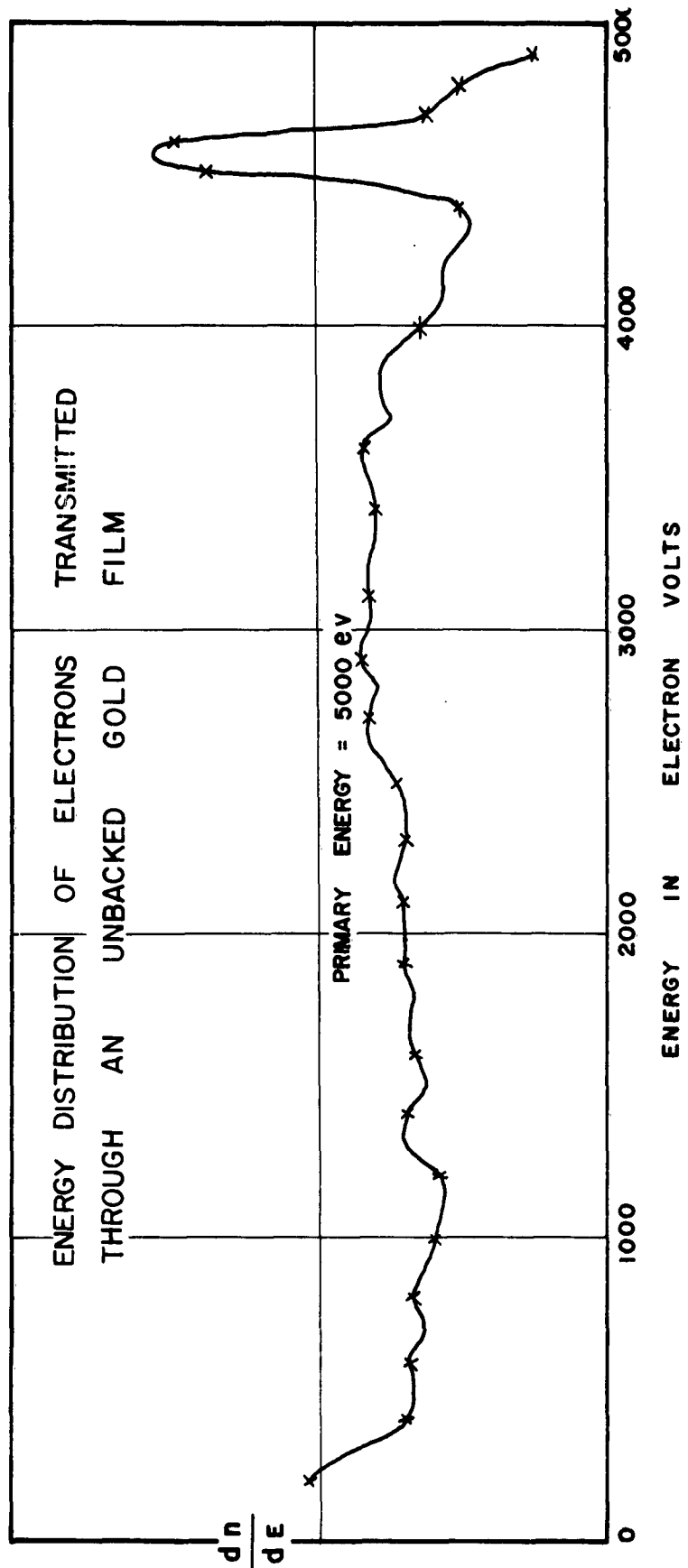


Fig. 10

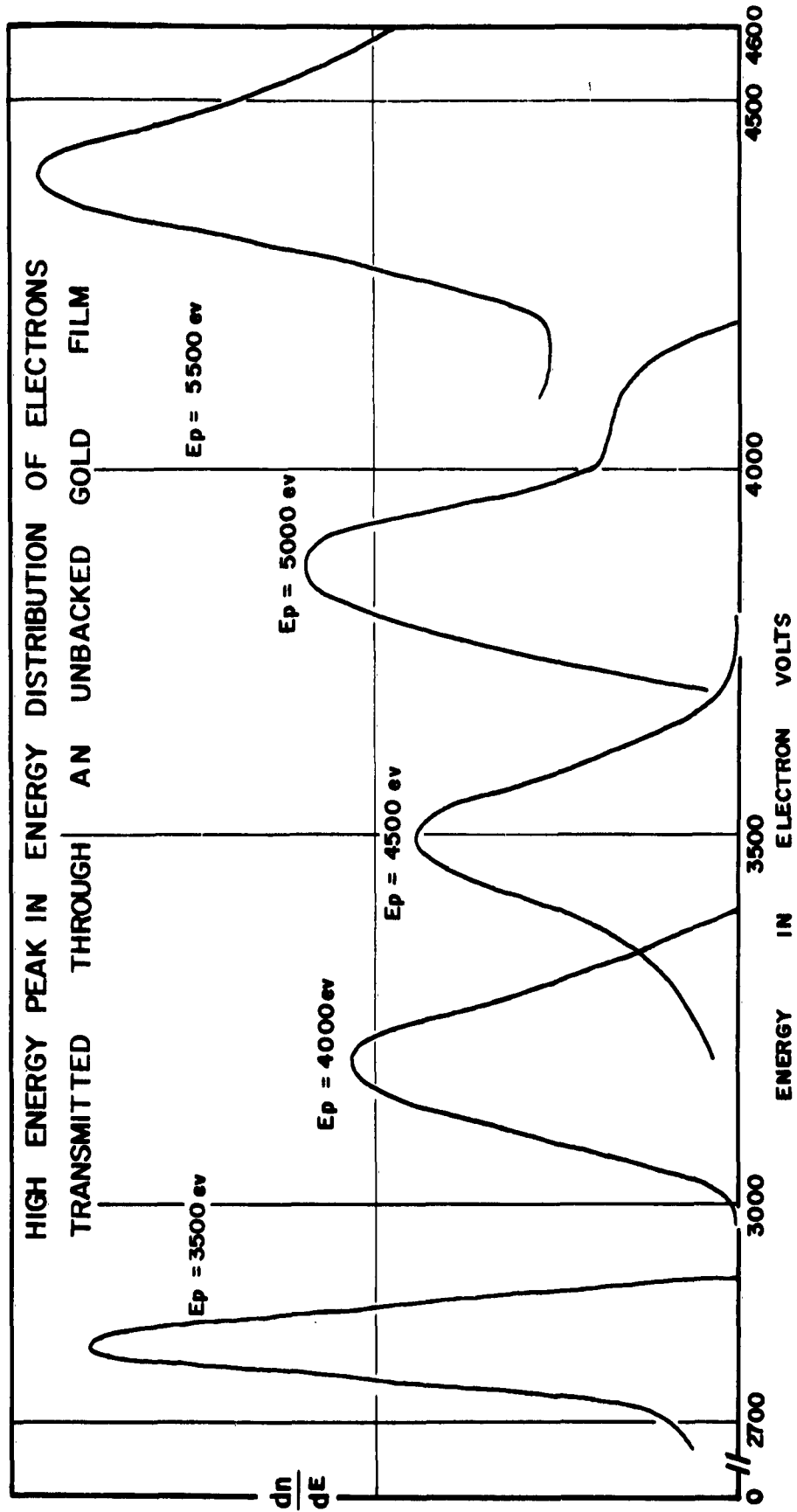


Fig. 11

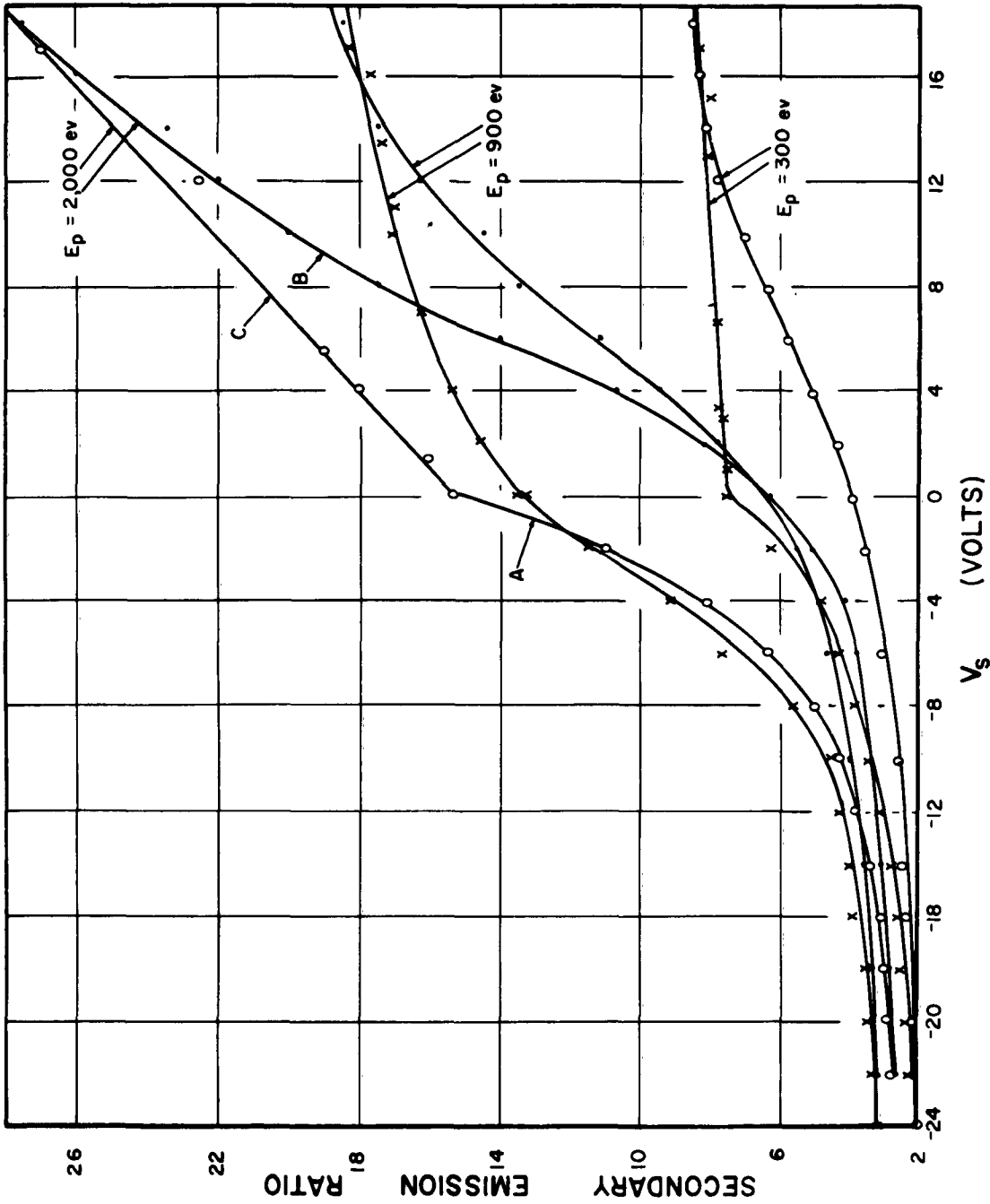


Fig. 12 The Dependence of Secondary Yield on the Surface Potential of a MgO Film (Film #1)

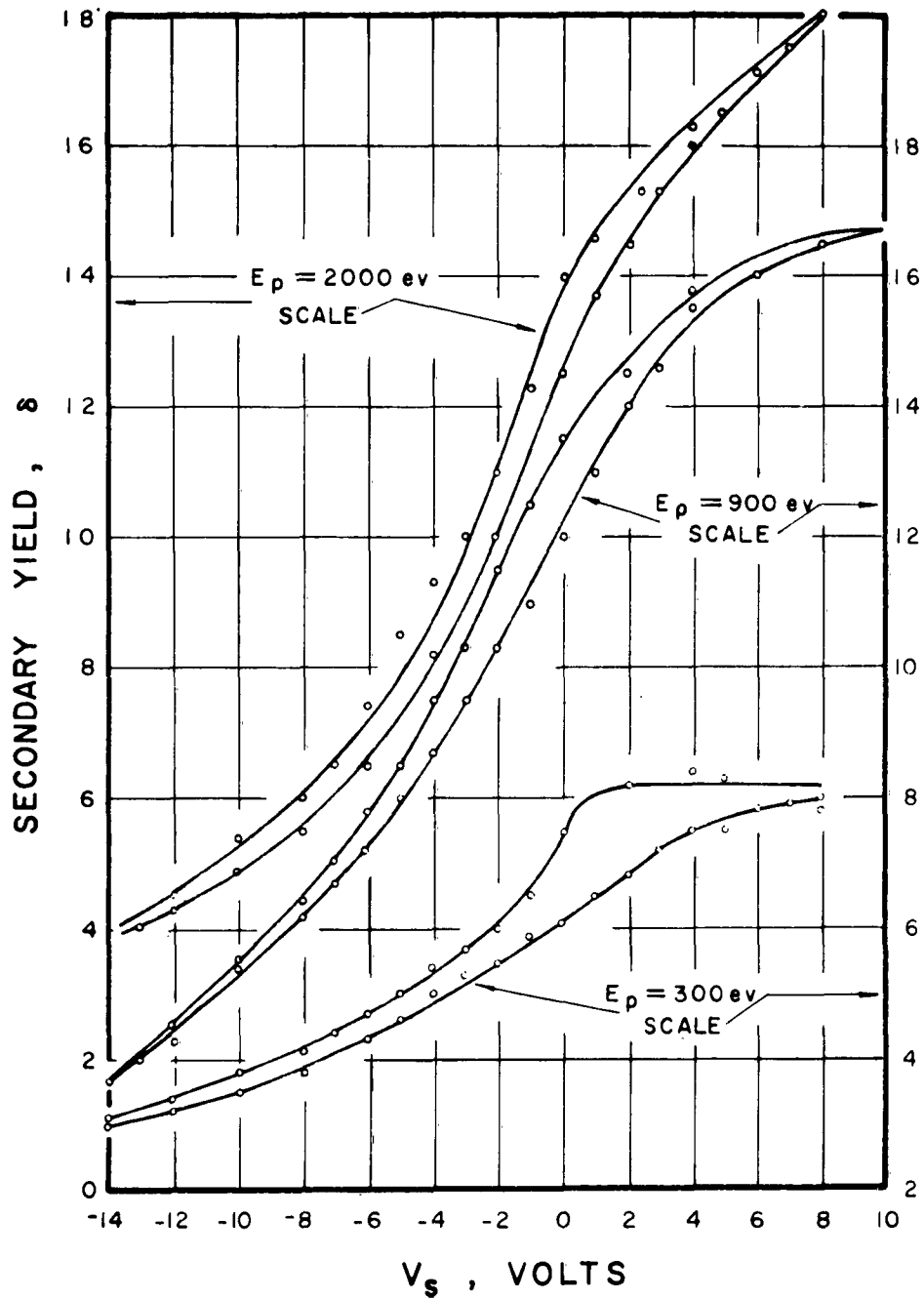


Fig. 13 The Dependence of Secondary Yield on the Surface Potential of Film No. 2

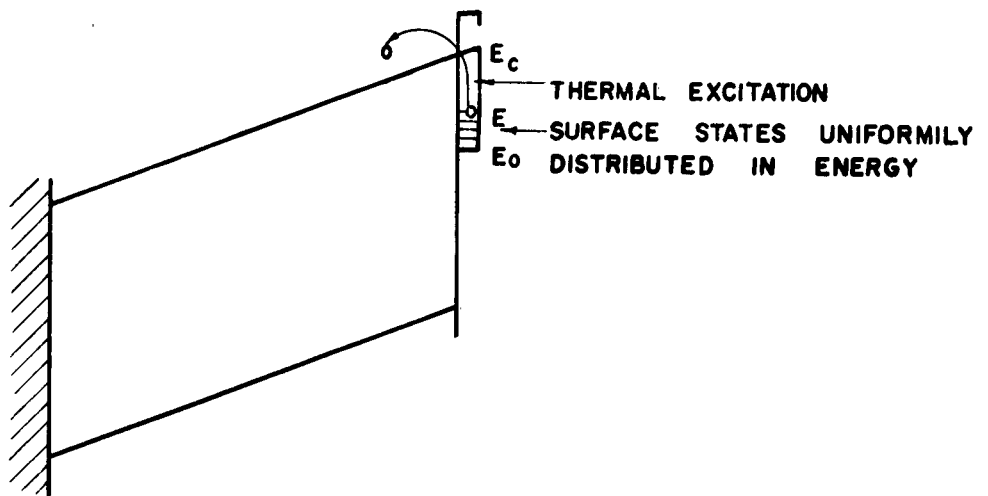


Fig. 14 Surface State Model

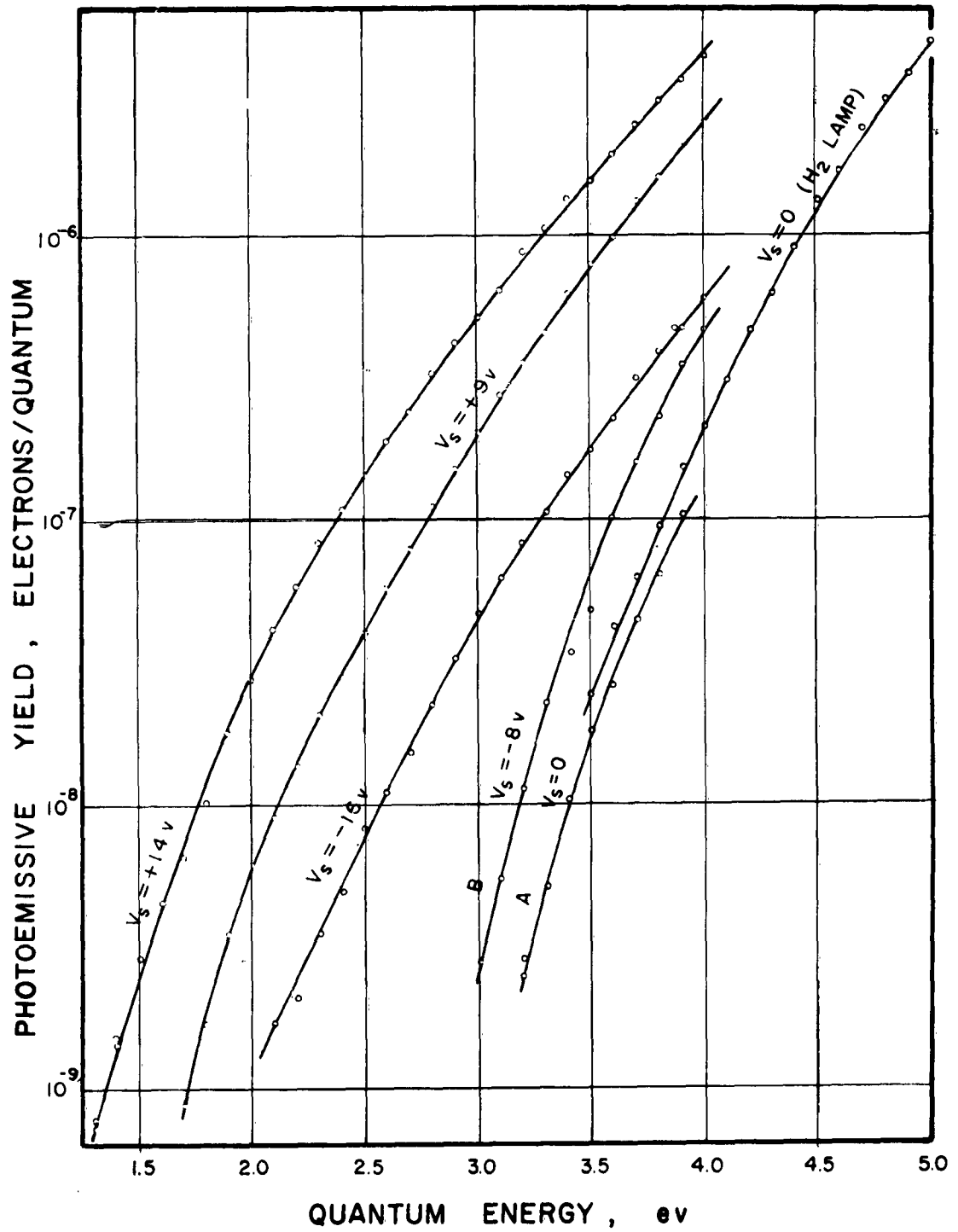


Fig. 15 Photoemissive Yield of Film No. 1

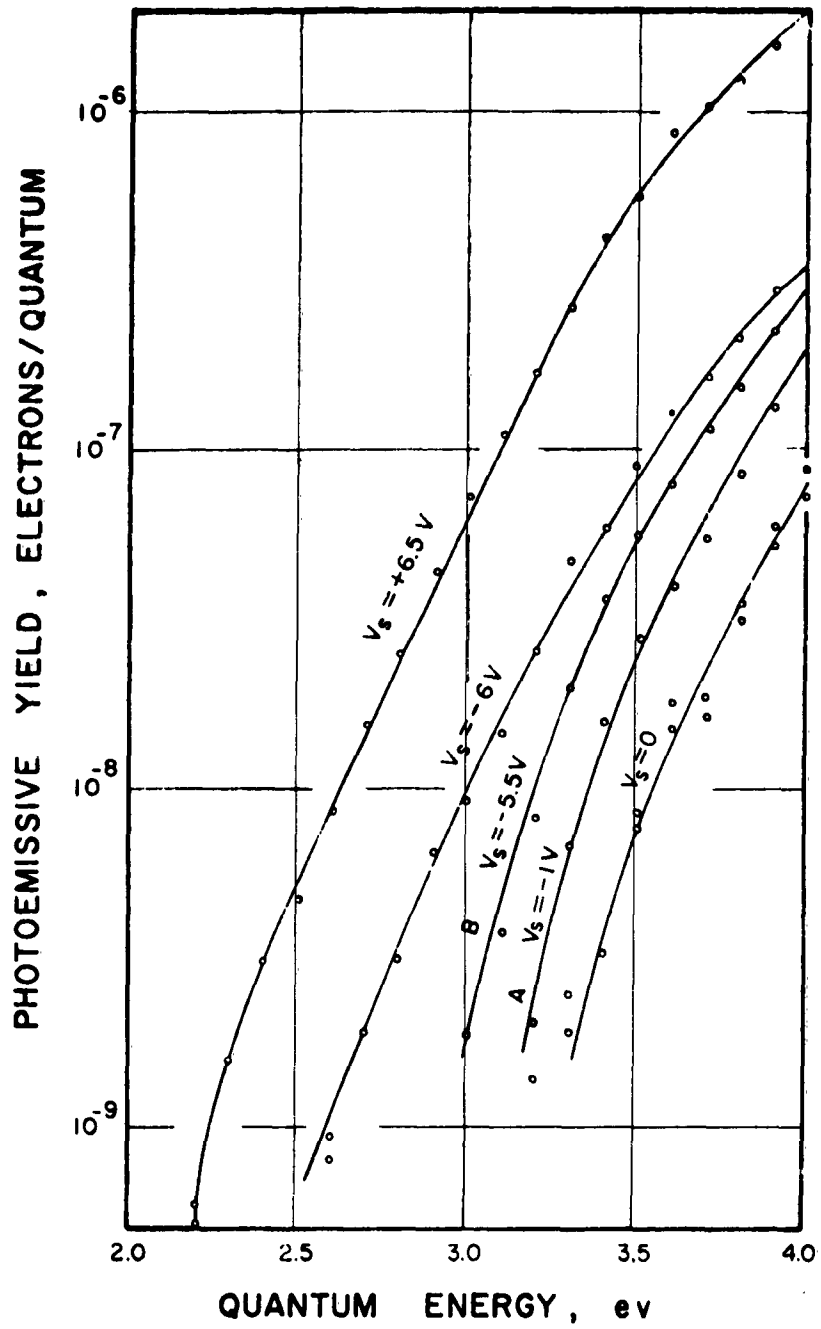


Fig. 16 Photoemissive Yield of Film No. 2

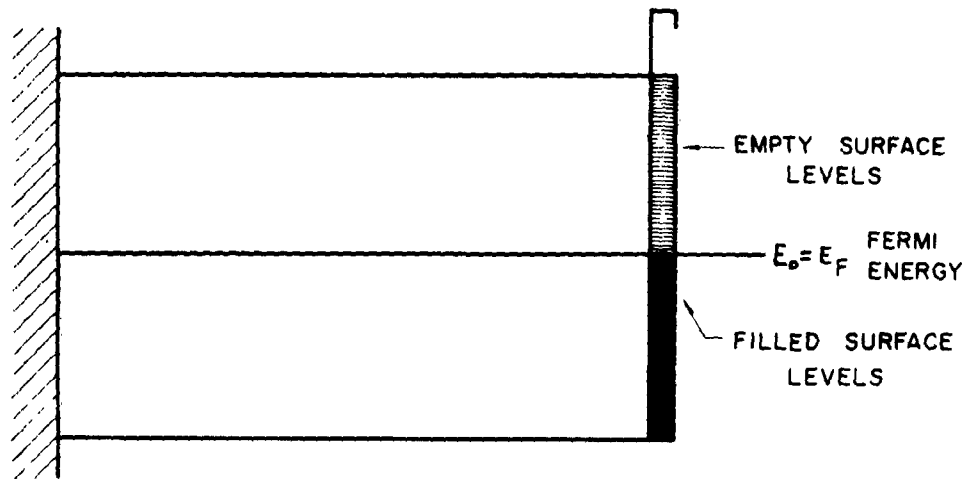


Fig. 17a Continuous Distribution of Surface States

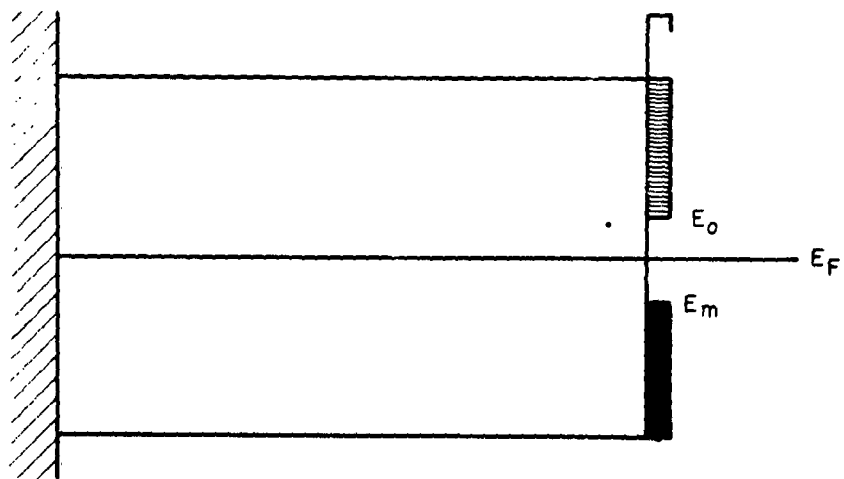


Fig. 17b Discontinuous Distribution of Surface States

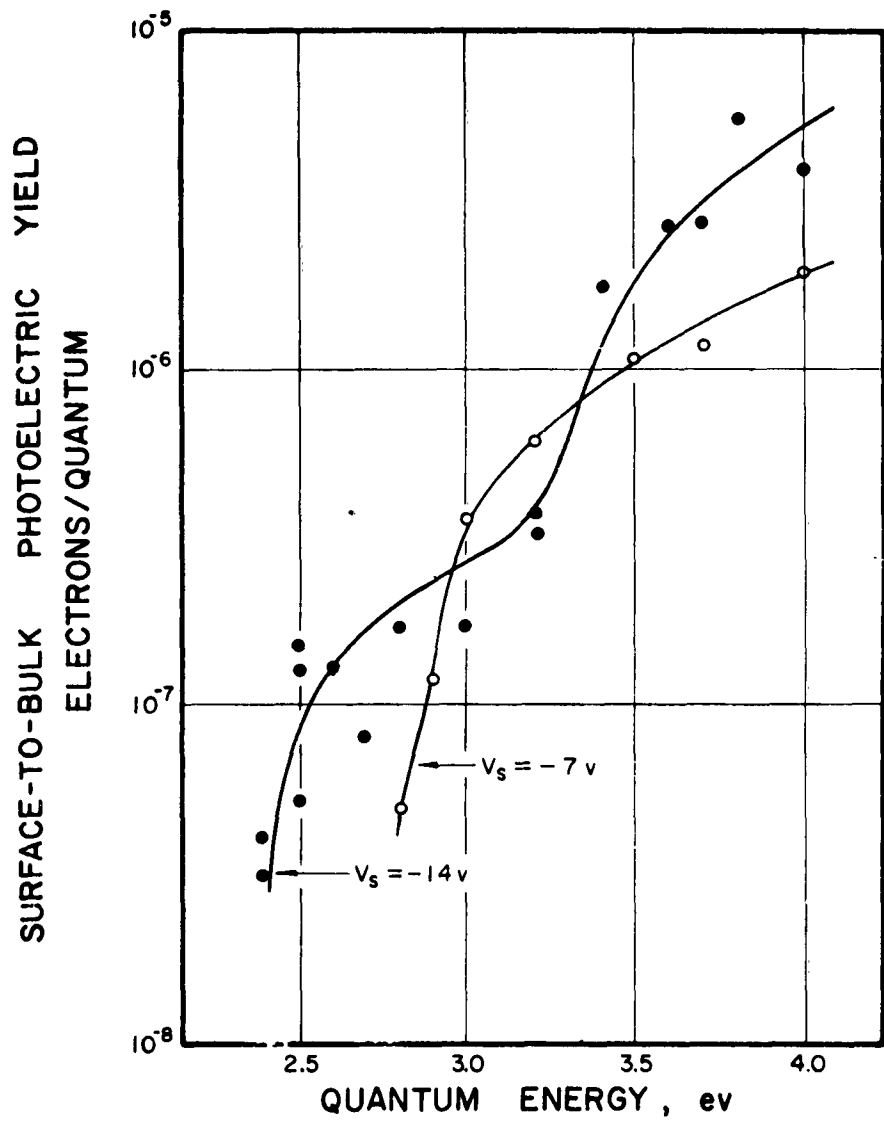


Fig. 18 Surface-to-Bulk Photoelectric Yield

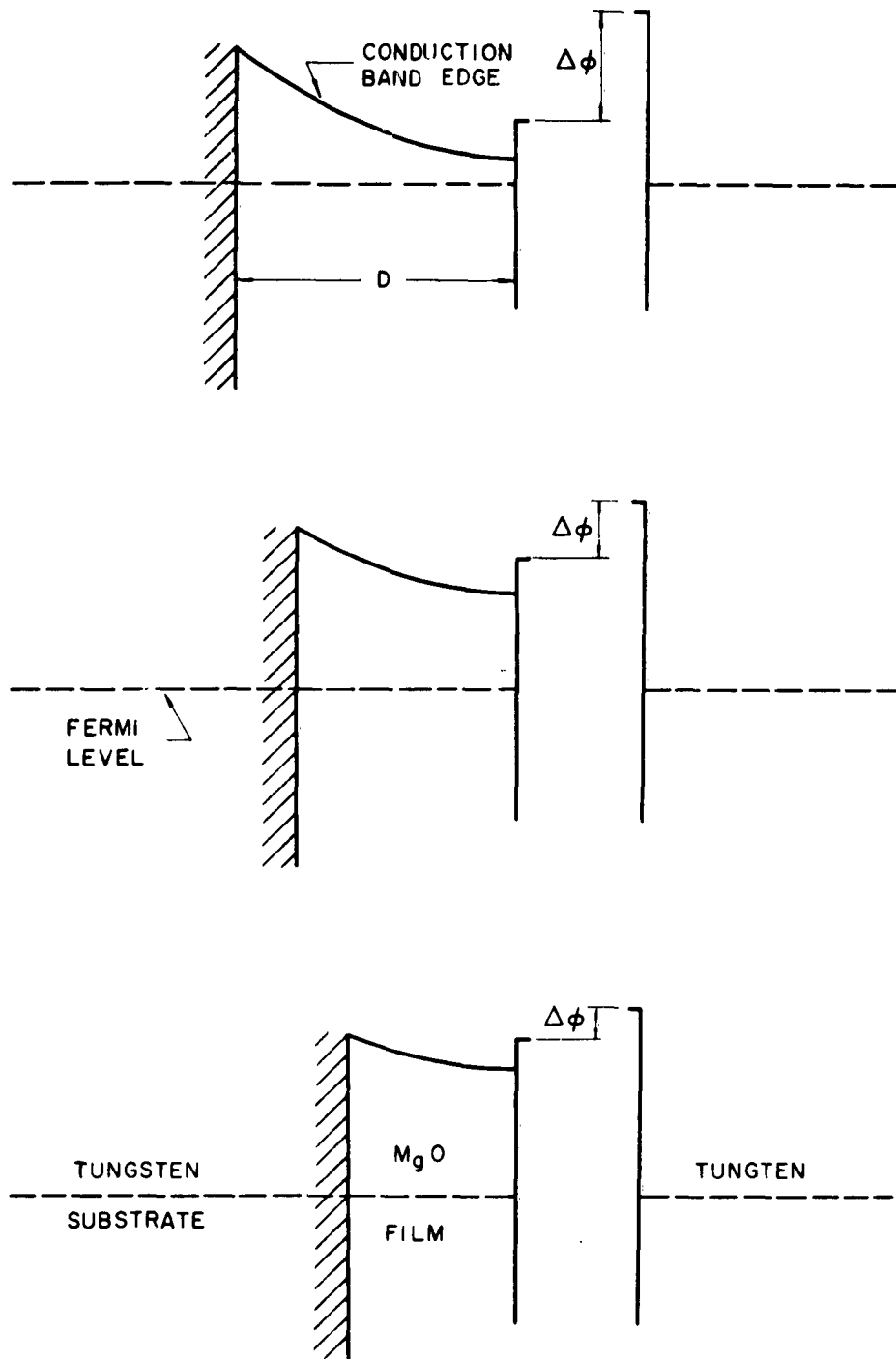


Fig. 19 Contact Potential Changes with Film Thickness

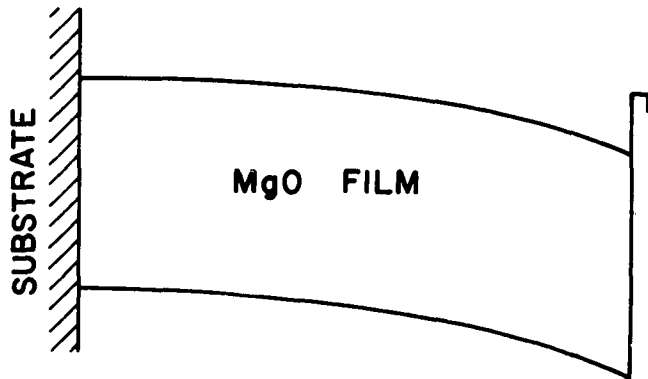
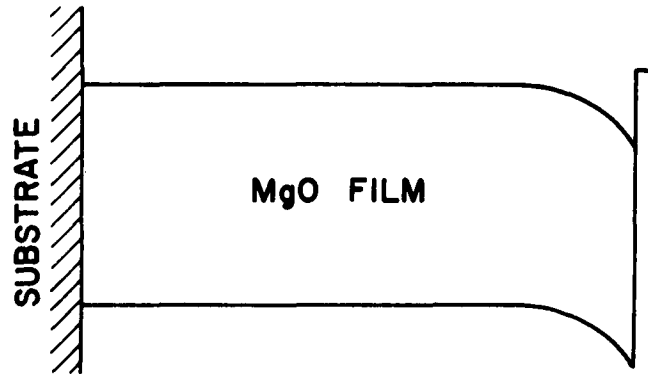
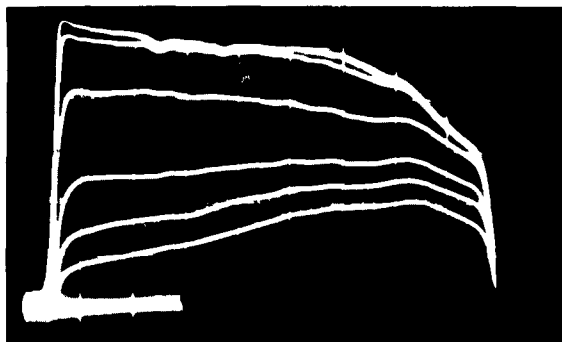


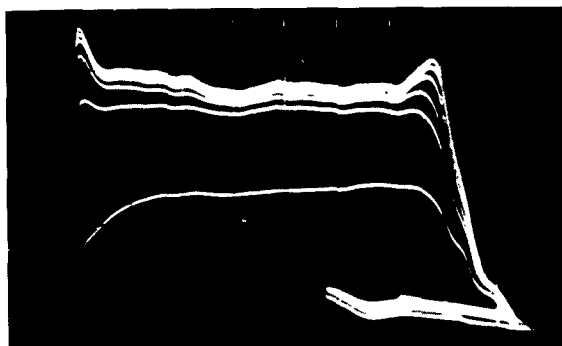
Fig. 20 Possible Potential Configurations near the Surface of the MgO Film.
 (a) High Temperature Case and
 (b) Room Temperature Case



TARGET #1



TARGET #2



TARGET #3

Fig. 21 Variation in δ as a Function of Primary Electron Beam Displacement for Several Collector Voltages

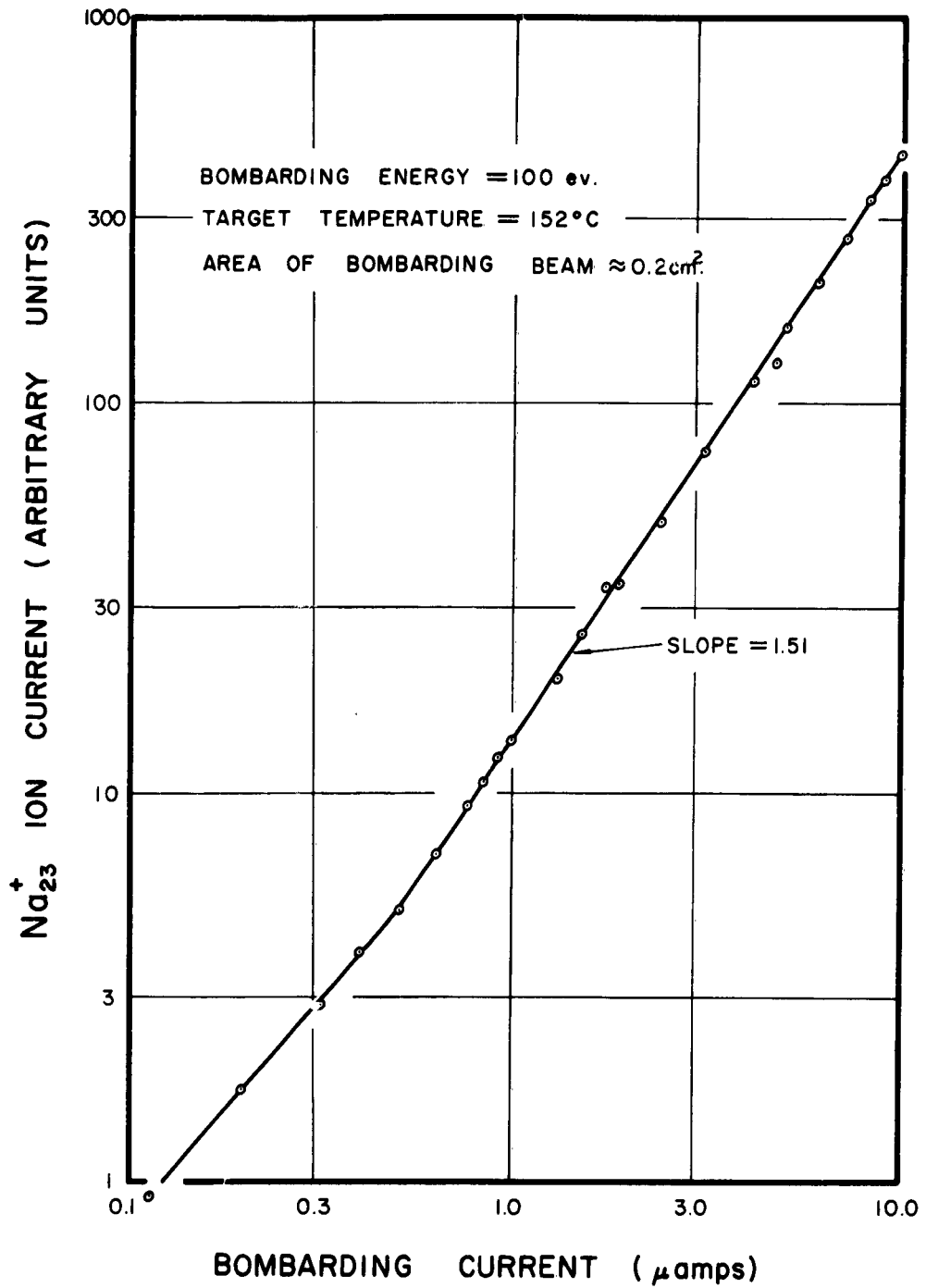
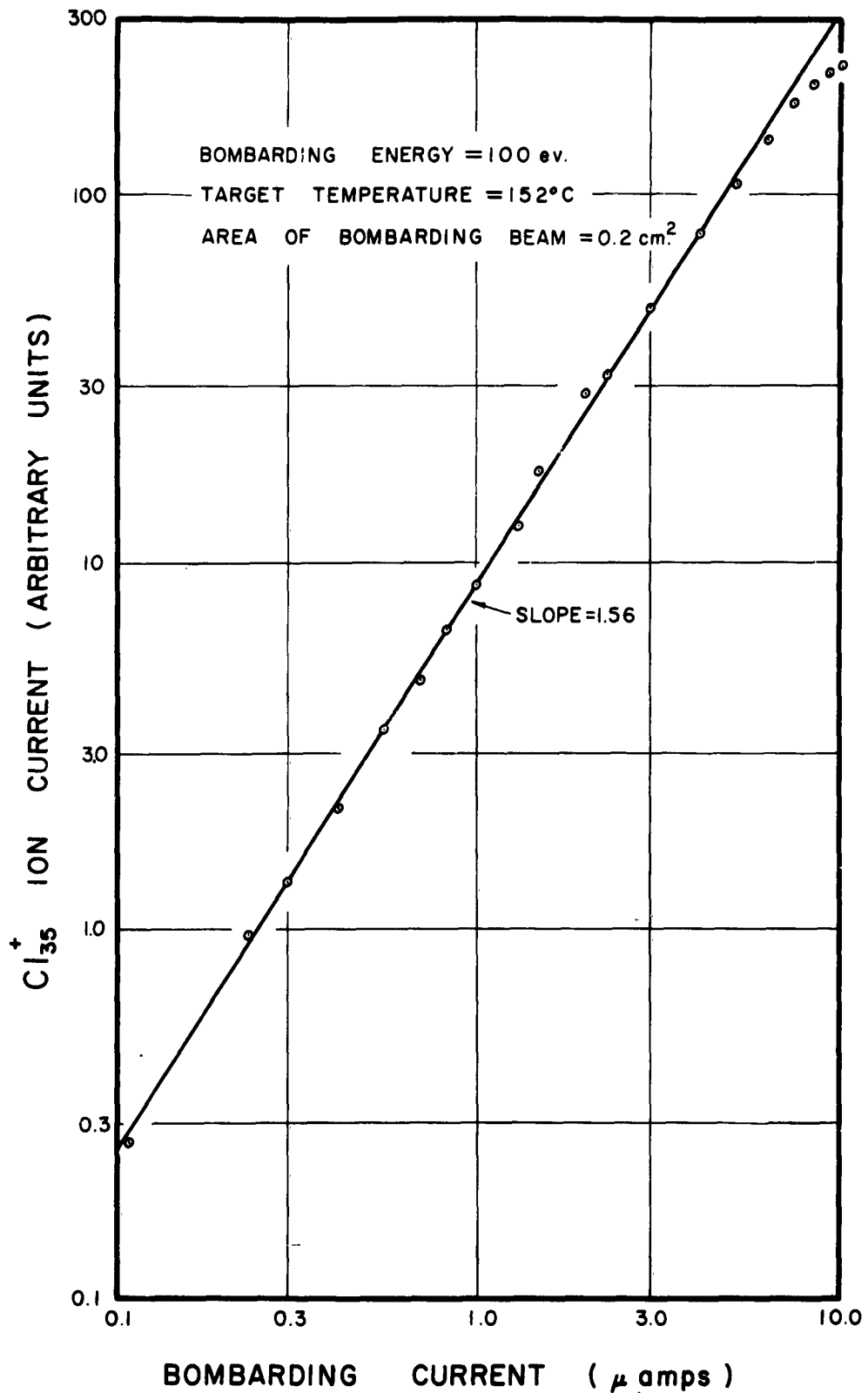


Fig. 22 The Dependence of the Na_{23}^+ Ion Current on the Bombarding Current for an Unbombarded NaCl Film



BOMBARDING CURRENT (μ amps)
 Fig. 23 The Dependence of the Cl_{35}^+ Ion Current on the Bombarding Current for an Unbombarded NaCl Film

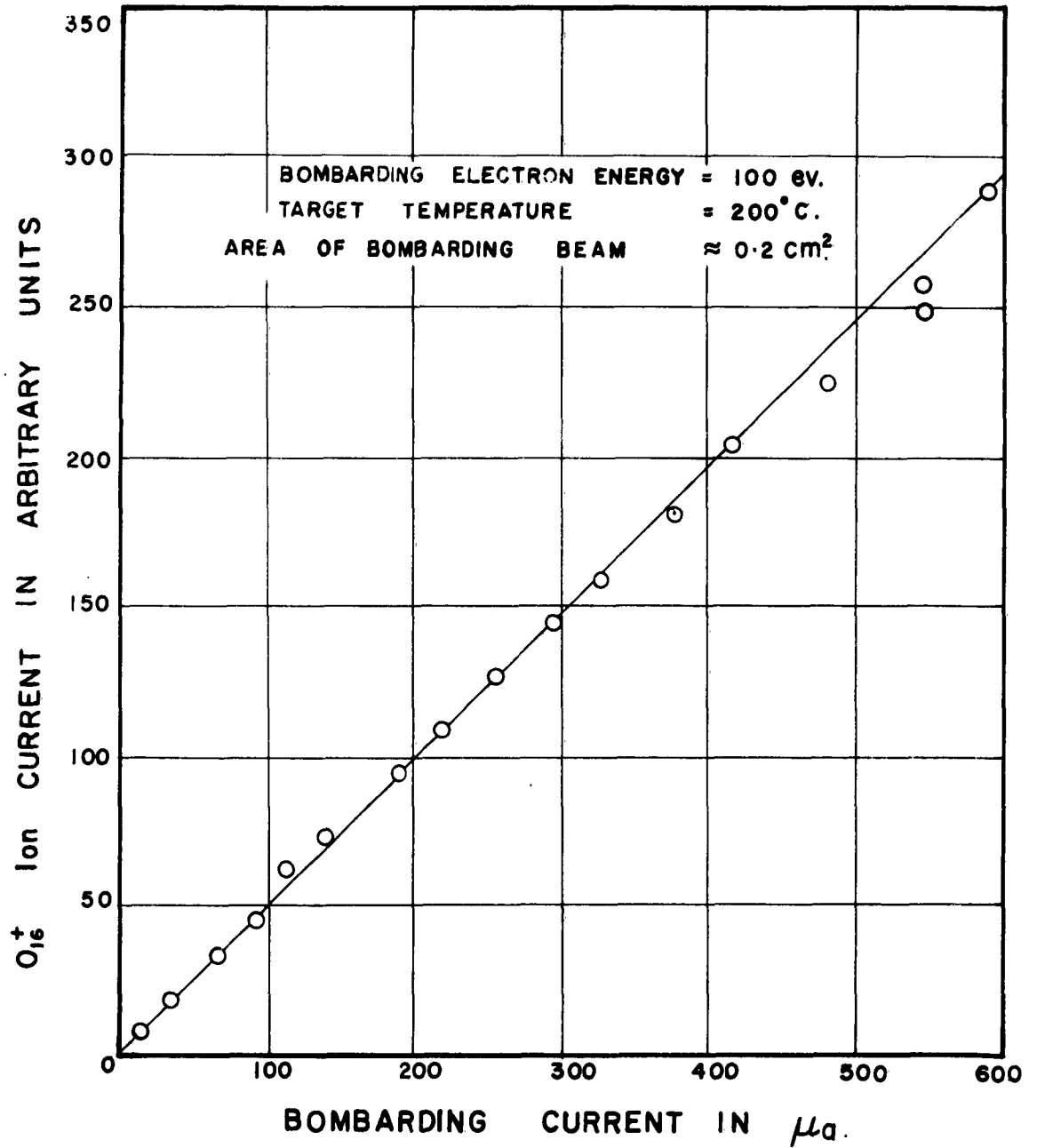


Fig. 24 The Dependence of the O₁₆⁺ Ion Current on the Bombarding Current for an MgO Film

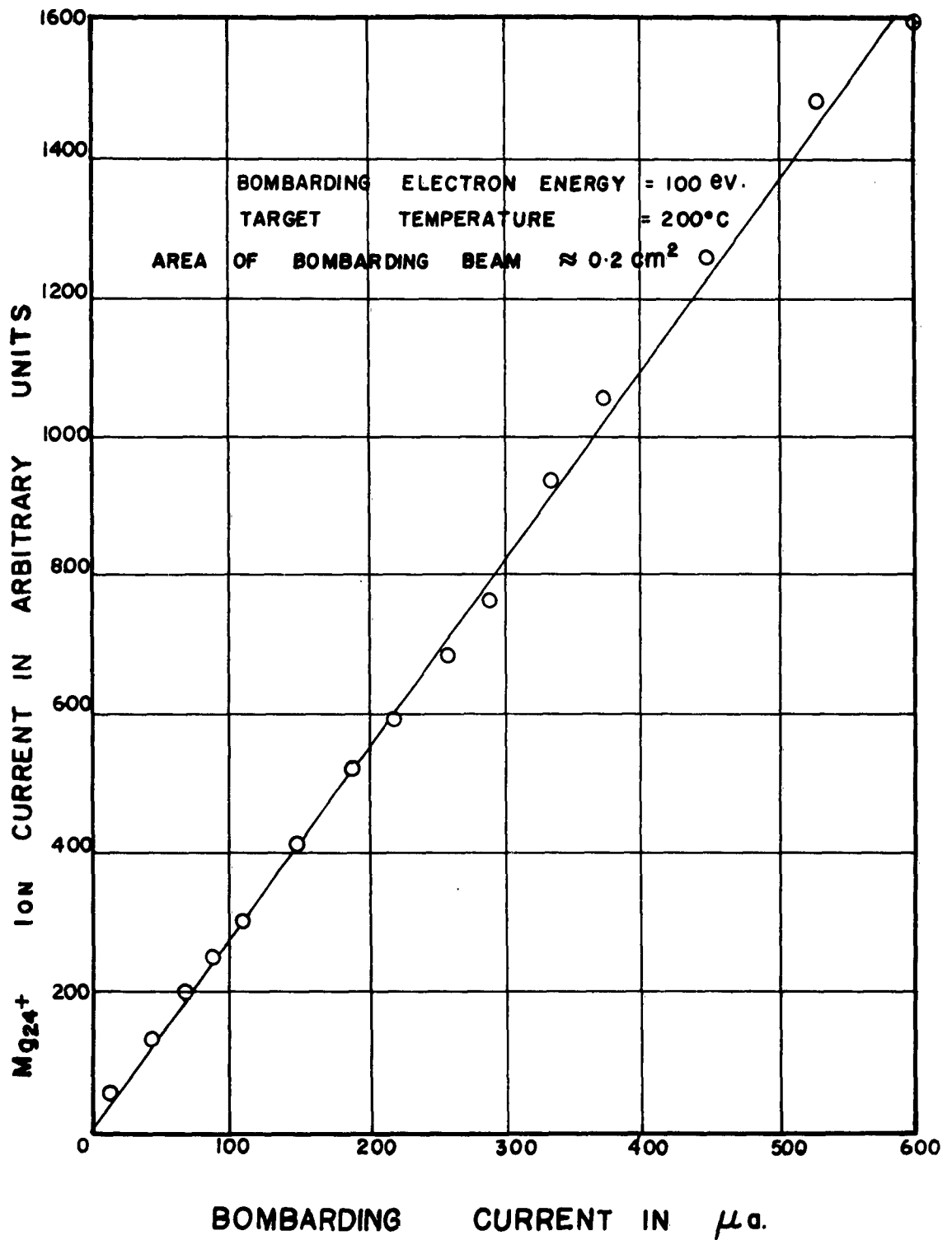


Fig. 25 The Dependence of the Mg_{24}^+ Ion Current on the Bombarding Current for an MgO Film

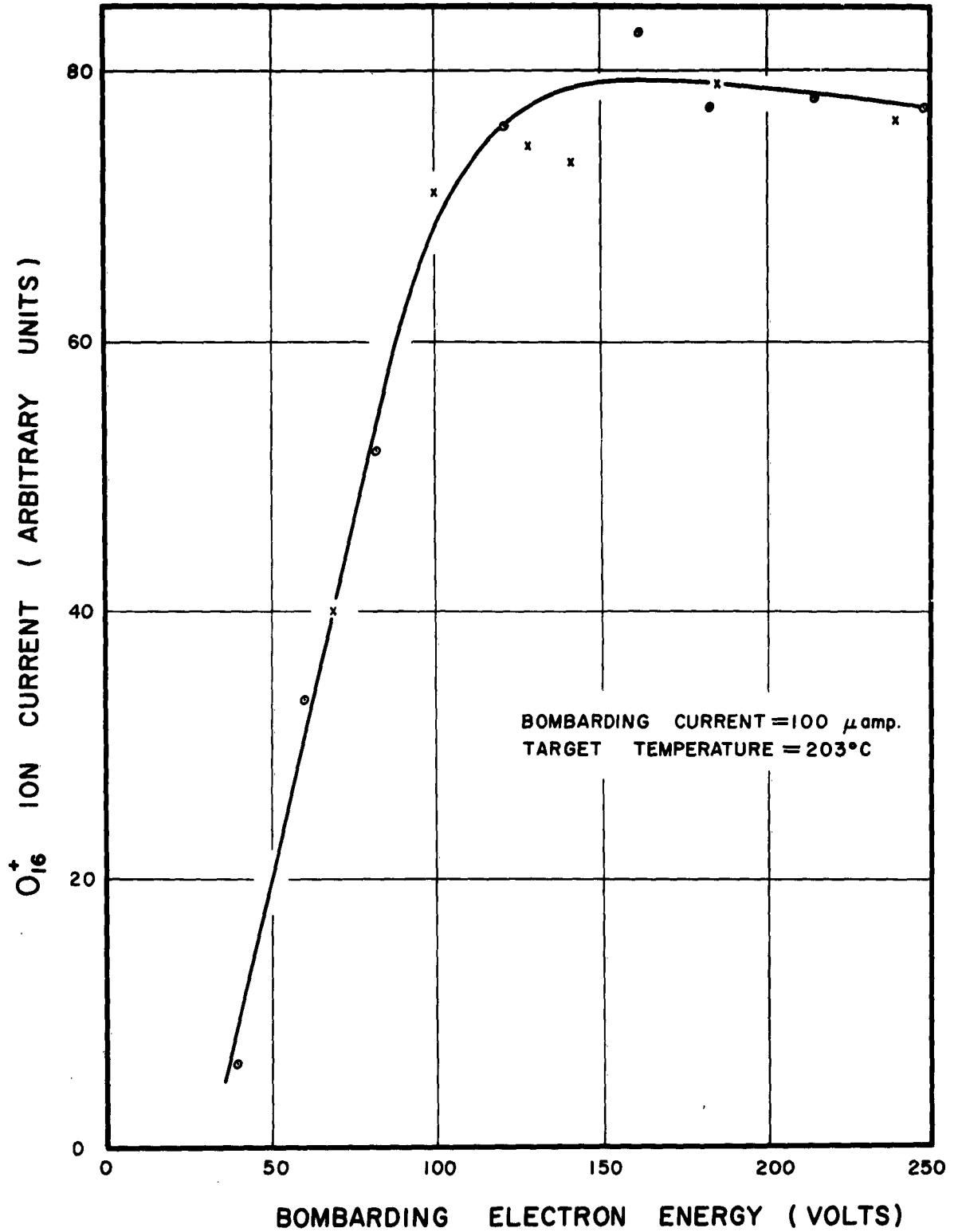
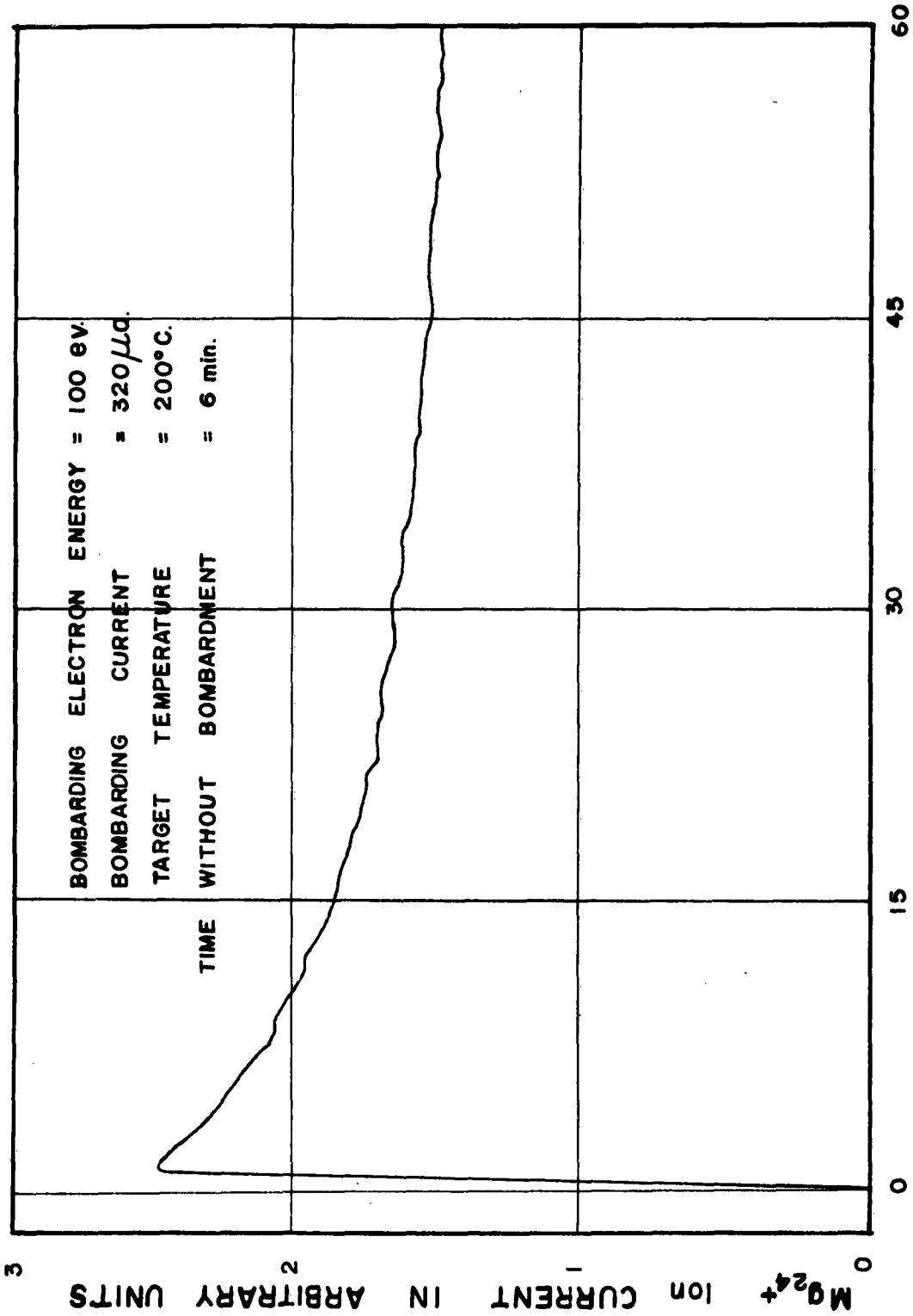


Fig. 26 The Dependence of the O_{16}^+ Ion Current on the Bombarding Electron Energy for a MgO Film



TIME IN SECONDS.

Fig. 27 The Transient Behavior of the Mg_{24}^+ Ion Current

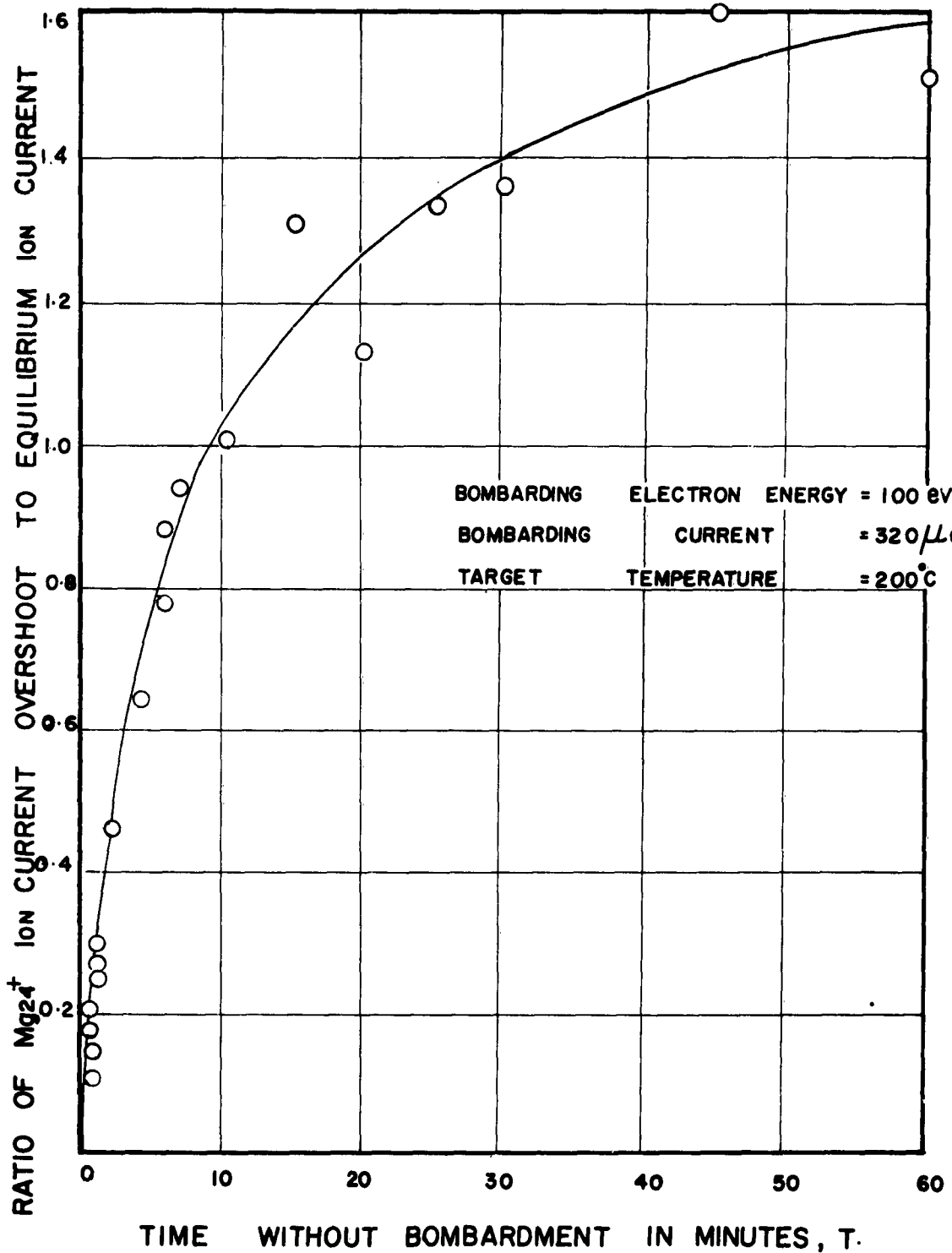


Fig. 28 The Dependence of the Overshoot of the Mg^{24+} Ion Current on the Time without Bombardment

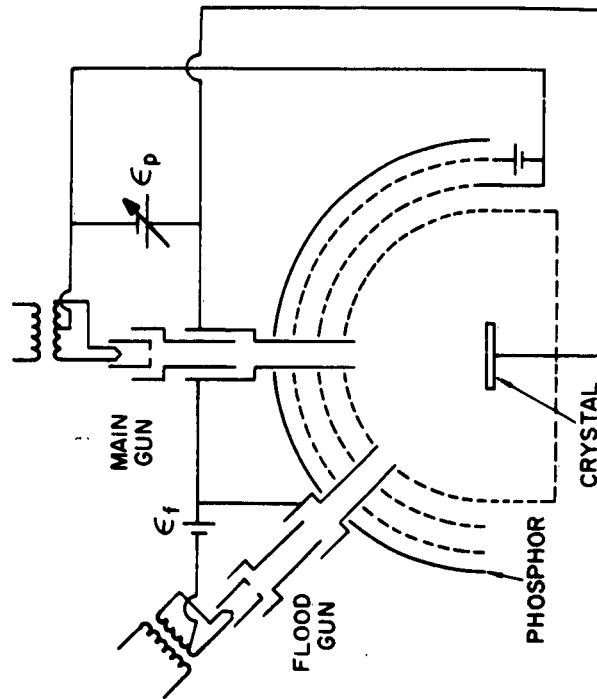


FIG. 29
ELECTRON DIFFRACTION CHAMBER

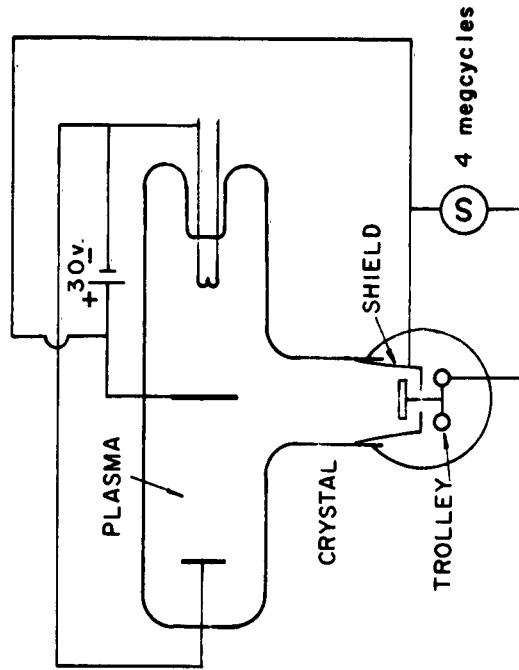


FIG. 30
CIRCUIT FOR SPUTTERING MgO

- (62) •(60)
- (53) •(51)
- (44) •(42) •(40)
- (33) •(31)
- (22) •(20)
- (11) •(00)

FIG. 31 ELECTRON DIFFRACTION PATTERN FROM (001) MgO

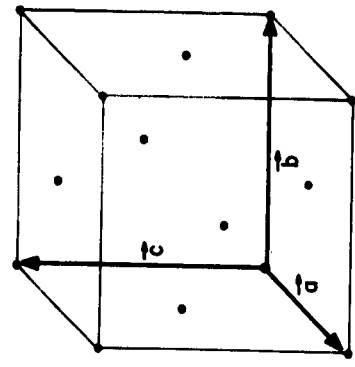


FIG. 32 THREE DIMENSIONAL fcc UNIT CELL

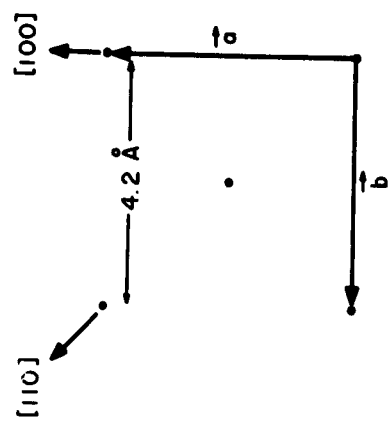


FIG. 33 TWO DIMENSIONAL fcc UNIT CELL

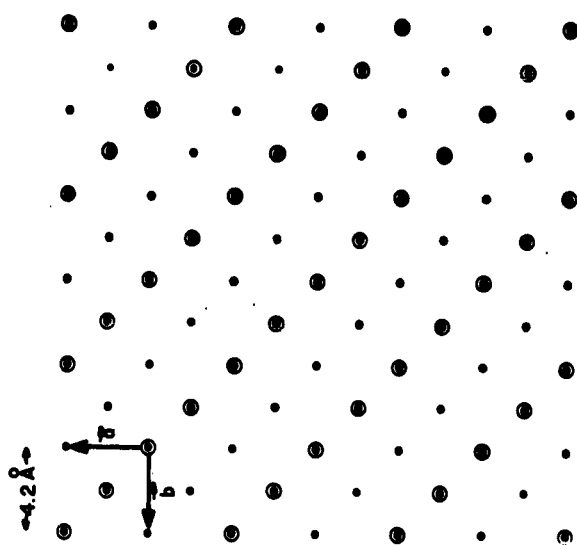


FIG.35 SURFACE STRUCTURE PRODUCING HALF ORDER BEAMS

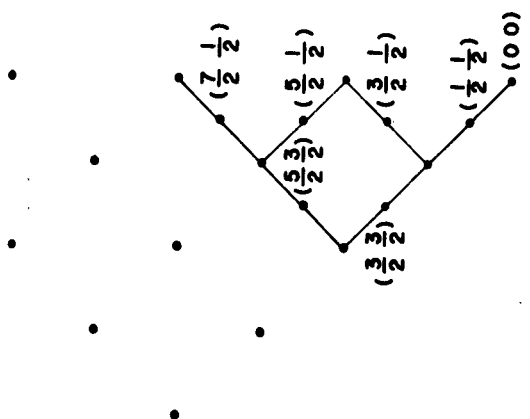


FIG.34 ELECTRON DIFFRACTION PATTERN FROM (001) MgO SHOWING HALF ORDER BEAMS

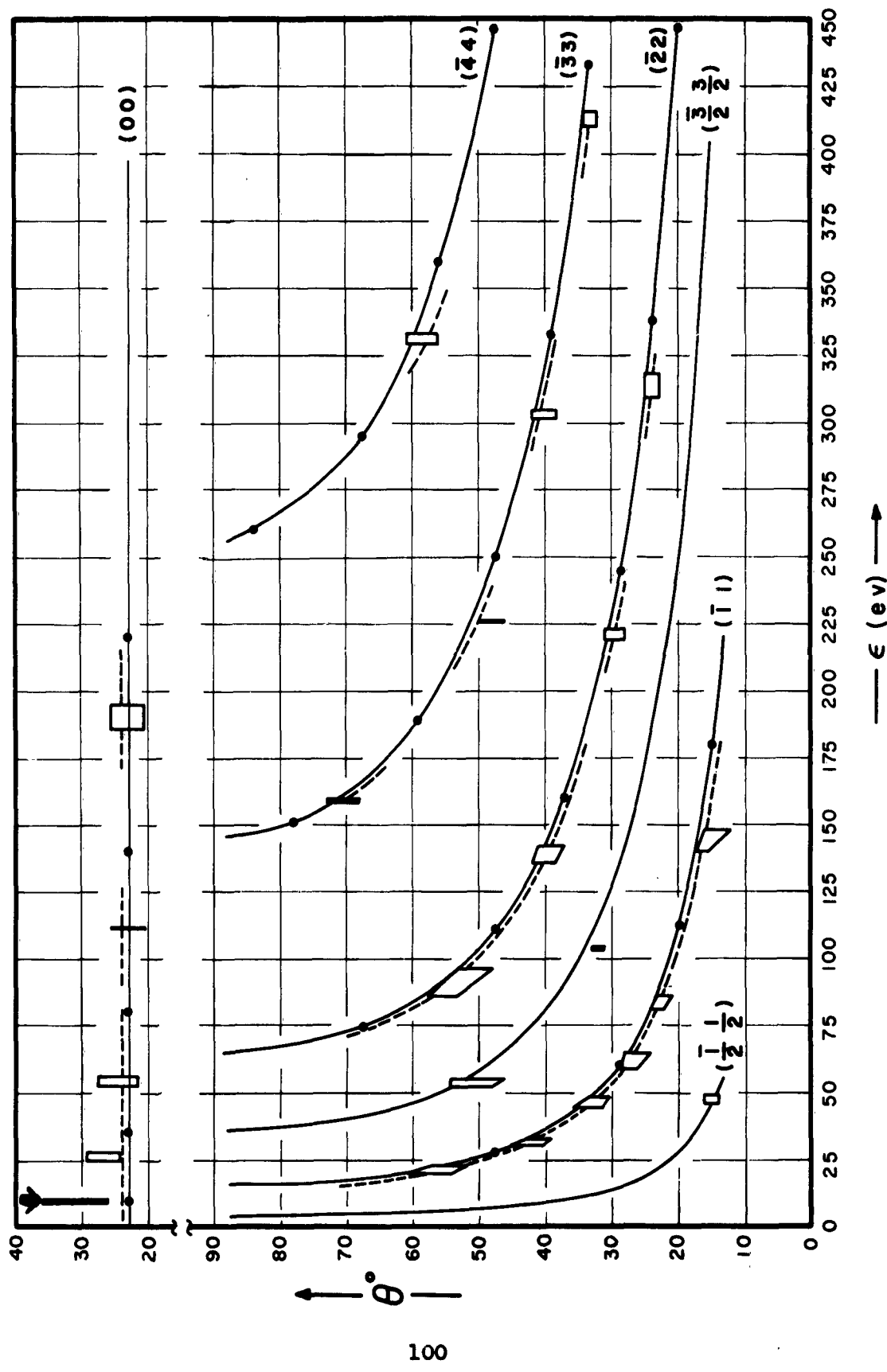


FIG. 36 ELECTRON DIFFRACTION FROM (001) MgO $[\bar{1}10]$ AZIMUTH

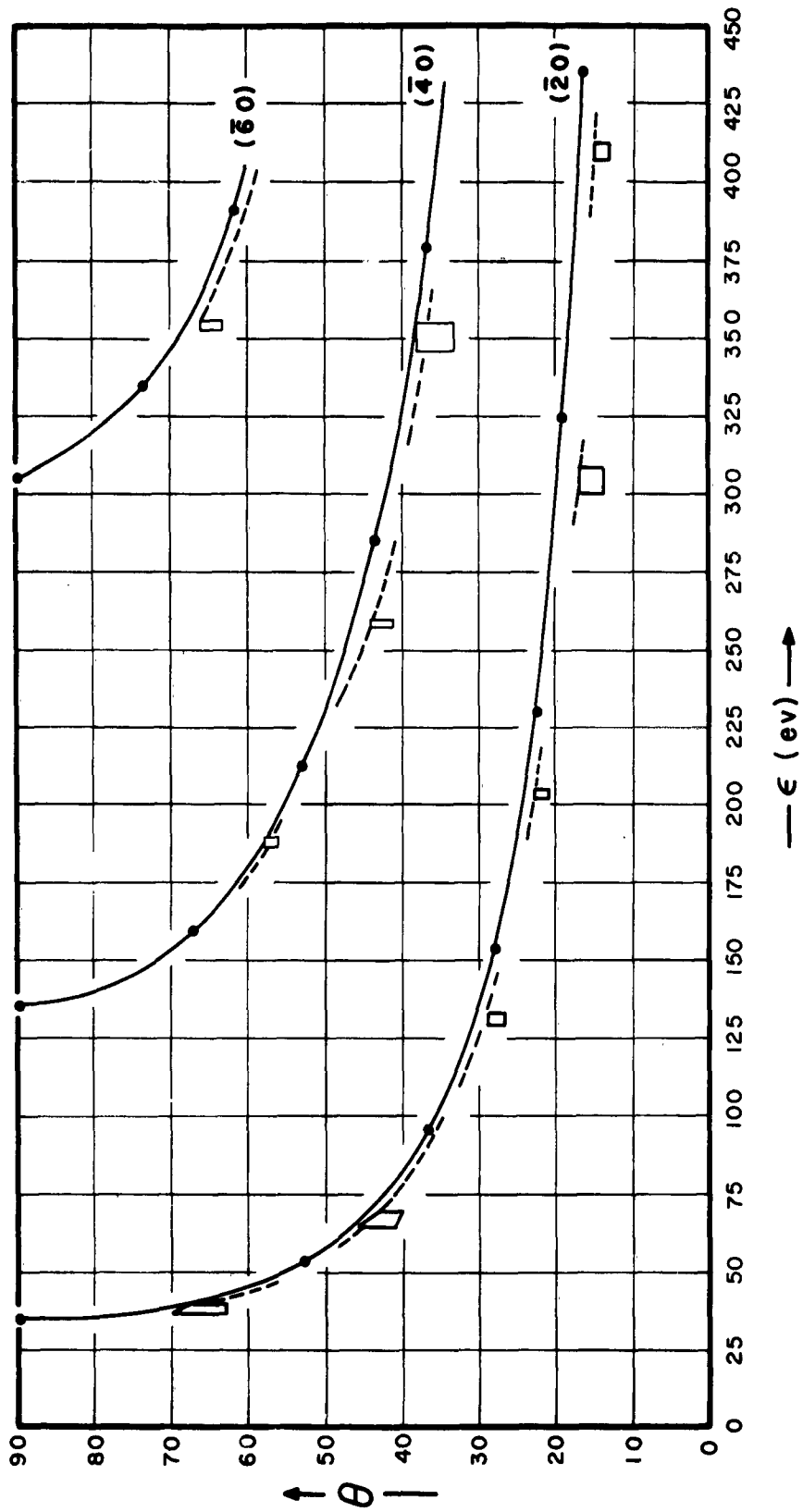


FIG. 37 ELECTRON DIFFRACTION FROM (001)MgO [100] AZIMUTH

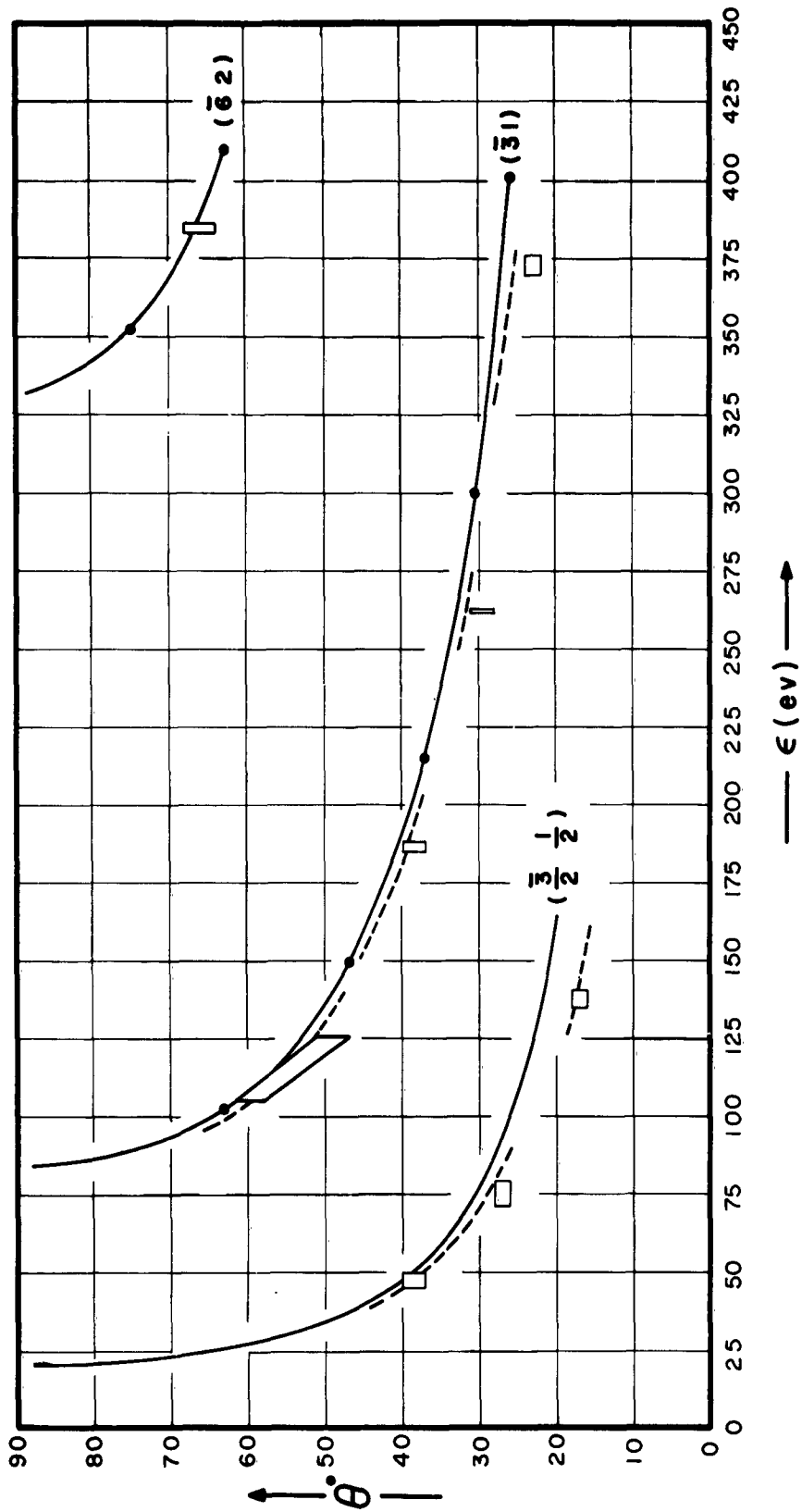


FIG. 38 ELECTRON DIFFRACTION FROM (001)MgO; $[\bar{3} 10]$ AZIMUTH

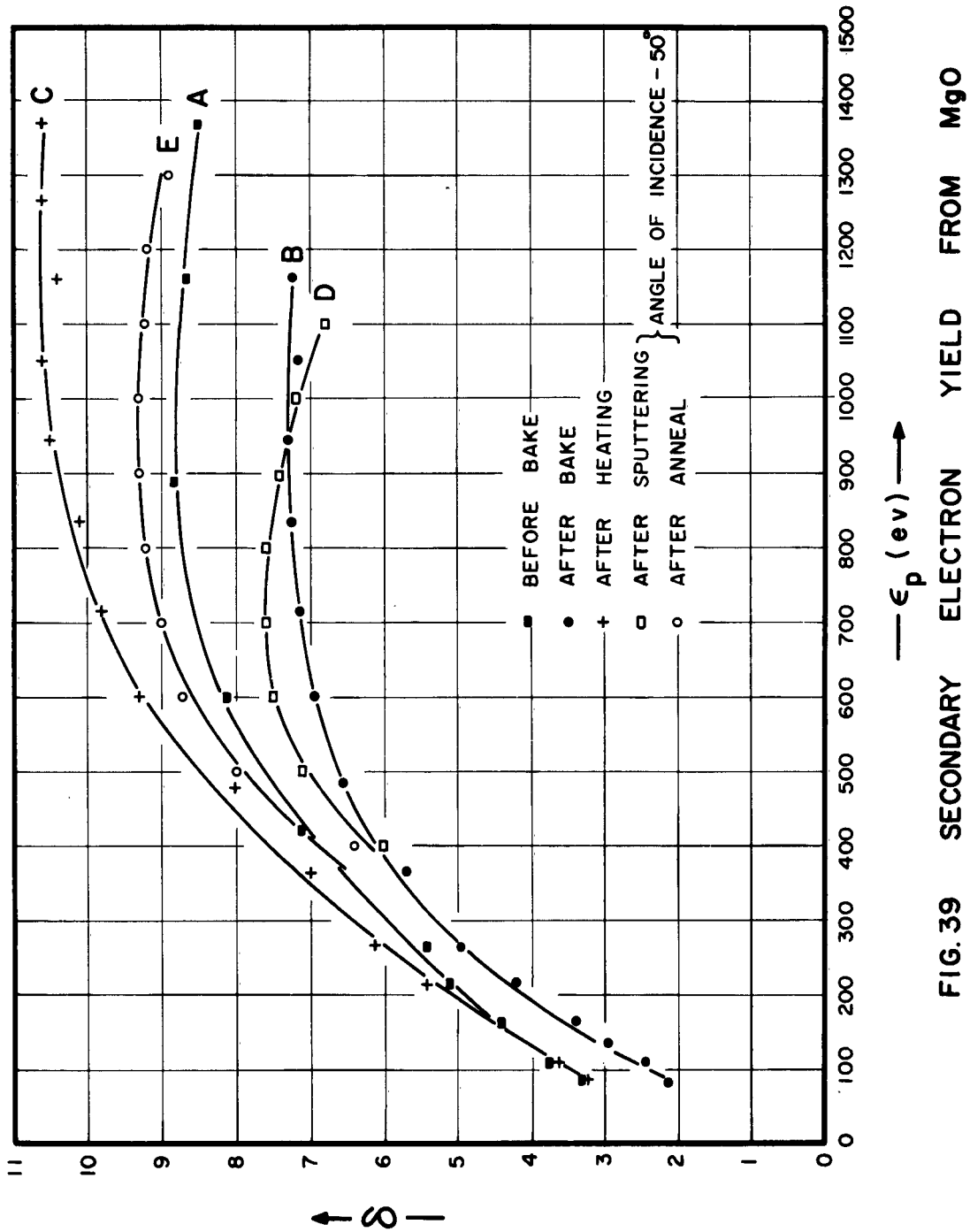


FIG. 39 SECONDARY ELECTRON YIELD FROM MgO

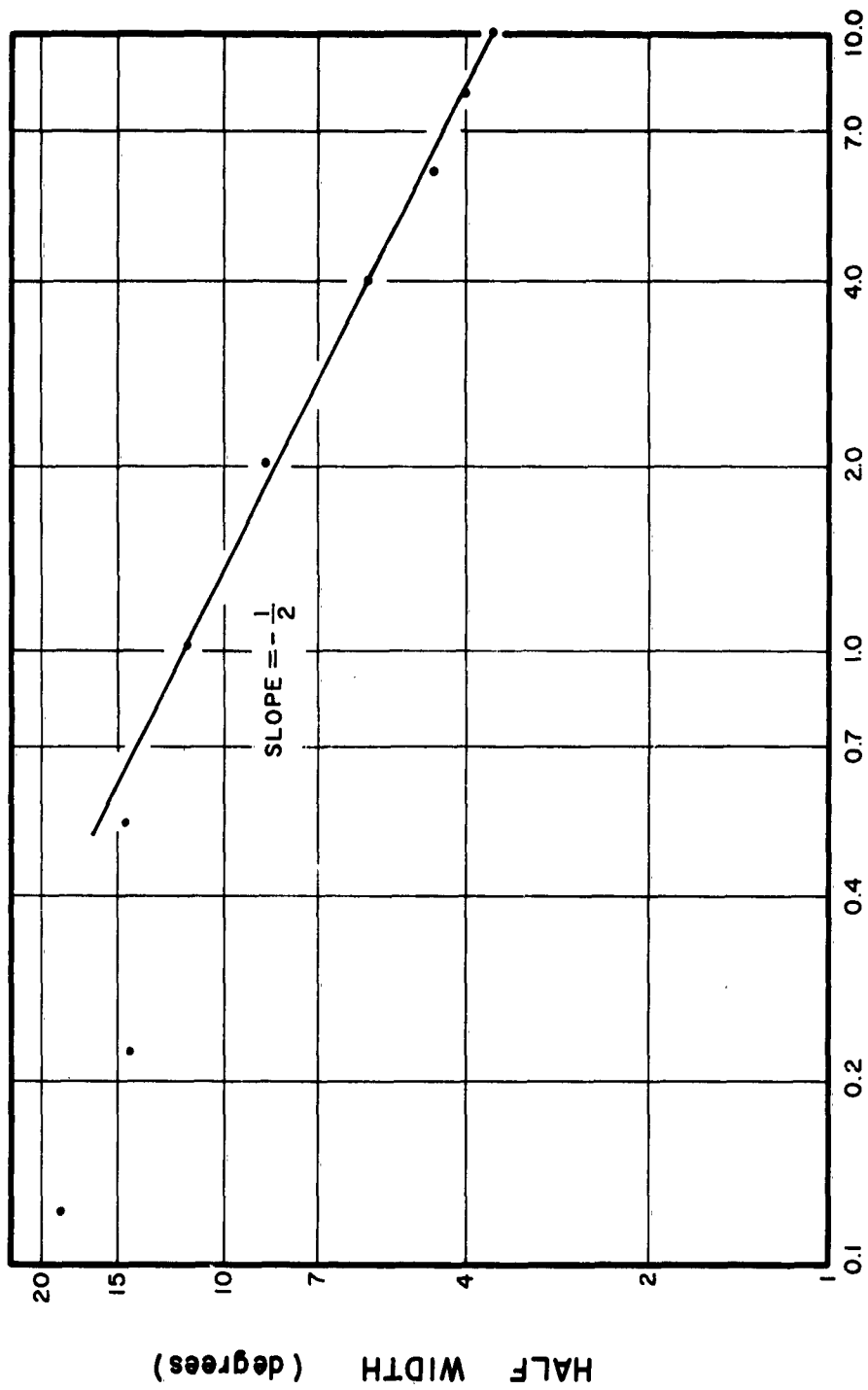


Fig. 40 Half Width of the Normal Incidence Peak for Titanium vs. Primary Energy (keV.)

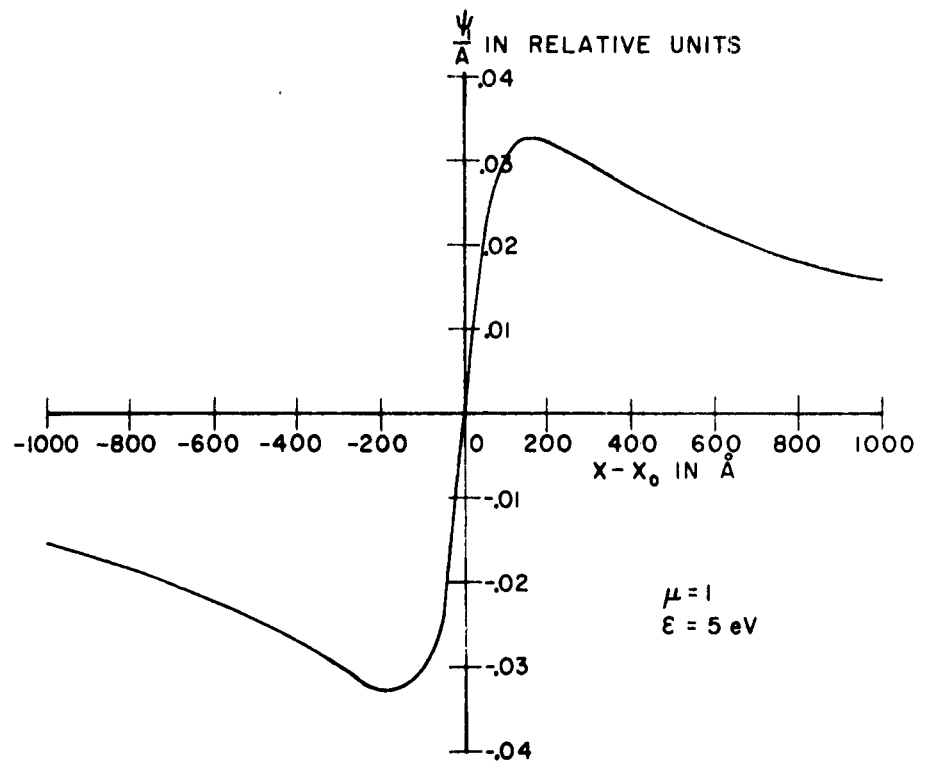


Fig. 41 Distribution Function ψ Against Distance $x - x_0$ from a Plane Source at x_0 for $a = 0.1$, $n = 2$, $\alpha = 1$

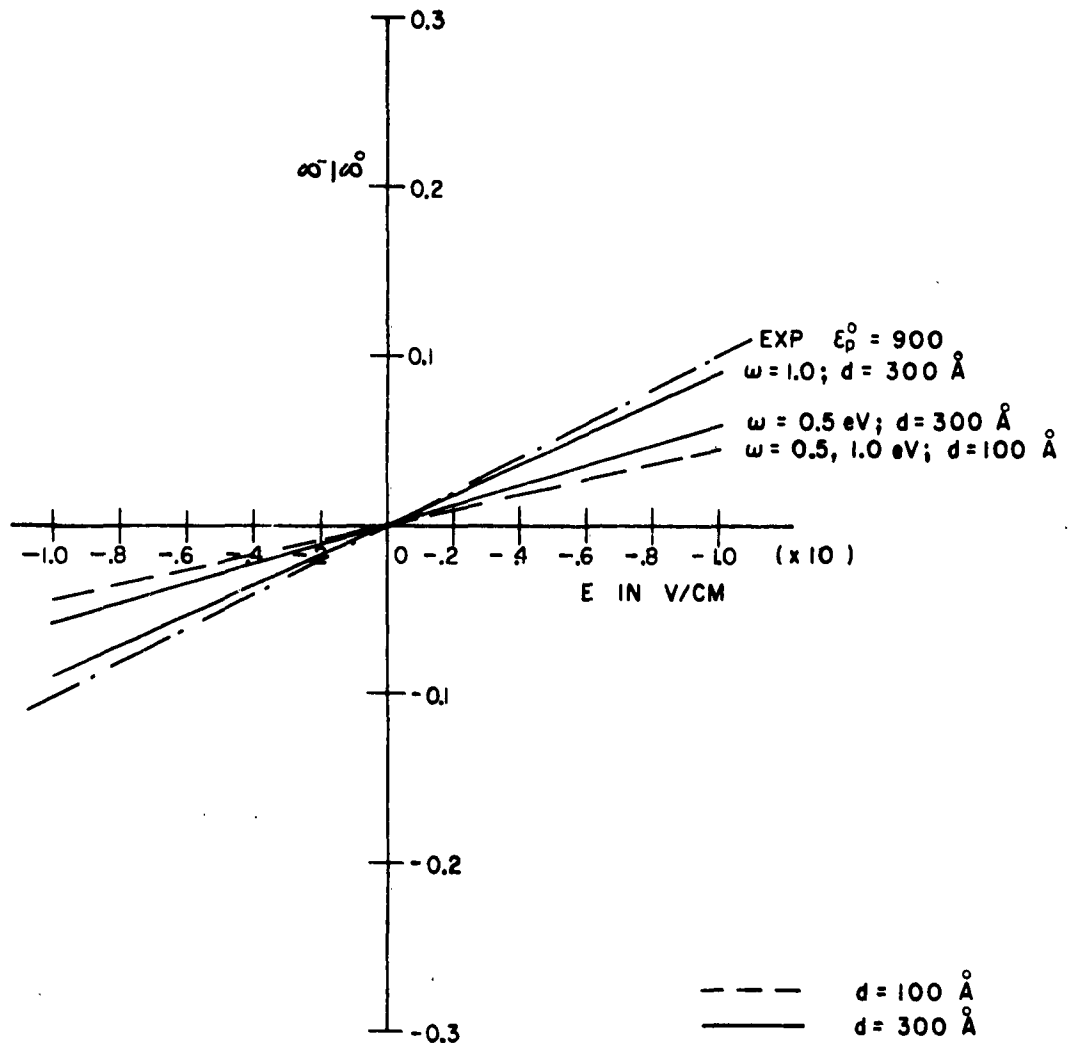


Fig. 42 Variation of δ_0 with Electric Field for a Plane Source Situated at Range d . The effect of electron affinity is also shown. Experimental curve obtained by Boll is shown for comparison

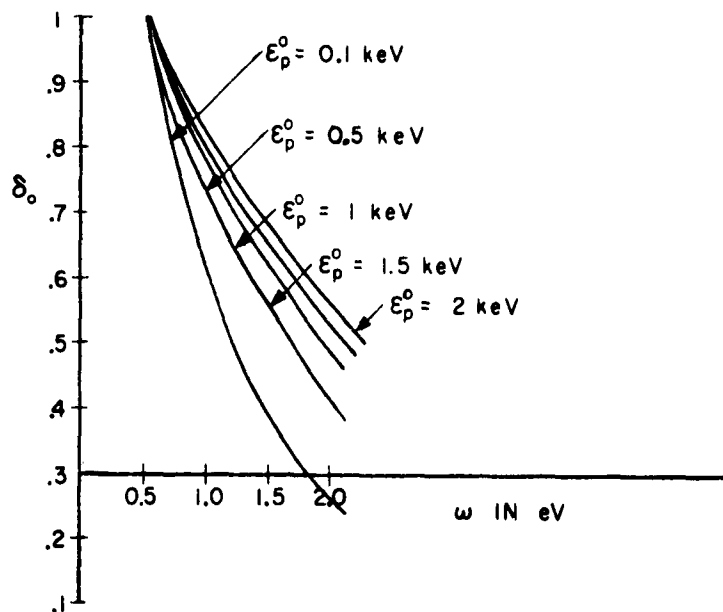


Fig. 43 Effect of Electron Affinity on Secondary Emission without Field for Uniform Source for Various Primary Energies Assuming Range $d = 300 (\epsilon_p^0)^{1.35}$. The curves are normalized to unity at $\omega = 0.5$ eV

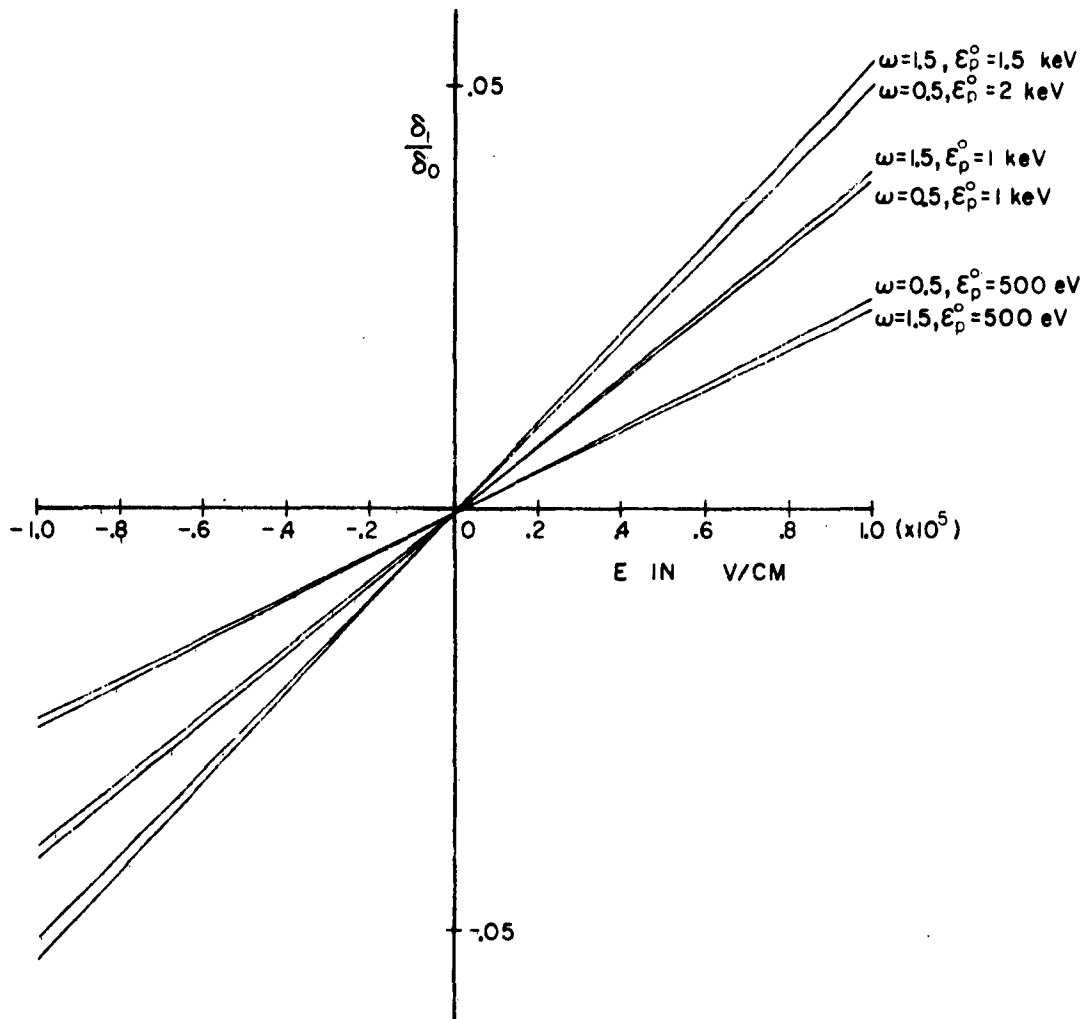


Fig. 44 Effect of an Electric Field on Secondary Emission Coefficient δ_1 for Uniform Source for Various Primary Energies. The effect of electron affinity is also shown

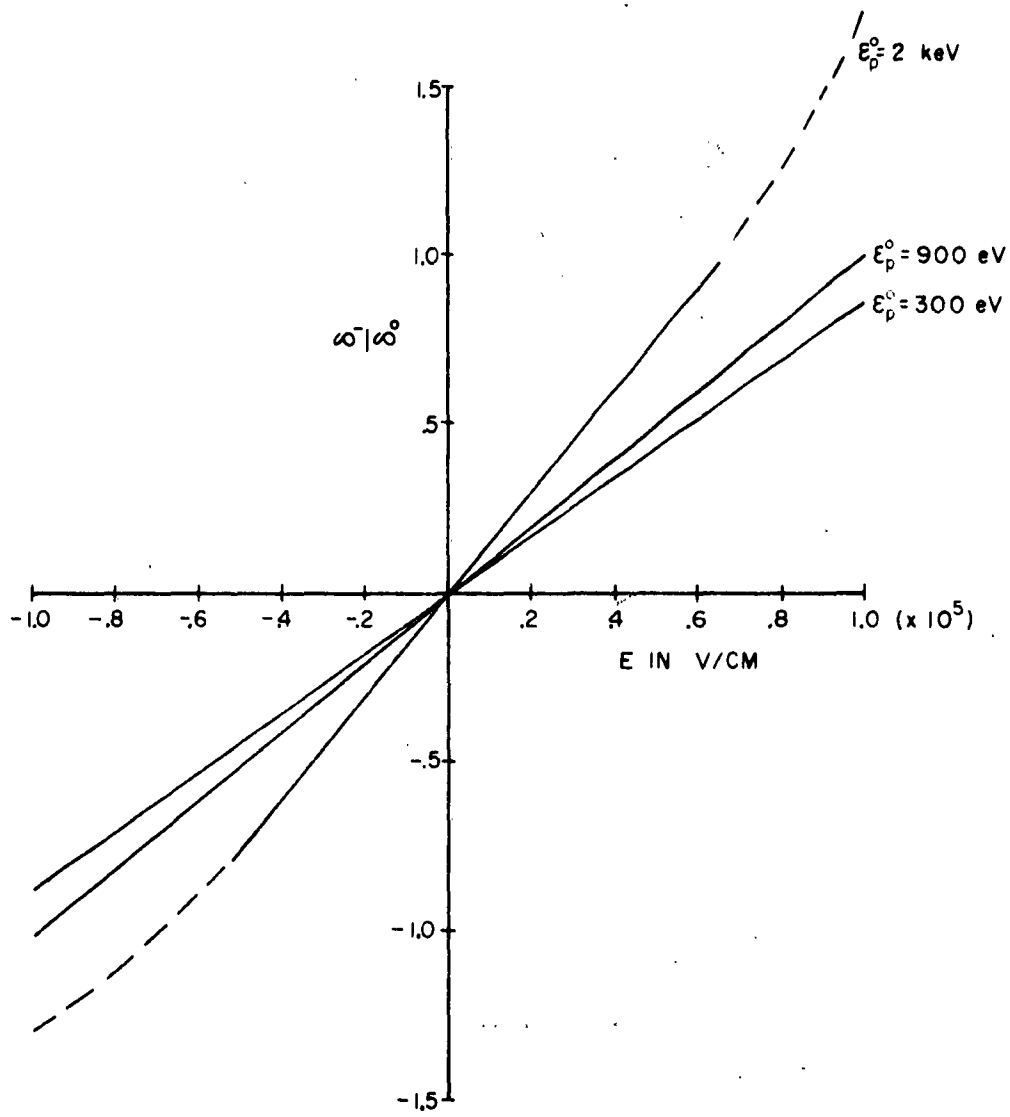


Fig. 45 Experimental Results Obtained by H. J. Boll for Small Values of the Electric Field

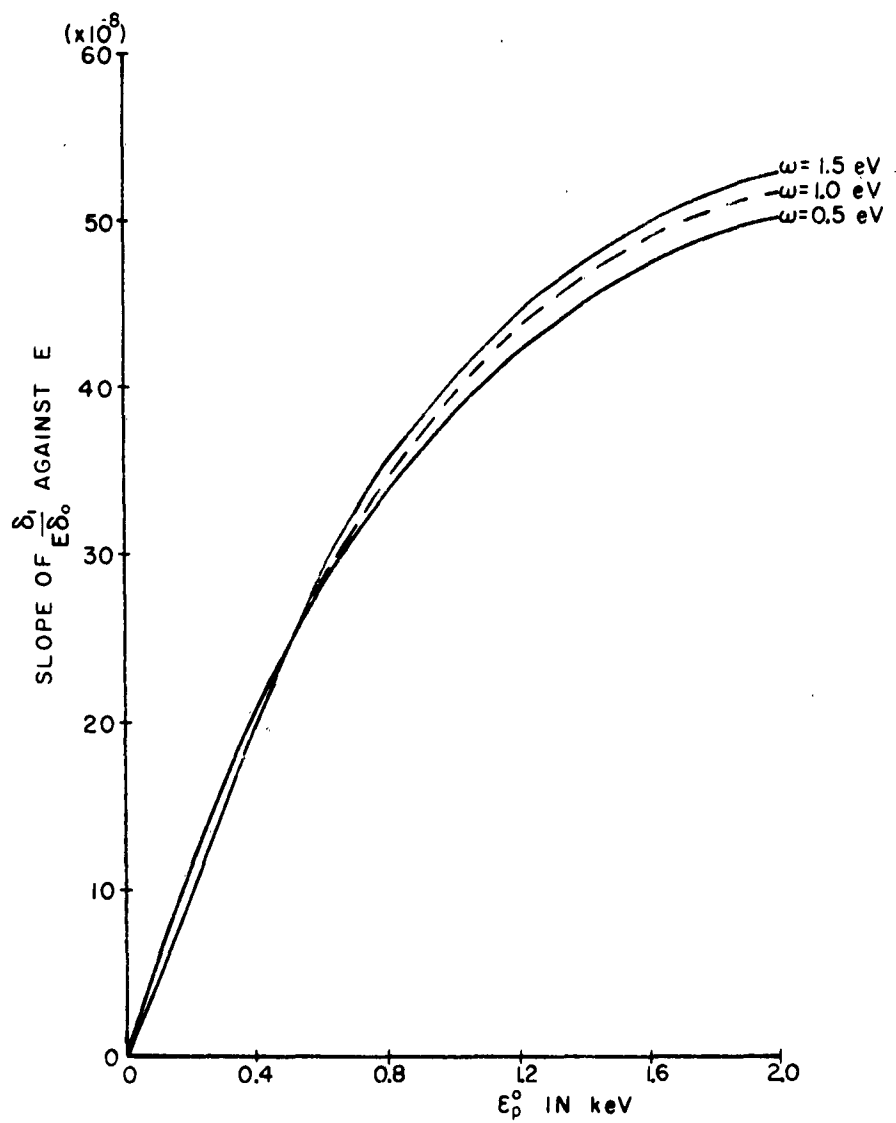


Fig. 46 Slope of δ_1/δ_0 vs. Electric Field Curves against Primary Energy for Various Values of Electron Affinity

Aeronautical Systems Division, Dir/Avionics,
Electronic Technology Lab., Wright-Patterson
AFB, Ohio.

Rpt Nr ASD-TDR-63-175, STUDY OF ELECTRICAL
AND PHYSICAL CHARACTERISTICS OF SECONDARY
EMITTING SURFACES, Final report, Jan. 1963
126 pp. incl. illus., tables, 41 refs.

Unclassified

Reproducible measurements of the variation
of the secondary electron emission with
angle of incidence of the primary beam are
reported for single-crystal titanium. It
was necessary to sputter-clean the crystal
in order that these results could be



(over)

obtained. Tungsten, on the other hand, re-
quired no such treatment. A model which ex-
plains, in a qualitative way, most features
of the experimental results is presented.
Further measurements of MgO films formed by
the oxidation of Mg films on metal substrates
are presented and the problem of adsorbed
gas on the target surface is discussed. Two
different surface structures on MgO crystals
are reported and the influence of sputtering
and annealing on these structures and on the
secondary emission coefficient are described.
The results of a theoretical calculation of
the influence of an internal electric field
on the secondary emission from polar crystals
are also given.



1. Secondary Emission
2. Electron Diffraction
3. Ion Bombardment
4. Electrons

I. AFSC Project 4156
Task 415605

II. Contract
AF 33(657)-8040

III. Department of
Electrical
Engineering,
University of
Minnesota,
Minneapolis 14,
Minnesota

IV. Edited by:
W. T. Peria

V. Avail for OTS

VI. In ASTIA collection

UNCLASSIFIED